SDEVELOPMENT OF NEW NMR TECHNIQUES FOR CONFORMATIONAL ANALYSIS OF ^{13}C-ENRICHED OLIGOSACCHARIDES

Graham R. Kiddle

A Thesis Submitted for the Degree of PhD
at the
University of St Andrews

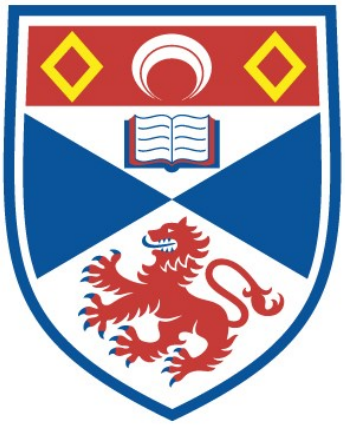

1998

Development of New NMR techniques for conformational analysis of ^{13}C-enriched oligosaccharides.

Graham R. Kiddle

A thesis submitted for the degree of Doctor of Philosophy.

School of Biomedical Sciences

University of St. Andrews

September 1998.

Table of Contents

Acknowledgements

Many thanks to my supervisor, Steve Homans, for his ideas, help and support during the past three years. I also appreciate the help, advice and friendship that I received throughout my Ph.D from Julia Richardson, Charlie Weller and Richard Harris who were a pleasure to work with.

I would like to thank the "Homans group" past and present for many helpful discussions and explanations and also for providing a good atmosphere in which to work.

Finally a special thanks to my parents, Bob and Shirley, for all there help and support over the years.

This work was funded by the BBSRC and Unilever.

Declarations

I, Graham Kiddle, hereby certify that this thesis, which is approximately 40 000 words in length, has been written by me, that it is the record of work carried out by me and that it has not been submitted in any previous application for a higher degree.

8th, September 1998 Graham R. Kiddle

I was admitted as a research student in October, 1995 and as a candidate for the degree of Doctor of Philosophy in October, 1995; the higher study for which this is a record was carried out in the University of St. Andrews between 1995 and 1998.

8th, September 1998 Graham R. Kiddle

I hereby certify that the candidate has fulfilled the conditions of the Resolution and Regulations appropriate for the degree of Doctor of Philosophy in the University of St. Andrews and that the candidate is qualified to submit this thesis in application for that degree.

8th, September 1998 Steve W. Homans

In submitting this thesis to the University of St. Andrews I understand that I am giving permission for it to be made available for use in accordance with the regulations of the University Library for the time being in force, subject to any copyright vested in the work not being affected thereby. I also understand that the title and abstract will be published, and that a copy of the work may be made and supplied to any *bona fide* library or research worker.

8th, September 1998 Graham R. Kiddle

Abstract

The three-dimensional conformations of various oligosaccharides have been investigated using high-resolution nuclear magnetic resonance measurements and molecular dynamics calculations. A fundamental problem with such studies is the lack of structural restraints across the glyosidic linkage as well as the short-range nature of these restraints. In this thesis this problem has been addressed by developing new techniques that increase the total number of structural parameters for inclusion in the molecular modelling simulations.

The measurement of inter-glycosidic heteronuclear NOEs is described and four ^{1}H-^{13}C NOEs were measurable in a model disaccharide with appropriate ^{13}C and ^{2}H enrichment. NMR studies were also carried out with a series of oligosaccharides dissolved in a dilute liquid crystalline medium. This resulted in a degree of molecular alignment for the oligosaccharides that in turn allowed the measurement of dipole-dipole coupling constants. These were incorporated in dynamic simulated annealing calculations in order to verify their usefulness in structural calculations.

The three-dimensional structure and dynamics of Galβ1-4Glc were investigated using the additional restraints mentioned above, as well as ^{13}C-^{13}C trans-glycosidic long-range coupling constants and ^{1}H-^{1}H NOEs. It was shown that the conformation cannot be represented by a single structure, but is best represented by a dynamic model.

Other techniques developed in this thesis include the measurement of three-bond ^{1}H-^{13}C scalar coupling constants to probe the existence of inter-glycosidic hydrogen

bonding, and the direct measurement of bond angles using relaxation via cross-correlated dipolar couplings. Finally the bound-state conformation of ^{13}C-enriched Sialyl Lewis-x in association with E-selectin was investigated using a three-dimensional nuclear Overhauser effect ^{13}C-^{1}H heteronuclear single quantum correlation experiment.

List of Figures

Chapter 1

Chapter 2

Chapter 3

Chapter 4

Chapter 5

Chapter 6

List of Tables

Chapter 2

Chapter 3

Chapter 4

Chapter 5

Chapter 6

List of Abbreviations

DHPC	Dihexanoylphosphatidylcholine
DMPC	Dimyristoylphosphatidylcholine
HMQC	Heteronuclear Multiple Quantum Coherence Spectroscopy
HSQC	Heteronuclear Single Quantum Coherence Spectroscopy
LRCC	Lon Range Carbon-Carbon Coupling Spectroscopy
NMR	Nuclear Magnetic Resonance
NOE	Nuclear Overhauser Effect
NOESY	Nuclear Overhauser Effect Spectroscopy
ns	nanosecond
ROE	Rotating Frame Nuclear Overhauser Effect
ROESY	Rotating Frame Nuclear Overhauser Effect Spectroscopy
ps	picosecond
TRNOE	Transferred Nuclear Overhauser Effect
TRNOESY	Transferred Nuclear Overhauser Effect Spectroscopy
[U-^{13}C]	Uniformly carbon-13 enriched (excluding *N*-acetyl groups of acetylated sugars)
[U-^{13}C, ^{2}H]	Uniformly carbon-13 and deuterium enriched.

List of Symbols

^{1}H	Hydrogen atom (proton)
^{13}C	Carbon-13 atom
$^{n}J_{CH}$	n-bond carbon-proton coupling constant
$^{n}J_{HH}$	n-bond proton-proton coupling constant
$^{n}J_{CC}$	n-bond carbon-carbon coupling constant
δ	Chemical shift
γ	Gyromagnetic ratio
$J(\omega)$	Spectral Density
τ_C	Correlation time for molecular reorientaion
τ_m	NOESY/ROESY mixing time
t_1	Acquisition time (1D experiment); first evolution period (nD NMR experiment)
t_2	Acquisition time (2D experiment); second evolution period (nD NMR experiment)
t_3	Acquisition time (3D NMR experiment)
φ	Dihedral angle H_1-C_1-O_1-C_X in a glycosidic linkage
ψ	Dihedral angle C_1-O_1-C_X-H_X in a glycosidic linkage
T_1	Time constant of spin-lattice (longitudinal) relaxation
T_2	Time constant of spin-spin (transverse) relaxation
T_m	Liquid crystalline phase transition

Chapter 1

Introduction

1.1 The Study of Carbohydrates

Modern carbohydrate chemistry can be dated to the late nineteenth century, when the German chemist Emil Fischer carried out his research. This included a proof of the structure of glucose. The name carbohydrate was brought into use under the impression that all members of the group were composed of the elements of carbon, hydrogen and oxygen with hydrogen and oxygen in the ration 2:1 as in H_2O. This is true for the majority (e.g. glucose $C_6H_{12}O_6$) but there are exceptions; for example rhamnose ($C_6H_{12}O_5$) and glucosamine ($C_6H_{13}O_5N$). Carbohydrates are in fact aldehyde or ketone compounds with multiple hydroxyl groups. They are essential components of all living organisms and are, the most abundant class of biological molecules. The metabolic breakdown of monosaccharides provides most of the energy used to power biological processes. Monosaccharides are principal components of nucleic acids, as well as important elements of complex lipids. Oligosaccharides consist of a few covalently linked monosaccharide units. They are often associated with proteins (glycoproteins) and lipids (glycolipids) in which they have both structural and regulatory functions.

The elucidation of the structures and functions of carbohydrates has lagged well behind those of proteins and nucleic acids. There are several reasons for this. For example, they are not subject to the types of genetic analysis that have been invaluable in the study of proteins and nucleic acids because saccharide sequences are not genetically specified but are built up through the sequential actions of specific enzymes. Also, it has been difficult to establish assays for monitoring biological

activities of these compounds because of their largely passive roles. Nevertheless it has become increasingly clear that carbohydrates are essential elements in many, if not most, biological processes (Varki, 1993).

1.2 Biological Function of Carbohydrates

Until the late 1960's the biological function of carbohydrates was generally thought to be limited to energy production and storage (starch and glycogen), and as a structural material (cellulose and chitin). The ability to sequence accurately the oligosaccharide units of glycogonjugates revealed a remarkable complexity and diversity of these molecules (Varki, 1993). Since that time various suggestions for the function of carbohydrates have been put forward. These include purely structural roles, such as aiding in the conformation and stability of proteins as well as cell-cell recognition, toxin adhesion and invasion, immune evasion and activation, leukocyte extravasation, and the clearance of glycoproteins from the circulation by hepatic reticuloendothelial cells (reviewed in Varki, 1993).

Research over the past 30 years has demonstrated that many proteins are, in fact, glycoproteins, that is they are covalently associated with carbohydrates. Glycoproteins vary in carbohydrate content from <1% to >90% by weight. These proteins occur in all forms of life with the carbohydrate moieties having many important biological roles. In mammalian systems the oligosaccharides involved in cellular recognition are normally found in glycolipids, linked to a ceramide tail, or in glycoproteins, covalently attached to the side chains of specific amino acids such as

asparagine (Asn) via a *N*-glycosidic bond (*N*-linked), or serine (Ser) and threonine (Thr) via an *O*-linked glycosidic bond (*O*-linked). The carbohydrate moieties of these glycoconjugates may range in size from 2 to 20 residues. They normally consist of neutral monosaccharides such as D-mannose (Man), D-glucose (Glc), and D-galactose (Gal); amino sugars such as *N*-acetyl-D-glucosamine, and *N*-acetyl-D-galactosamine; C-6 deoxy sugars for example L-fucose (Fuc); and the nine carbon atom sugars of the sialic acid family, of which *N*-acetyl neuraminic acid (Neu5Ac) is the most commonly found representative (Schauer, 1982) (for structures see figure 1.1).

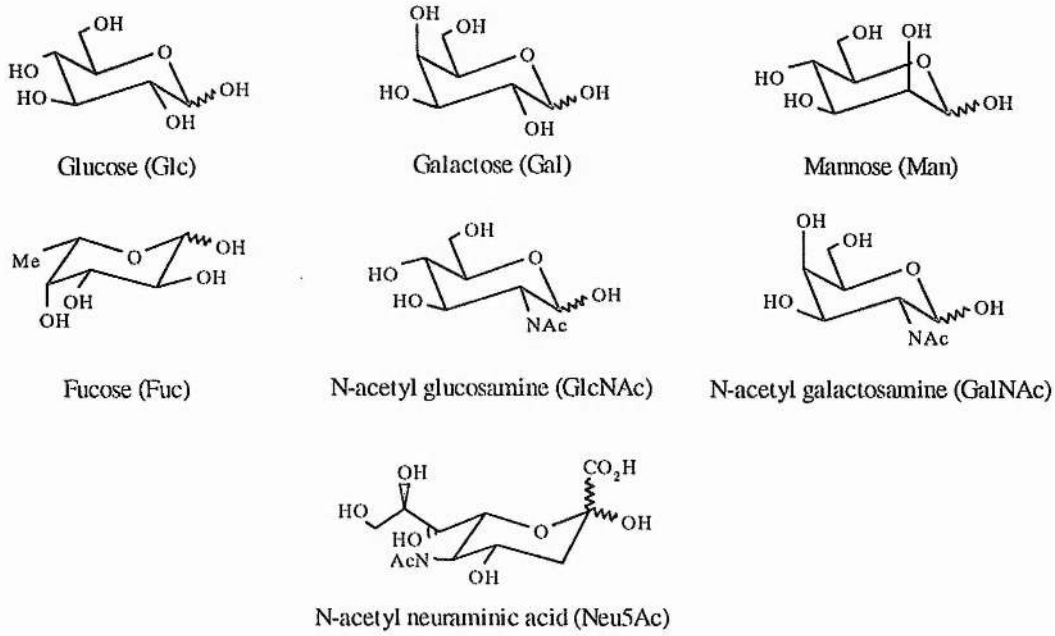

Figure 1.1 - Schematic representation of the most commonly found constituent monosaccharide units of glycoproteins and glycosphingolipids

In contrast to nucleotides in nucleic acids and amino acids in proteins, which can only interconnect in one way, the monosaccharide units in oligosaccharides can bond together in multiple ways to form a vast repertoire of compounds using only a few simple sugars. Glucose alone has six functional groups and five asymmetric carbons, each different from the others. Despite the potential structural diversity of oligosaccharide chains, glycosphingolipids and the glycoprotein glycans commonly found in mammalian systems can be classified into a few distinct groups. Glycolipids may be arranged into "ganglio", "globo", "isoglobo", "lacto", and "neo-lacto" series (figure 1.2).

Ganglio	
Galβ1-3GalNAcβ1-4Galβ1-4Glc-Cer	asialo-G_{M1}
Globo	
GalNAcβ13Galα1-4Galβ1-4Glc-Cer	globoside, G_{b4}
Isoglobo	
GalNAcβ1-3Galα1-3Galβ1-4Glc-Cer	isogloboside
Lacto	
Galβ1-3GlcNAcβ1-3Galβ1-4Glc-Cer	lacto-*N*-tetraose
Neo-lacto	
Galβ1-4GlcNAcβ1-3Galβ1-4Glc-Cer	lacto-*N*-neotetraose

Figure 1.2 - Examples of the core structures of animal glycosphingolipids

***1.2.1 N*-linked glycoproteins** exhibit numerous glycoforms; cells tend to synthesis a large repertoire of a given *N*-linked glycoprotein, in which each variant species differs somewhat in the sequences, locations, and numbers of its covalently attached oligosaccharides. *N*-linked glycoprotein glycans fall into three broad families (figure 1.3): oligo-mannose, complex, and hybrid type oligosaccharides. All *N*-linked oligosaccharides contain the pentasaccharide Manα1-6(Manα1-3)Manβ1-4GlcNAcβ1-4GlcNAc as a common core (the "trimannosyl core"). Oligo-mannose type sugars contain only α-mannosyl residues in addition to the trimannosyl core. Complex type oligosaccharides contain no mannose residues other than those in the core, and the chains normally terminate with variations of the Neu5Acα2-3/6Galβ1-4GlcNAcβ1-R (where R = trimannosyl core), and hybrid type oligosaccharides have a combination of the complex and oligo-mannose type characteristics.

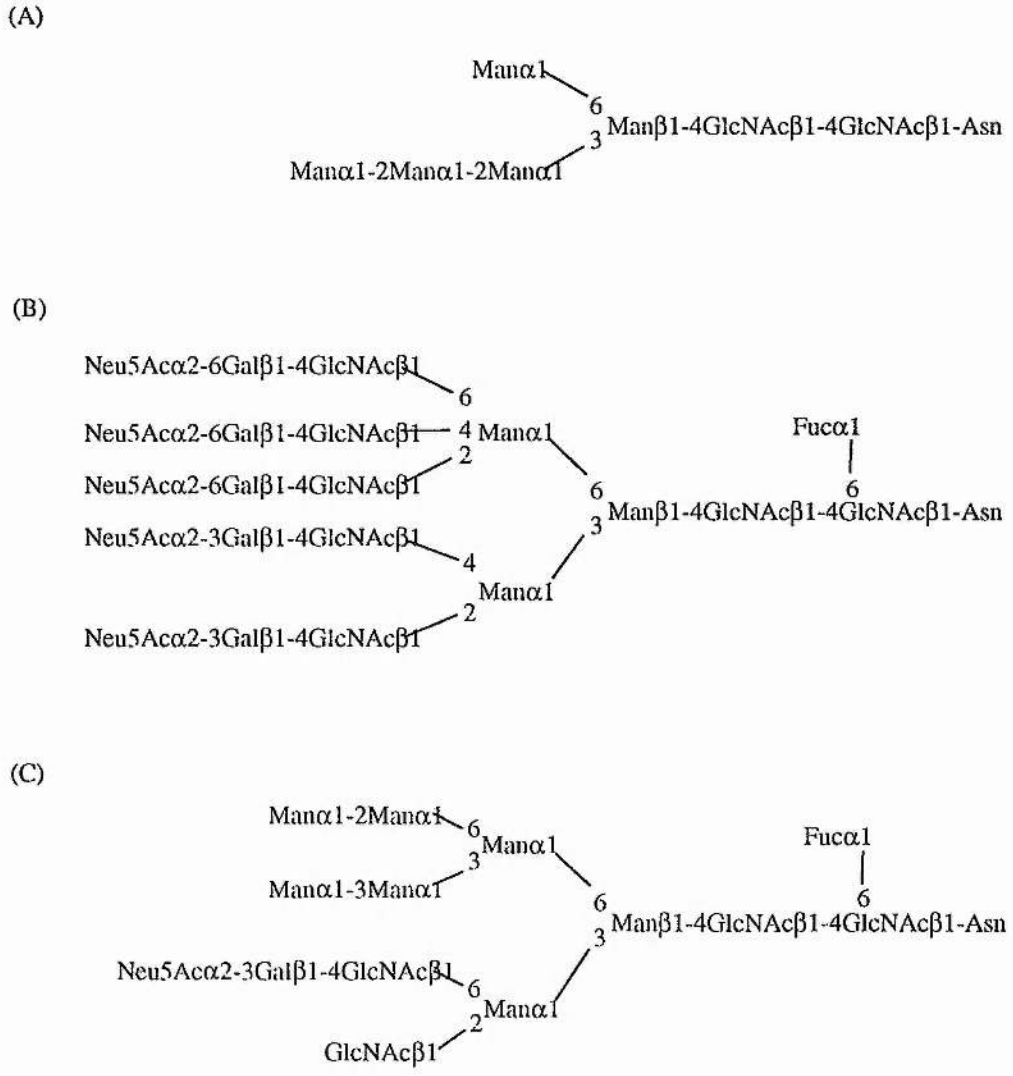

Figure 1.3 - Examples of the three major subgroups of *N*-linked sugar chains: (A) Oligo-Mannose type; (B) Complex type; and (C) hybrid type

***1.2.2 O*-linked glycoproteins** do not share a common core structure, but are classified as belonging to one of six groups according to different core structures (figure 1.4). These cores can be elongated to form the backbone region by addition of galactose in β1-3 and β1-4 linkages, and *N*-acetylglucosamine in β1-3 and β1-6 linkages. Although the glycans are often linked to a serine or threonine residue via GalNAc, they may link through other residues such as fucose.

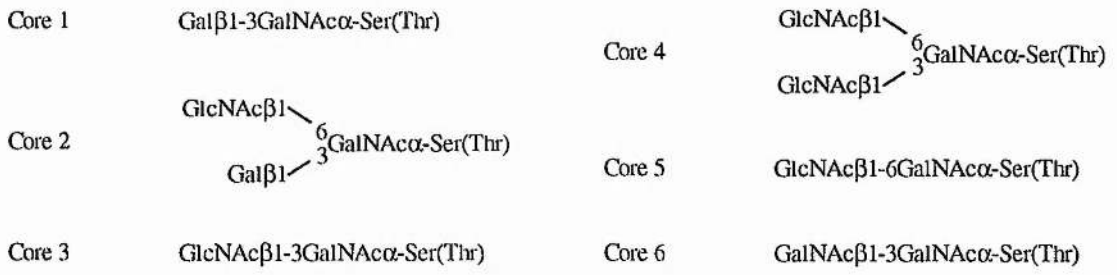

Figure 1.4 - Core structures found in *O*-linked glycans

1.3 Carbohydrates Associated with Disease

1.3.1 Oncology

A change in the glycosylation profile of cells is often associated with disease and is a manifestation of defects in sugar metabolic pathways caused by cells undergoing oncogenesis. For example, certain cancerous cell lines (reviewed in Oettgen, 1989) have higher densities of simpler gangliosides such as G_{M3} (Neu5Acα2-3Galβ1-4GlcCer) and G_{D3} (Neu5Acα2-8Neu5Acα2-3Galβ1-4GlcCer) at the expense of more complex gangliosides such as G_{M1} (see figure 1.1). Monoclonal antibodies (mAbs)

raised against these sugars or plant lectins that recognise the G_{M3}/G_{D3} epitopes are often used in the clinical diagnosis of cancer cell-lines.

The tetrasaccharide, sialyl Lewis-x (sLex) has also been shown to play a role in tumour metastasis. Expression of sLex on the surface of cancer cells promotes metastasis by providing adhesion and invasion points for circulating metastatic cells.

1.3.2 Bacterial and Viral Infection

Certain oligosaccharides can act as highly specific receptors for a variety of viruses, bacteria and parasites. For example terminal sialic acids are recognised by receptors for a variety of virus haemagglutinins. Recognition is affected by linkage and/or substitution of a sialic acid. This can be the first step in the infectious process of a virus, the consequences of which, range from lethal disease to a mild infection. Oligosaccharides are also receptors for many plant and bacterial toxins, and serve as antigens for autoimmune and alloimmune reactions.

Some bacteria bind to epithelial cells by means of carbohydrate-protein interactions (reviewed in Edge, 1994). In most of these instances, there is exquisite specificity for the sequence of the oligosaccharide involved. Examples include the preferential binding of *Helicobacter pylori* to the surface of gastric epithelial cells in the stomach using the Lewis^b antigen as its receptor; cholera toxin, an A-B toxin produced by *Vibrio cholerae*, which uses the B-subunit to bind the glycosphingolipid GM_1. This enables the A subunit to enter the cell and activate cAMP production; and the

influenza virus which recognises and binds to glycoconjugates on cell surfaces through one of its surface proteins, haemagglutinin.

1.3.3 Inflammation

The high fidelity of carbohydrate binding proteins is crucial for the health of an organism. However, this specificity may also have disadvantages if the carbohydrate recognition is unregulated. The recognition of oligosaccharides produced on the surface of endothelial cells by circulating leukocytes is essential for the correct function of the immune system. Injured or infected cells defensively secrete cytokines that stimulate endothelial cells to express lectins and display them on their surfaces. These lectins, often called selectins or leukocyte-cell adhesion molecules, have different affinities for sialyl Lewis-x, an oligosaccharide present on the surface of white blood cells. Leukocytes are thus "snared" by endothelial cells expressing these selectins, and once attached, a leukocyte can leave the bloodstream by squeezing through adjacent endothelial cells. Unfortunately, this same mechanism which recruits leukocytes to areas of inflamed tissue can ultimately lead to over-recruitment. This allows leukocytes to accumulate in tissues causing tissue damage, swelling and pain. Certain forms of rheumatoid arthritis and thrombosis are caused by the unregulated accumulation of white blood cells. Reperfusion injury is a disorder that occurs after the flow of blood is temporarily cut off from tissue, such as during heart attack. When the blood flow resumes, leukocytes destroy tissues damaged by lack of oxygen leading to necrosis and dangerous swelling.

1.4 Carbohydrate Therapeutics

With the diverse role that oligosaccharides play in biological functions, it is apparent that the manipulation of carbohydrate recognition may have important therapeutic benefits. Carbohydrate based drugs may also have other advantages such as low toxicity and immunogenicity. In addition, in the treatment of microbial infections, these drugs merely prevent the adhesion of microbes and not their death. There is therefore less evolutionary pressure for mutation, so resistance is less likely. Presently pharmaceutical companies are testing the sialyl Lewis-x antigen in clinical trials for reperfusion injury, as well as other carbohydrate drugs undergoing clinical trials for ailments including cancer, diarrhoea, thrombosis, diabetes, ulcers, epilepsy, and Parkinson's disease (reviewed in McAuliffe, 1997).

1.4.1 Carbohydrate drugs may be designed to work in several ways

1. Inhibition of protein attachment

The most common method so far is to design a drug, based on the natural carbohydrate ligand, which would bind irreversibly to a protein involved in pathogenesis, thus preventing cellular adhesion. This method has been used in the treatment of reperfusion injury with both Cytel and Glaxo Wellcome currently designing small sialyl Lewis-x mimics to prevent the accumulation of leukocytes in tissues damaged by heart attacks or surgery. The clearance of bacteria and their toxins from the gastrointestinal tract with oligosaccharides has long been used in nature: mammalian milk, which contains high concentrations of oligosaccharides

often found on the surface of the gut, is believed to protect infants from infections. Synthetic attempts to mimic this process include the development of a Gb_3 conjugate linked to an insoluble powder to prevent verotoxin adhesion.

2. Alteration of carbohydrate biosynthesis

Many diseases are associated with defects in oligosaccharide metabolism. Several azasugars (nitrogen analogues of carbohydrates) may help in the treatment of certain forms of diabetes by inhibiting sucrase and amylase, responsible for the breakdown of polysaccharides in the gut, and therefore prevent the adsorption of glucose into the bloodstream. The spread of metastatic cells may be prevented by inhibiting the synthesis of glycoconjugates such as sLex known to aid the colonisation of healthy tissues by cancerous cells. Inhibiting the catabolism of Neu5Ac terminating oligosaccharides has been used successfully in the treatment of influenza (von Itzstein, 1993).

3. Eliciting an immune response

Cells undergoing oncogenesis often express a different range of glycoconjugates compared to their healthy counterparts. The treatment of cancer patients by stimulating anti-ganglioside antibodies has had some limited success (Livingston, 1987). Recently a similar methodology has been applied successfully to the treatment of lung, breast, colon, and ovarian cancers: this treatment consists of injecting the patient with a glycopeptide hapten found on the surface of these cancer cell lines which elicits an immune response against these cells.

1.4.2 Rational Drug Design

A prerequisite for a rational approach to drug design is a detailed understanding of the interaction of a carbohydrate with its receptor. Of primary importance to this understanding is a high-resolution three-dimensional structure of the complex, and several crystallographic studies have been described recently that illustrate in detail the precise nature of certain carbohydrate-protein interactions. The most celebrated example of model based drug design was the work performed in von Itzetein's laboratory on the development of an influenza sialidase inhibitor (von Itzstein, 1993). Sialidase is critical in the release of newly synthesised influenza virons from infected cells by the cleavage of terminal Neu5Ac residues from host cell-surface glycans. Inhibition of this enzyme limits the establishment and progression of infection. Computer-aided molecular modelling was used to analyse the active site and predict the functional group changes that would increase the binding affinity of the sialic acid residue. Modelling studies predicted that the substitution of the 4-OH group with an amino or guanidino group would produce an increase in overall binding. Results show that the 4-guanidino derivative has an inhibition constant, for various strains of influenza, in the 1×10^{-10} range. Additionally the affinity of this compound against human sialidases is a million times lower, therefore offering excellent selectivity for virus sialidases.

Detailed x-ray crystal structures of biologically important oligosaccharide complexes are rare, as the relatively flexible oligosaccharide often results in poor electron densities for the carbohydrate residues, and when observed they are often stabilised

by crystal packing forces which may orient the sugar in an unnatural conformation. Many lectins only weakly bind isolated oligosaccharide analogues of their receptor glycans, and so may not be co-crystallised (Stein, 1992). An additional problem is that carbohydrate binding sites in the well ordered solid state may not be active in the less well ordered solution state (*c.f.* Wright, 1992, with Wright, 1996, and reviewed in Rossi, 1992).

In contrast, high-resolution structural studies of glycan protein interactions by nuclear magnetic resonance spectroscopy can offer complimentary information on the structure of the carbohydrate in sugar-protein interaction. Solution studies have important advantages compared to crystal studies since a comparison of the solution structure of the free and bound conformations of the ligand is more meaningful, and moreover, the dynamics of the system are accessible.

NMR has been used to study carbohydrates, since the 1950's, and is uniquely suited to the investigation of carbohydrates and their complexes. NMR has been used to determine the type, number, and primary sequence of oligosaccharides, including the occurrence of branch points and the location of appended non-carbohydrate groups, and their three-dimensional conformations and dynamics in free solution and in complex with proteins (van Halbeek, H., 1994b).

1.5 NMR Spectroscopy

The first NMR signals were observed in 1945. In 1949 and 1950 the phenomenon of the chemical shift was discovered. In more recent times the development of pulsed Fourier transform NMR and the conception of multidimensional NMR spectroscopy has lead to the widespread use of NMR as a non-destructive technique for the molecular analysis of both organic and inorganic compounds. NMR techniques can provide information on structure, conformation, and internal mobility. Comprehensive introductions include Sanders and Hunter (1987), and Derome (1987).

The fundamental basis of the NMR experiment is perturbation by a radio-frequency pulse of the equilibrium bulk magnetisation from an axis parallel to the external static magnetic field (B_0) into a vector perpendicular to this axis. The individual spins precess around this plane at a characteristic frequency known as the Larmor frequency (ω), which is dependent upon the shielding of the nucleus from the external field by nearby electron-inductive groups:

$$\omega = \gamma B_0 \qquad [1.1]$$

where γ is a constant for a given nucleus known as the magnetogyric ratio.

Once perturbed from its equilibrium position the magnetisation can be detected as an oscillating current in a coil orthogonal to the B_0 field. The detected signal, known as the Free Induction Decay (FID), is a function of time, that upon Fourier

transformation is converted into a function of frequency, with frequencies characteristic of the nuclei that are precessing.

1.5.1 Conformational Analysis

For NMR studies of oligosaccharides in free solution, there are three main parameters that can be measured to give structural information:

(a) Conformation and structure dependent chemical shifts

(b) Spin-spin coupling constants (J)

(c) Relaxation properties (NOE, T_1, T_2)

The conformation of oligosaccharides in complex with proteins may be determined from:

(d) Line shape analysis

(e) Transferred NOE

1.5.2 Relaxation

There are two main reasons why relaxation is important in NMR. Firstly, relaxation has a significant effect on the way in which NMR experiments are designed. The rate of relaxation for many important nuclei is fortuitous, for if it were either much slower, or much faster, pulsed NMR would not be as useful a technique as it is. Secondly, relaxation parameters correlate with structural features of molecules and particularly with their motions.

Detailed explanations of NMR relaxation phenomena are given by Noggle and Schirmer (1971), and Neuhaus and Williamson (1989).

After the application of a pulse or other perturbation, nuclei relax back to equilibrium by one of two mechanisms. Longitudinal relaxation (T_1) causes the population difference between two spin states of a given nucleus to return exponentially to equilibrium, due to transfer of energy to the surroundings or 'lattice'. In terms of the classical formalism, bulk magnetisation in the X-Y plane returns to the Z axis. The second mechanism, transverse relaxation (T_2) causes a loss of phase coherence in the X-Y plane due to mutual exchange of spin energy and resultant decay in the bulk intensity of transverse vectors. The process is not changing the energy of the sample, as no transitions between levels are occurring, but the amount of order present is decreasing. In other words the enthalpy remains constant but the entropy increases.

Both mechanisms of relaxation are due to time-dependent magnetic or electric fields derived from random thermal motions within the sample. For both ^{1}H and ^{13}C nuclei, the major sources of such fields are the magnetic moments of neighbouring protons, and the intensity is termed the spectral density function, $J(\omega)$. Relaxation is most efficient for both T_1 and T_2 when the time scale of such interactions is at or near the Larmor frequency, and T_2 is additionally sensitive to low frequency modulations of spin energy levels. The effects of dipole-dipole interactions with adjacent ^{1}H nuclei therefore dominate relaxation mechanisms. The strength of these dipolar interactions is primarily dependent upon the internuclear distance and the mobility of the vector

within the static field. An understanding of the dipole-dipole interactions can give information about both geometric and dynamic behaviour.

1.5.3 Nuclear Overhauser Effect

1.5.3.1 The Truncated Driven NOE

Consider a two-spin system, IS, that is not dipolar coupled, but is close in space. Transition probabilities between states can be defined as shown (figure 1.5), with the populations of each energy level given by the Boltzmann distribution.

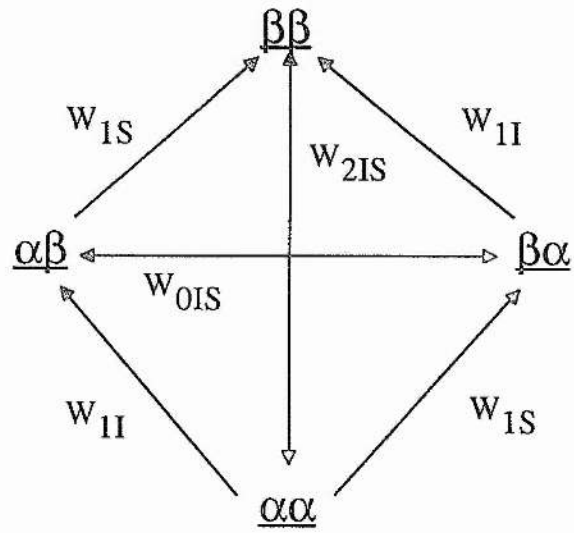

Figure 1.5 - Energy level diagram for two non-coupled spins, I and S, in close spatial proximity. W_1, W_2 and W_0 represent the transition probabilities for single, double, and zero quantum processes, respectively.

The application of a radio-frequency pulse at the frequency of spin S saturates this spin causing the equalisation of the populations across the S spin transitions, and relaxation will proceed by various pathways including double (W_2) and zero (W_0) quantum spin transitions. W_2 transitions are promoted by magnetic fields fluctuating at ~2ω, and W_0 by low frequency fluctuations. In slowly tumbling molecules relaxation by the W_0 pathway will predominate causing a reduction in the intensity of the I spin, resulting in a -100% NOE at the limit, whilst in rapidly tumbling molecules, W_2 relaxation processes dominate causing a positive enhancement on the intensity of the I spin. When these energy level populations are disturbed from equilibrium, the I spin will also relax by transferring energy to other nearby spins, these indirect enhancements are negative. After prolonged saturation of the S spin, the transfer of indirect NOE enhancements (spin-diffusion) causes saturations of all the spins in the molecule, and the distance proportionality of the NOE magnitude is lost. Therefore, rate of cross-relaxation, σ which is also proportional to r^{-6}, is a more convenient parameter to use than the enhancement itself.

In a multi-spin system, the rate of intensity change for spin I is:

$$\frac{dI_z}{dt} = -R_I\left(I_z - I_z^0\right) - \sigma_{IS}\left(S_z - S_z^0\right) - \sum \sigma_{IM}\left(M_z - M_z^0\right) \qquad [1.2]$$

where I_z and I_z^O are I spin intensities along the Z-axis at time zero and time t respectively. R_I is the relaxation rate of I, and M represents all other spins in the system. The initial rate, when $I_z = I_z^O$, and $S_z = 0$, is given by:

$$\frac{dI_z}{dt} = \sigma_{IS} S_z^0 \qquad [1.3]$$

For homonuclear ^{1}H-^{1}H interactions, σ is given by:

$$\sigma_{IS} = \left(\frac{\mu_0}{4\pi}\right)^2 \frac{\gamma_I^2 \gamma_S^2 h^2}{10 r_{IS}^{-6}} \left[6J(\omega_I + \omega_S) - J(\omega_I - \omega_S)\right] \qquad [1.4]$$

where h is Planck's constant divided by 2π, μ_0 is the permeability of free space, r_{IS} is the internuclear distance, and γ is the gyromagnetic ratio of proton spins, I and S. $J(\omega)$, the spectral density function is defined as:

$$J(\omega) = \frac{\tau_c}{1 + \omega^2 \tau_c^2} \qquad [1.5]$$

where τ_c, the correlation time for isotropic molecular reorientation, is inversely proportional to rates of molecular motions, and is identical for each ^{1}H-^{1}H vector in a rigid isotropically tumbling molecule.

Using the initial rate approximation, immediately after saturation of spin S, the NOE at spin I is affected by only one distance-dependent term, σ_{IS}. Therefore, when the saturation period is within the linear build-up region, all enhancements behave as though they were in a two-spin system. NOEs measured during a truncated driven experiment are therefore in proportion to the inter-nuclear separation from spin S.

With longer pre-saturation times, indirect enhancements develop, and the distance specificity is lost.

If all constant terms in equation 1.4 are gathered together as a single term, k, the equation simplifies to:

$$\sigma_{IS} = k r_{IS}^{-6} \qquad [1.6]$$

Then, when an NOE enhancement is observed between two other spins (I and M) and the distance between I and S is known, the I-M distance can be estimated from a simple ratio calculation:

$$r_{IM} = r_{IS}\left(\frac{\sigma_{IS}}{\sigma_{IM}}\right)^{\frac{1}{6}} \qquad [1.7]$$

Due to the r^{-6} dependence, small inaccuracies in measured NOE enhancements have negligible effects in calculated inter-nuclear distances. As a result, this reference distance method, also referred to as the isolated spin pair approximation (ISPA), may be used to model theoretical NOE intensities from static or dynamic structures provided that the following caveats are appreciated:

1. The accuracy of the calculated I-M distance relies upon that of the reference distance.
2. Inaccuracies are introduced by non-instantaneous saturation.
3. The method is only valid for the initial rate approximation.

4. Integration of spectra, particularly with overlapping signals may be inaccurate.

5. Inter-nuclear vectors connecting IS and SM must have the same effective correlation time (τ_c). This will not be the case if the molecule exhibits anisotropic tumbling or has flexibility in the S-M distance.

6. In the event of internal motions, enhancements are heavily weighted by conformations with the closest contact, due to the r^{-6} dependence, with the inter-nuclear distance rather than the enhancement itself, which is averaged.

7. Nuclei I, S, and M must have the same gyromagnetic ratio, and must not be relaxed by a directly attached NMR 'active' nucleus.

8. Nuclei I, S, and M must not be undergoing chemical exchange.

Providing these conditions are satisfied, the I-M distance can be calculated to within ~10%. However, in flexible oligosaccharides inequalities of τ_c become relevant, and internal mobility adds uncertainties to the proportionality of σ and r^{-6} (Genest, 1989). For a flexible molecule in multi-site conformational exchange that is slow on the τ_c time-scale, the effective inter-nuclear distance is simply a time-average of the separation at each individual conformation $\langle r^{-6} \rangle^{-1/6}$.

1.5.3.2 Transient and NOESY experiments

The truncated driven experiment, involves the presaturation of a resonance for a short time, during which the enhancement is driven to some value short of steady state and is then sampled by a pulse. Alternatively an NOE can be measured using a transient experiment. For a 1D transient experiment, a selective inversion pulse is

applied to one resonance, during a time (τ) the NOE develops at other resonances. The populations can then be sampled with an observe pulse. During the delay τ (or τ_m if considering 2D experiment) two competing processes are occurring. The first, cross-relaxation from the perturbed spins, is acting to alter intensities of neighbouring spins. The second, spin-lattice relaxation, acts to restore all intensities to their equilibrium value. The initial rate of build up in the transient experiment is given by equation [1.8]:

$$dI_z/d\tau = 2\sigma_{IS} S_z^0 \qquad [1.8]$$

This is twice the build up rate seen in the saturation type experiment (compare equation [1.3]). This would be expected since the initial perturbation of S is twice the size, *i.e.*, inversion rather than saturation.

The 2D or NOESY technique is very similar to the 1D transient experiment, except that the selective inversion of a single resonance in the 1D experiment is replaced by frequency labelling of all resonances in the 2D experiment. The pulse sequence consists of three 90° pulses separated by delays (t_1 and the mixing time, τ_m), followed by acquisition of the FID. If the FID from one such experiment is transformed to give a spectrum, the intensity of the line depends on the particular value of t_1 and τ_m. In the full 2D experiment many such individual experiments are carried out. The value of t_1 is incremented in a regular manner from one experiment to the next so as to generate a matrix of FIDs. The amplitude of the line in the spectrum varies regularly

as a cosine function of t_1. Considering a two-spin system (I, S), the spins are assumed to be spin ½ nuclei, close together in space but not J-coupled. After the first 90_x pulse of the sequence, I and S precess around in the xy plane. The precession rate of I in the rotating frame (ω_I), is the difference between I and the carrier; similarly ω_S is the frequency difference between S and the carrier. At the end of t_1, the two spins I and S have precessed through angles $\omega_I t_1$ and $\omega_S t_1$, respectively and a second 90_x pulse rotates the vectors representing I and S through 90° into the xz plane. An important feature of the NOESY experiment is that it is designed to record only that part of the magnetisation that was longitudinal during the mixing period (τ_m). This means that the x component of magnetisation present after the second pulse must be rejected, and this is achieved using a suitable phase-cycling scheme.

The z components present after the second pulse are dependent on t_1. By measuring the intensity of the z components at this point as a function of t_1, using a third 90_x pulse immediately after the second to convert them into transverse signals, the precession frequency that each vector had during t_1 could be determined. This would be a NOESY experiment with τ_m set to zero yielding only diagonal peaks at the precession frequencies in t_1. Useful information only emerges if the two spins exchange magnetisation during τ_m either by cross-relaxation that acts to alter intensities of neighbouring spins or by chemical exchange. In general, the size and direction of the transient enhancements depend on the difference in the values of the z components of I and S at the start of τ_m. These values depend in turn on the extent of precession that I and S underwent during t_1. Thus, by the end of the mixing period

τ_m, the intensity of the I vector has acquired an additional dependence on ω_s. The extent of this new modulation at frequency ω_s depends on the magnitude and sign of the transient enhancement. Similarly, the intensity of S at the end of τ_m has acquired an equivalent new modulation at ω_I leading to a cross-peak connecting S to I.

As discussed above cross-peaks are absent when the mixing period is very short. When τ_m is very long, equilibrium is restored between the second and third pulses, so that the frequency labelling is lost and all contributions to the 2D spectra decay away. The cross-peaks being the weakest part of the spectrum are the first to go. The choice of τ_m is therefore of great importance.

1.5.4 Spin-Spin Coupling

The basis of spin-spin coupling can be simply explained by consideration of two coupled spins, AB. In the static magnetic field (B_O), the magnetic field of nucleus A is effected by both its own nuclear shielding and the magnetic field due to B. B has two orientations in the field (*i.e.* $M_B = \pm 1/2$) which will produce a small field $\pm \Delta B$. These two orientations are equally probable and therefore H_A gives two equally intense peaks. The same arguments also apply to H_B.

The magnitude of spin-spin coupling constants is affected by the degree of atomic orbital overlap, and is therefore related to the dihedral angle (θ) between vicinal coupled spins (Karplus, 1959 and Karplus, 1963). The generalised Karplus

relationship, applicable to both homonuclear and heteronuclear spin-coupling constants, takes the form [1.9]

$$J = A\cos^2\theta + B\cos\theta + C \qquad [1.9]$$

where A, B and C are constants for which different values have been proposed depending on the torsional angles under investigation. Haasnoot has also included additional terms for substituent electronegativities (Haasnoot, 1980). The ^{1}H-^{1}H spin-coupling constants and chemical shifts of pro-R and pro-S hydroxymethyl resonances have been assigned unequivocally for several hexapyranosides, where $H6_{proR}$ invariably resonates at a higher frequency and larger H5-H6 coupling constants compared to $H6_{proS}$. The rotamer distribution about the C5-C6 bond can therefore be found from the analysis of the ^{1}H-^{1}H spin-coupling constants (Wu, 1983; Ohrui, 1985).

1.5.5 Two and Three Dimensional NMR Spectroscopy

Resonance assignment of even simple oligosaccharides is often complicated by resonance overlap. This is because of the tendency of the majority of resonances in both ^{1}H and ^{13}C spectra to lie within an unresolved envelope spanning only a few hundred Hertz. Anomeric proton and carbon resonances usually lie outside this envelope, being well resolved down-field due to the electron withdrawing effect exerted by the ring oxygen. Resonance overlap problems can often be resolved by separation into a second or third dimension, increasing the spectral dispersion. The precise nature of the information contained in the spectrum depends upon the details

of the pulse sequence and phase cycling used, however, a number of key points are shared by all multidimensional experiments. All multi-dimensional experiments consist of 'building blocks' (Edison, 1994) consisting of a sequence of pulses and delays to generate the required coherences which are then allowed to evolve under a free precession Hamiltonian during an incremented delay (t_1). In multi-dimensional experiments, magnetisation is transferred to other nuclear spins (often ^{13}C, or ^{15}N) where additional information is encoded, for instance ^{13}C chemical shift, which is recorded in an additional incremental delay. The signal generated is then detected directly during acquisition, with two-dimensional spectra processed by application of two orthogonal Fourier transformations, and three-dimensional spectra requiring a third orthogonal transformation.

1.5.6 Transferred NOE experiments

The transferred NOE or TRNOE occurs when a ligand is in exchange between free solution and a bound state in which it is complexed with a protein (Clore, 1982; Clore, 1983a) and reviewed extensively in (Clore, 1991; Campbell, 1993; Ni, 1994; Ni and Scheraga, 1994). Measurement of negative NOEs on the easily detectable free or averaged ligand resonances following the irradiation of other ligand resonances whilst bound to the protein, allows information about the bound conformation to be obtained. As oligosaccharides are often in fast exchange with their receptor proteins, K_D values are between ~10^{-3} to 10^{-6}M, a variety of glycan-protein interactions have been probed by TRNOE experiments (Bevilacqua, 1990; Bevilacqua, 1992; Bundle, 1994; Cooke, 1994; Milton, 1995; Scheffler, 1997).

For a ligand in fast exchange between free and bound on the relaxation time-scale, $\langle\sigma\rangle$, the overall cross-relaxation rate, is given by:

$$\langle\sigma_{IS}\rangle = N^F\sigma_{IS}{}^F + N^B\sigma_{IS}{}^B \qquad [1.10]$$

where N^F and N^B are the number of molecules in the free and bound states, respectively, and $\sigma_{IS}{}^F$ and $\sigma_{IS}{}^B$ are the cross-relaxation rates between spins I and S in the free and bound states. For the measurement of TRNOEs $\langle\sigma\rangle$ should be dominated by σ^B, and corresponds to the inequality:

$$|N^B\sigma_{IS}{}^B| \gg |N^F\sigma_{IS}{}^F| \qquad [1.11]$$

The extent to which this inequality is fulfilled depends upon the relative correlation times (τ_c) of the free and bound states, the distances, r_{IS}, in both states, and the equilibrium dissociation constant K_D. If the complex is only weakly bound, then N^B will be small, and the TRNOE will disappear simply because there is insufficient ligand present in the bound state to contribute to the overall relaxation. Clearly, the minimum value of K_D required for a viable TRNOE will depend on values of $\sigma_{IS}{}^B$ and $\sigma_{IS}{}^F$, where, the more slowly the complex tumbles the larger $|\sigma_{IS}{}^B|$ becomes, consequently the simpler it is to satisfy equation 1.11. One advantage of this condition is that ligands in complex with very large proteins, such as photon

rhodopsin (>1000kDa) (Ni, 1994), which would normally be too large to study by conventional NMR spectroscopy, may be probed by TRNOEs.

At the opposite extreme, the TRNOE depends upon the rate of exchange between free and bound states being sufficient for an appreciable magnetisation flux to occur between them. If S^B is irradiated, the condition for appreciable enhancement transfer to occur from the bound signal I^B to the free signal I^F is:

$$k_{on}[P] >> R_I^F \qquad [1.12]$$

where R_I^F is the relaxation rate of spin I in the free state. Similarly, if the signal S^F is selectively irradiated, the saturation transfer from S^F to S^B is also a requirement for a viable TRNOE, and the relevant equality is:

$$k_{off} >> R_S^B \qquad [1.13]$$

where R_S^B is the relaxation rate of spin S in the bound state. Inequalities in equations 1.11 and 1.12 are likely to be broken for tightly bound complexes, and so for TRNOEs to be observed, inequalities equations 1.11, and 1.12, and for certain experiments equation 1.13 must be observed.

The build-up and decay of TRNOEs over a series of NOESY mixing times can also be used to study the relative mobility of ligand residues when bound to a protein. For a typical example, TRNOEs which show an increase in intensity followed by a decay

over a small range of mixing time ($t_m \leq 100$ms) indicates the presence of spin diffusion as a result of restricted mobility of this residue and the close proximity of the protein. In comparison, TRNOEs which show significant increase in intensity even up to relatively long mixing times (t_m>500ms) are characteristic of a group which has significant conformational mobility in the bound state. Thus, it is possible to map oligosaccharide residues that makes significant contact with their receptor lectin (Casset, 1997).

Due to the restricted mobility of a ligand in the bound state and the close proximity of proteins which are often large, spin-diffusion effects play an important role in the TRNOE phenomena, and failure to take this into account has resulted in misinterpretation of TRNOESY data. A notable example of this was the work by Glaudemans and co-workers, who examined the conformation of a disaccharide in complex with an antibody Fab fragment. The original study TRNOESY data suggested that there was a large conformational change between free and bound states (Glaudemans, 1990). In a following paper however (Arepalli, 1995), the authors concluded that the intra-residue TRNOE which was indicative of this new bound state conformation was in fact spin-diffusion as a result of magnetisation transfer via the protein. Such indirect (TR)NOEs may be identified by measuring transferred NOE enhancements in the rotating frame (TRROE) where, σ_{ROE} is positive regardless of the rate of rotational reorientation, giving rise to cross peaks with negative phase, and where ROE-ROE relays (equivalent to spin-diffusion in NOESY spectra) will always lead to cross-peaks having sign $(-1)^m$, where m is the

number of ROE transfers (Farmer II, 1987). Hence a ROE transfer from proton A to C via B will give rise to a cross-peak of opposite phase to a direct A to C ROE.

1.6 Carbohydrate Conformation

Carbohydrate conformations (reviewed in Stoddart, 1971) are defined by the conformations of individual residues and their linkage geometries. Hexapyranose rings occur predominantly in the chair configuration and, for the purpose of description, the atoms are numbered with the ring oxygen as zero and the carbons follow sequentially from the anomeric carbon (atom one). A reference plane is defined as passing through four of the six heavy atoms in the ring, with the lowest numbered atom lying above or below the plane (IUPAC-IUB, 1980). A letter relating to the conformation ('Cchair for chair) then describes alternative configurations. Superscript and subscripts denote the atoms lying above and below the plane of the ring, respectively. The $^{4}C_{1}$ configuration predominates in D-pyranose due to the relief of steric crowding, except D-arabinopyranoses that adopt $^{1}C_{4}$ configuration due to the distribution of hydroxyl groups and the absence of a 6-carboxy moiety (figure 1.6). *N*-acetyl neuraminic acid adopts a similar configuration to the arabinopyranoses except due to the different numbering, this system is defined as $^{2}C_{5}$. Measurement of homo-nuclear spin-coupling constants does not indicate large deviations from theoretical predictions, suggesting that in solution pyranose rings are essentially rigid structures.

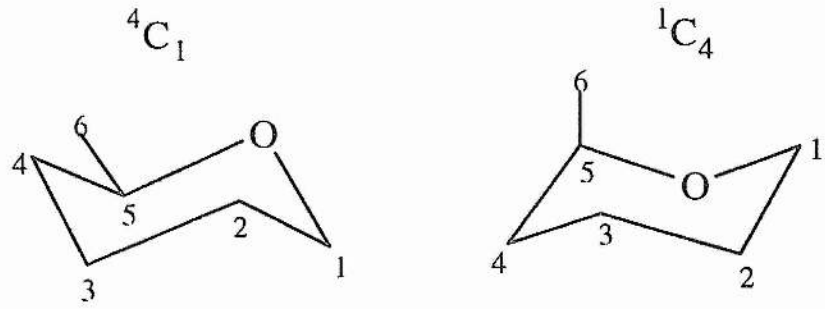

Figure 1.6 - Chair conformations of pyranose rings.

Linkage geometry is defined by the orientation of the glycosidic linkage. IUPAC-IUB describes these in terms of heavy atoms, however in discussing NMR-derived conformations it is more convenient to define them with respect to protons as follows:

$$\varphi_H = H1\text{-}C1\text{-}O1\text{-}Cx, \qquad \psi_H = C1\text{-}O1\text{-}Cx\text{-}Hx.$$

The subscript 'H' distinguishes these from the IUPAC definitions, and the 'Cx' and 'Hx' refer to the aglyconic atoms.

1.6.1 Theoretical Determination of Conformation

The incorporation of experimentally derived distance restraints (NOE measurements) in the determination of the structures of proteins and nucleic acids is now well established. In contrast, due to the small number of inter-residue contacts, experimental NOE data alone are not sufficient to define the geometry of oligosaccharides in solution. Therefore, theoretical support is required from computerised energy calculation routines, which modify/optimise the atomic co-ordinates of an input structure to determine the optimum (minimum energy) conformation. Methods for conformational searching and energy calculation procedures are reviewed by French and Brady (French, 1989).

Full *ab initio* quantum mechanical computations of oligosaccharide conformations are unattainable for even small disaccharides due to the computationally intensive calculations required, thus computations of oligosaccharide conformations have relied almost entirely on molecular mechanical methods (Brady, 1986; Homans,1987; Brady, 1987; Yan, 1990). In this approach the atoms are treated as point masses and charges, and the bonds are treated as springs. Each bond type has an optimum value derived empirically from x-ray crystallography or *ab initio* studies on small molecules, and distortion from the ideal increases the potential of the model in an analogous manner to compression of a spring (i.e. $E=1/2\ Kx^2$). Using analogous classical descriptions, an energy function can be defined for the model. Additional terms to account for empirical observations that are particular to carbohydrates, particularly the anomeric and exo-anomeric effects (reviewed by Tvaroska, 1989)

which drive the aglyconic carbon to take orientations of $\varphi_H \sim +60^\circ$ in β-D-glycosides, and $\varphi_H \sim -60^\circ$ in α-D-glycosides can also be used.

The approach was adopted for the commonly used hard sphere exo-anomeric (HSEA) approach (Thorerson, 1982), where results obtained were in good agreement with experimental and theoretical data for the blood-group oligosaccharides (Lemieux, 1980; Thogerson, 1982), sucrose (Bock, 1982), and structures relating to the complex type *N*-linked glycans (Bock, 1982). These studies proposed that oligosaccharides have essentially fixed orientations about the glycosidic linkages, with the exception of 1-6 linkages for which a number of orientations were predicted. However, in extending this approach to structures larger than 4-5 residues, agreement is poorer, and it becomes apparent that a degree of conformational flexibility may be present.

HSEA calculations give good results for static minimum energy structures with restricted values for φ and ψ torsion angles, but to investigate dynamic models where the potential energy surface encompasses a wide range of φ and ψ angles, a full molecular mechanical force field is more appropriate. The AMBER parameterisation is a full force-field (Weiner, 1984; Weiner, 1986), originally designed for use with nucleic acids and proteins, and has been extended to include carbohydrates (Homans, 1990), based upon the work by Ha *et al.* (Ha, 1988).

HSEA calculations suggest deep potential wells supporting the concept of rigid conformations. However all bonds, angles, and torsion angles are allowed to vary during minimisation. Flexible geometry increases the area of conformational space accessible to a given glycosidic linkage (Homans, 1987; Ha, 1988; Scarsdale, 1988; French, 1989; Imberty, 1989; Yan, 1990), Resulting in a shallower topography which often exhibits minor minima that are not observed on rigid surfaces. Relaxed potential energy surfaces (French, 1989) in which φ_H and ψ_H are systematically varied in small steps (10^O or 15^O) and the geometry optimised for this value of the glycosidic angles may be presented as an iso-energy contour plot (Ramachandran plots) in which occupation is temperature dependent and governed by the Boltzmann law. Calculation of relaxed maps is preferable to the use of the rigid-residue approach, since bad contacts may be avoided by relatively small deviations of the internal co-ordinates (French, 1988; Ha, 1988). Clearly this becomes impractical for larger molecules, since the number of degrees of freedom rapidly increases the number of calculations and therefore the computational time. Additionally, the problem of false or multiple minima is accentuated since it cannot be ensured that at each φ/ψ point the molecule is at the global minimum energy.

An alternative approach for the determination of the accessible conformational space is the calculation of molecular dynamics simulations, and studies of the behaviour of model saccharides during molecular dynamics simulations has highlighted several important points. First, whilst structures may be restricted to low-energy regions of conformational space, they exhibit some degree of conformational flexibility, with a

number of conformations consistent with experimental data. Second, internal motions occur on the time-scale of picoseconds, substantially faster than the rate of overall tumbling for even moderately sized molecules.

An additional advantage of MD simulations is that NMR parameters, such as NOEs and spin-coupling constants, may be back calculated and compared with those measured experimentally. Significant improvement in the back-calculated data in comparison to the experimental data may be achieved by using experimentally derived restraints, r_{NOE} introduced into the force field as 'pseudo energy' functions (Holak, 1987). In conventional MD based NMR refinement (Nilges, 1988) these distances are applied on the model structures using a harmonic potential term of the form:

$$V_{NOE} = K_l(r_{model}(t)-r_l)^2 \qquad r_{model}(t) < r_l \qquad [1.14]$$

$$V_{NOE} = 0 \qquad r_u \geq r_{model}(t) \geq r_l \qquad [1.15]$$

$$V_{NOE} = K_u(r_{model}(t) - r_u)^2 \qquad r_u < r_{model}(t) \qquad [1.16]$$

where $r_{model}(t)$ is the instantaneous distance in the model molecule at time t. K_l and K_u are weak force constants (20KJmol^{-1}), and the NMR derived distance, r_{NOE}, typically lies in the middle of the range (r_l, r_u). The flat bottom region between r_l and r_u, where the penalty function is zero regardless of $r_{model}(t)$ accounts for the uncertainty of the NOE derived distances and because it is not possible to distinguish between a fixed inter-nuclear distance and a variable inter-nuclear distance caused by motional

averaging. In the MD simulation these distance restraints are included as a penalty function which along with the analytic function (the potential energy of the system) gives the total energy of the molecule as a function of conformation.

The distance restraints serve to restrict the motion of the MD simulation to areas of potential energy surface which are well parameterised (*i.e.* around the global energy minimum), and represent the minimum extent of torsional variation consistent with the experimental data. Unrestrained MD simulations in comparison represent the maximum torsional freedom consistent with the force field. This often takes the molecule into regions of potential energy surface divorced from the global energy region that are poorly parameterised.

The problem with this approach is that the energy of the system is derived from snapshots along the MD simulation that comprise of static structures. Obviously the distance, r_{NOE}, derived from an NMR experiment represents an ensemble of the distance over the time-scale of the cross-relaxation period during the experiment, and it is therefore more appropriate to use $\langle r_{model(t)}^{-6} \rangle^{-1/6}$ in the equation, where $\langle r_{model} \rangle$ is a time-averaged value. For practical reasons the time-averaged distance is taken over a memory time τ, so that an effective NMR distance might be given by:

$$r_{eff}(t)^{-6} = \frac{1}{t}\int_0^{\tau} e^{-\frac{t'}{\tau}} \left[r(t-t') \right]^{-6} dt' \qquad [1.17]$$

where r and r_{eff} are the distance and time-averaged distance respectively, and t is time. Since only the average (and not instantaneous) distances need to satisfy the restraints, the restrictions on the conformational space sampled are generally less severe than for "conventionally" restrained MD simulations. This becomes important as the number of NMR restraints increases which may provide sets of conflicting distance restraints which can only be modelled well by time-averaged restraints.

Determination of the minimum energy structure may be reached by means of restrained simulated annealing, where convergence upon a similar final conformation from a number of different starting geometries ensures that a larger proportion of conformational space has been sampled compared to minimisation by differentiation of the energy function.

1.7 Outline of Investigation

The main aim of this work was to develop new techniques for studying the three-dimensional conformation of oligosaccharides.

Chapters 2-5 detail the development of NMR techniques for gaining additional restraints, for use in molecular modelling simulations. These include the measurement of inter-glycosidic heteronuclear NOEs; the measurement of three-bond coupling constants to hydroxyl protons, to probe the existence of inter-glycosidic hydrogen bonding; the direct measurement of angles between bond vectors, using a method which makes use of cross-correlated dipolar couplings; and finally the use of a dilute liquid crystalline medium for the direct measurement of angles. Chapter 4 describes an investigation into the free solution state structure of lactose, incorporating the NMR restraints obtained from newly developed experiments

Chapter 6 details work carried out using TRNOEs to study the bound state of sLex with E-selectin. A three-dimensional nuclear Overhauser effect ^{13}C-^{1}H heteronuclear single quantum correlation experiment was employed in order to give additional dispersion.

Chapter 2

Heteronuclear Overhauser effects in Carbohydrates

Abstract

A fundamental problem in the charaterisation of the structure and dynamics of oligosaccharides is the lack of structural restraints across glycosidic linkages. In order to overcome this, new NMR techniques for gaining additional restraints must be developed. In this regard, the measurement of heteronuclear NOEs would be useful. A theoretical full-relaxation matrix analysis of heteronuclear Overhauser effects in oligosaccharides is described. This analysis predicts that trans-glycosidic heteronuclear $^{1}H\{^{13}C\}$ NOEs should be measurable in a model disaccharide with appropriate ^{13}C and ^{2}H enrichment. These predictions are confirmed experimentally, and the value of these measurements is discussed for conformational analysis.

2.1 Introduction

In order to define the conformation of a carbohydrate and to study its dynamics, it is necessary to define the conformation of the individual monosaccharide units that form the carbohydrate, and the way in which these units are linked together, that is the conformation about the glycosidic linkage. The linkage region is relatively flexible in comparison to the rigid monosaccharide units, and it is therefore necessary to have as much information about this region as possible. Unfortunately a fundamental problem in the characterisation of the structure and dynamics of oligosaccharides in solution by NMR is the lack of experimentally accessible structural restraints across glycosidic linkages (see Homans, 1994 and van Halbeek, 1994b for review). For a given glycosidic linkage, no more than three ^{1}H-^{1}H inter-glycosidic nuclear Overhauser effects (NOEs) are generally measurable, and therefore, any conformational study using these restraints alone will tend to be under restrained. Measurement of inter-glycosidic ^{1}H-^{13}C NOEs would lead to another valuable source of restraints, perhaps doubling the amount of distance information for each glycosidic linkage, and hence providing a potential improvement in structural determination.

The enhancement by the nuclear Overhauser effect of ^{13}C resonance intensities in small molecules is well known. In the case of directly attached ^{13}C-^{1}H pairs, the enhancement is substantial and can reach the theoretical maximum of ~200%, resulting in a three-fold increase in ^{13}C resonance intensity (Neuhaus, 1989). It has been demonstrated that heteronuclear Overhauser effects in small molecules can be measured for ^{1}H-^{13}C distances in the range 0.1-0.4nm, including the measurement of

^{1}H-^{13}C NOEs to quaternary carbons (Kover, 1986; Rinaldi, 1983; Kover, 1988; Neuhaus, 1989; Neuhaus, 1992; Stott, 1996).

2.2 Practical aspects of measuring inter-glycosidic Heteronuclear NOEs

Obtaining useful information from the measurement of inter-glycosidic heteronuclear NOEs is not simple; problems due to spin diffusion and spectral overlap are encountered. Full relaxation matrix simulations were used to study the effects of spin diffusion and perdeuteration. Theoretical simulations were also used to compare different experimental approaches to discover the most appropriate experimental scheme for measuring inter-glycosidic NOEs. The theoretical predictions were then confirmed experimentally, using a model system of appropriately labelled Galβ1-4Glc.

2.2.1 Indirect Spin Diffusion ('Three Spin effect')

The use of ^{1}H-^{13}C NOEs in conformational analysis has been restricted, largely because of the inherent problem that ^{13}C nuclei are relaxed efficiently by directly attached protons which reduces the sensitivity of any experiment involving ^{13}C magnetisation. A further problem is that there are two different pathways that lead to a NOE enhancement. The first pathway is due to the direct ^{1}H-^{13}C NOE that is the desired NOE and gives a positive enhancement. Unfortunately, because of the strong dipole-dipole interaction between the ^{13}C and its attached ^{1}H, there is also a secondary pathway via the relevant attached proton, to the ^{13}C spin in question. This

indirect NOE occurs because of spin diffusion and leads to a negative NOE enhancement. The effect is a phenomenon historically termed the 'three-spin effect' and was originally observed in homonuclear ^{1}H spin systems (Noggle and Schirmer, 1971).

This problem can be demonstrated by considering the effects on Galβ1-4[U-^{13}C-Glc] (figure 2.1). An NOE is observable from the H-1 of the Gal to C-3 of the Glc (solid arrow, figure 2.1), but in addition to this the indirect NOE, H-1 Gal → H-3 Glc → C-3 Glc is observed, indicated by the dashed arrows. Any observed effect is the combination of the direct NOE and the indirect 'three-spin' NOE.

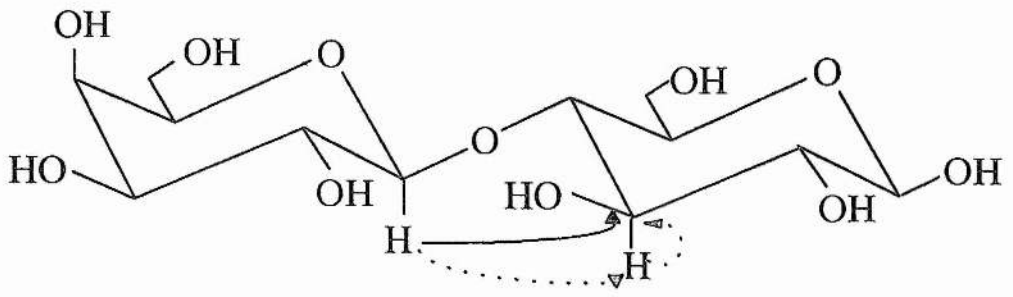

Figure 2.1: Galβ1-4Glc. The solid arrow is the direct NOE between Gal H1 and Glcβ C3; the dashed arrows indicate the indirect NOE or 'three-spin' NOE due to spin diffusion.

Since only a combination of these two NOEs is observable in Galβ1-4[U-^{13}C-Glc], it is interesting to consider whether the 'three spin' NOEs are sufficiently sensitive to torsional variation about the glycosidic linkage to be of value as conformational restraints.

2.2.2 Perdeuteration

Heteronuclear NOEs to carbons without directly attached protons for example quaternary carbons have been observed (Kover et al., 1986; Poppe, 1992). Therefore a possible mechanism whereby the conformational sensitivity of trans-glycosidic heteronuclear NOEs could be improved is by perdeuteration of the aglycon. The advantage of deuteration is twofold: First deuterons are less efficient than protons at relaxing the carbons they are attached to, with benefits for the maximum observable enhancement, and second, the homonuclear NOEs, and thus any three spin effects, are removed. In principle therefore, if Galβ1-4[U-^{2}H, ^{13}C Glc] could be prepared, direct heteronuclear NOEs could be measured from the galactose protons to the glucose carbons.

2.2.3 Saturation Experiment vs HOESY

For a heteronuclear two spin system, IS, the maximum NOE at the extreme narrowing limit is given by equation [2.1]:

$$\eta_{max} = \gamma_S / 2\gamma_I \qquad [2.1]$$

If ^{13}C (I) is observed whilst the ^{1}H (S) is saturated, the maximum NOE is 198.8%. If ^{1}H (I) is observed and ^{13}C (S) is saturated, the maximum NOE is 12.6%. In other words in a saturation type experiment, in order to achieve the maximum theoretical NOE enhancement, it is necessary to saturate ^{1}H and observe ^{13}C. This however means observing the low natural abundance nucleus. In the general case for larger molecules, selective saturation of proton resonances is inconvenient, especially in oligosaccharides where the majority of resonances experience severe overlap (Vliegenthart *et al.*, 1983). An alternative strategy is therefore to employ the two-dimensional heteronuclear Overhauser effect spectroscopy experiment (HOESY) (Rinaldi, 1983; Yu, 1984). This is a relatively simple experiment as can be seen from the pulse sequence in figure 2.2. Moving into two dimensions reduces the overlap problem, and although this experiment is potentially less sensitive than the saturation type experiment, it does have the compensation that proton detection can be utilised.

The pulse sequence shown in figure 2.2 is a relatively simple experiment and can be considered in terms of the vector model. A relatively long equlibration delay (8s) is required to allow relaxation of ^{13}C nuclei, this is followed by a 90° ^{13}C pulse which flips the ^{13}C spins into the *xy* plane. Their components precess during t_1 according to the resonance frequencies of the chemically distinct nuclei. Coupling between ^{13}C and ^{1}H spins, is removed by the 180° ^{1}H pulse at $t_1/2$ and by the end of the t_1 period, the ^{13}C spins are frequency labelled. The second ^{13}C pulse converts the transverse magnetisation into *z* magnetisation, and during the mixing period (mix) cross relaxation between the ^{1}H and ^{13}C spins occurs. The final 90° ^{1}H pulse creates

detectable transverse magnetisation that is modulated according to the amount of cross relaxation that occurred during the mixing period.

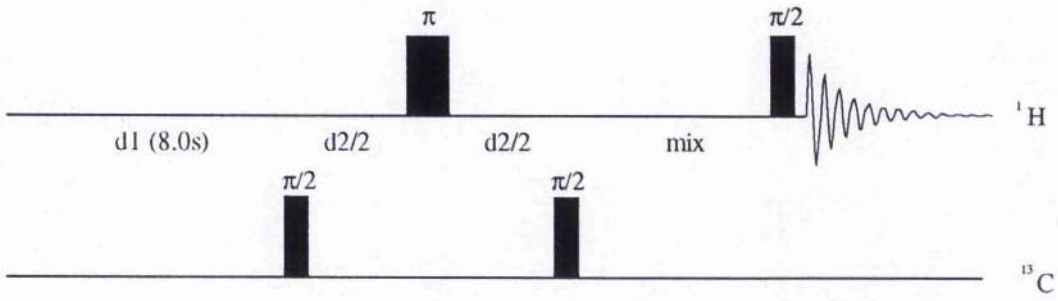

Figure 2.2: Heteronuclear nuclear Overhauser effect experiment (HOESY)

2.3 Full Relaxation Matrix Simulations of Heteronuclear Overhauser Effects

2.3.1 Experimental

In order to derive the most suitable experimental strategy, a series of simulations were carried out. The simulations compared the time dependence of steady-state NOE intensities with the time dependence of the transient experiment for Galβ1-4[^{13}C-Glc] and Galβ1-4[^{13}C, ^{2}H-Glc] and the conformational dependence of steady state and transient NOEs during rotation of the glycosidic torsion angle φ

Heteronuclear NOEs were simulated using the in-house written program MDNOE2, that is a package for the full-relaxation matrix analysis of NOESY, ROESY, steady-state NOEs and transferred NOEs for an arbitrary heteronuclear spin system. In these simulations the influence on ^{13}C spins of scalar relaxation of the second kind (Abragam, 1961; London 1990) derived from ^{2}H was not included, since its influence on the longitudinal relaxation of ^{13}C under the described conditions is negligible. Simulations were performed on the Galβ1-4Glc either in the global minimum energy configuration (φ,ψ + 60°, 0°) (Duda, 1990), or from a 500 ps *in vacuo* molecular dynamics simulation performed as described (Homans and Forster, 1992) without experimental NOE restraints.

2.3.2 Results and Discussion for the full Relaxation Matrix Simulations

Simulations were carried out in order to examine the effects of spin diffusion and deuteration, and also to compare the relative merits and disadvantages of the saturation and HOESY type experiments. Figure 2.3 A-F shows the results of these calculations. Panels A, B and C show results for Galβ1-4[U-^{13}C-Glc] and panels D, E and F are results for Galβ1-4[U-^{13}C, ^{2}H-Glc]. Panel A shows some theoretical NOE intensities with the saturation experiment for the protonated sample. These NOEs are negative as they are a combination of the direct NOE ($^{1}H\rightarrow^{13}C$) which is positive and the 'three-spin' NOE ($^{1}H\rightarrow^{1}H\rightarrow^{13}C$) which is negative. Panel B also shows negative NOEs for the HOESY simulation. In some cases the positive 'direct' NOE and the negative 'three-spin' NOE can almost cancel. However the question remains, for those NOEs that are observable, whether they are of value as conformational

restraints. As a simple test of this, both $^{13}C\{^1H\}$ and $^1H\{^1H\}$ NOEs were simulated for various geometries during complete rotation about the φ torsion angle of the disaccharide. Ignoring, for illustrative purposes the fact that certain orientations about φ are energetically unfavourable, it is seen in panel C that only the NOE between Gal H-1 and Glc C-4 displays substantial variation. However, this is principally as a result of the fact that the NOE between Gal H-1 and Glc H-4 is sensitive to conformation. By virtue of the fact that the Glc H-4 -Glc C-4 bond distance is invariant to conformation to first order, the 'three-spin' NOE between Gal H-1 and Glc C-4 shows an essentially identical dependence to the homonuclear NOE. It can therefore be concluded that trans-glycosidic 'three-spin' $^{13}C\{^1H\}$ NOEs are not useful parameters for conformational analysis in this disaccharide.

In contrast for the Galβ1-4[U-^{13}C, ^2H-Glc] sugar, both steady state (panel D) and HOESY (panel E) intensities are positive. This is as a result of the attenuation of the trans-glycosidic pathway for indirect enhancement. Unlike the 'three-spin' trans-glycosidic NOEs, the direct NOEs are much more sensitive to torsional variations across the glycosidic linkage (F) and at least three such NOEs are predicted to be measurable.

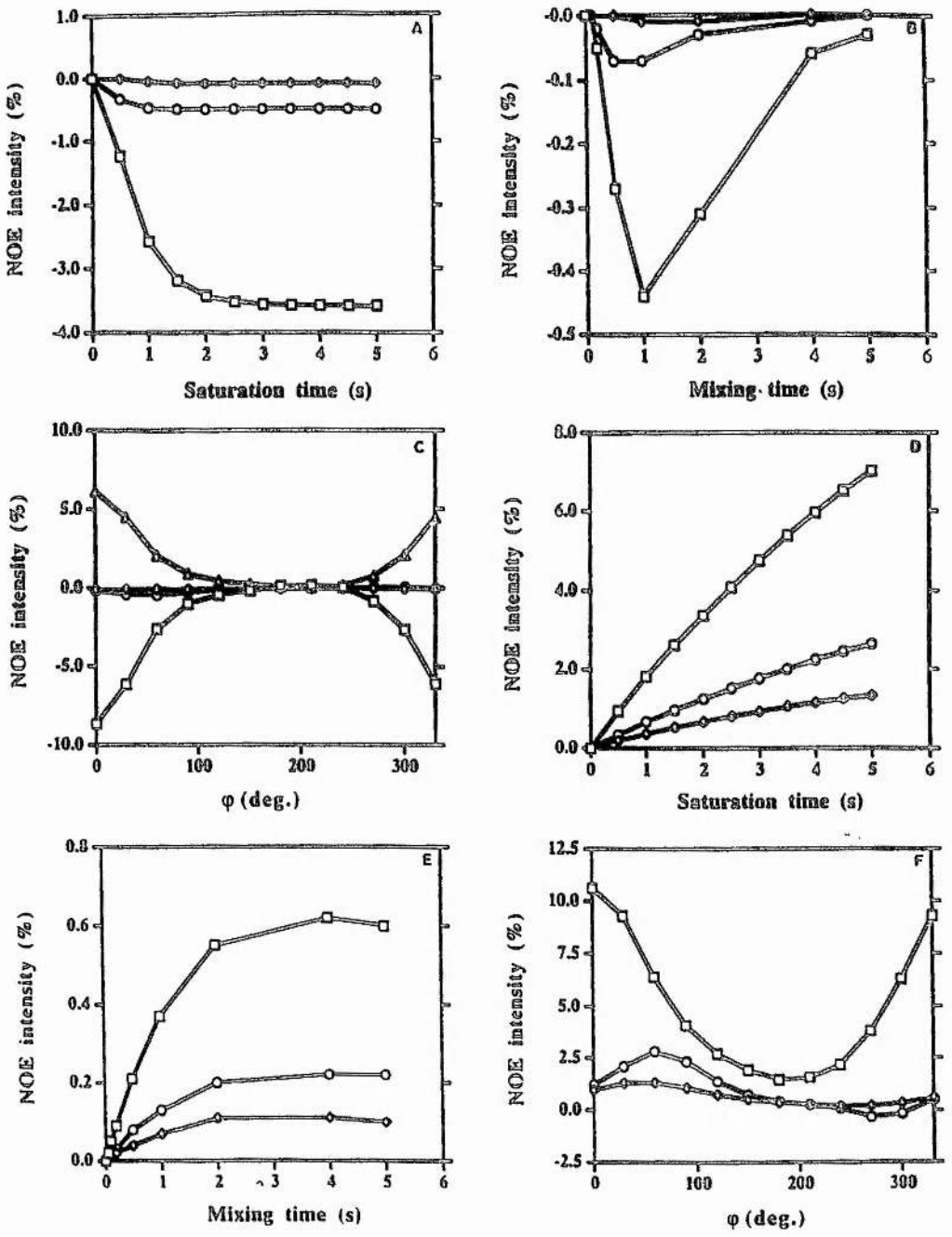

Figure 2.3 – Full-relaxation matrix simulation of trans-glycosidic heteronuclear NOEs in Galβ1-4[U-^{13}C-Glc] (panels A-C) and Galβ1-4[U-^{13}C, ^{2}H-Glc] (panels D-F).

Key to figure 2.3:

A and D - time dependence of the steady-state NOE intensities experienced by Glc C4 (square), C5 (diamond) and C6 (circle) on saturation of Gal H1.

B and E - time dependence of the transient (HOESY) cross-peak glucose resonance intensities on saturation of Gal H1.

C and F – Conformational dependence of steady-state NOE glucose resonance intensities on saturation of Gal H1 during rotation of the glycosidic torsion angle φ, including to Glc H4 (triangle).

2.3.3 Choice of Experimental Scheme

It is seen by comparison of panel A with B (or D with E) that HOESY intensities are substantially smaller than steady-state enhancements, in complete analogy with homonuclear ^{1}H systems (Neuhaus and Williamson, 1989), and reach maxima at times substantially shorter than steady-state measurements. Comparison of the NOE buildup rates in D and E shows that the steady-state NOEs reach a value more than tenfold greater than the transient NOE, suggesting that the former would be the experiment of choice on grounds of sensitivity. However, there are additional factors that need to be considered for practical applications. First, application of steady-state NOE measurements requires the application of a selective, saturating radio-frequency field on protons. In the case of oligosaccharides, the resonance overlap in the proton NMR spectrum is generally so severe that steady-state measurements are of limited applicability. Also, steady-state $^{13}C\{^{1}H\}$ NOE measurements by definition involve detection of ^{13}C, whereas in contrast, transient HOESY experiments can be

performed with detection of either nucleus. The symmetry of the relaxation matrix in homonuclear systems also holds for heteronuclear systems, hence the transient simulations in Figure 2.3 are relevant to either detection of ^{13}C or ^{1}H. Since it can be demonstrated that ^{1}H detection offers approximately eightfold enhancement of signal-to-noise in comparison with ^{13}C detection (Stott and Keeler, 1996), the sensitivity disadvantages for measurement of transient NOEs become less severe with proton detection. It is also necessary to consider the sensitivity advantage per unit time of each approach. In the case of steady-state experiments, the repetition rate is determined not only by the build-up rates of the NOE enhancements (Figure 2.3D), but also by the need for the ^{13}C atoms to recover their equilibrium magnetisation between experiments. In the transient $^{1}H\{^{13}C\}$ experiment, the repetition rate is again determined by the need for ^{13}C atoms to recover to their equilibrium magnetisation since the initial polarisation derives from them. However the mixing time can be relatively short since the maximum enhancement is obtained in a relatively short time (Figure 2.3E).

2.3.4 Conclusions based on Simulations

Inter-glycosidic NOEs resulting from spin diffusion effects are not useful parameters for conformational analysis of Galβ1-4Glc, however the deuteration of the glucose moiety overcomes this problem by attenuating the 'three-spin' effect.

Transient experiments with ^{1}H detection offer comparable sensitivity per unit time with steady-state experiments with ^{13}C detection, and indeed should offer greater

sensitivity with conventional 'inverse' probes which are not optimised for ^{13}C detection, since these offer ~50% of the sensitivity offered by their ^{13}C-optimised counterparts.

2.4 Measurment of Heteronuclear NOEs in Galβ1-4[U-^{13}C, ^{2}H Glc] by NMR

2.4.1 Experimental

In order to assess the validity of the transient NOE simulations in Figure 2.3, the HOESY type pulse sequence (figure 2.2) was applied to a sample of Galβ1-4[U-^{13}C, ^{2}H-Glc].

2.4.2 Preparation of Galβ1-4[U-^{13}C, ^{2}H]Glc

Chemoenzymatic synthesis was performed in a 2.5ml solution containing 10mM UDP-galactose and 1-mM U-^{13}C, ^{2}H glucose in 50mM phosphate buffer (pH 7.4). One unit of galactosyltransferase was added with 1mM lactalbumin and $MnCl_2$ to a concentration of 5mM, and the mixture was incubated at 37°C overnight. The disaccharide product was purified by Biogel P-2 column (2.5 cm × 100 cm) chromatography, with H_2O as eluant.

2.4.3 NMR measurements

Two-dimensional heteronuclear $^{1}H\{^{13}C\}$ nuclear Overhauser effect (HOESY) spectra were acquired at a proton frequency of 500.13 MHz and a probe temperature of 303 K on a Varian Unity^{+} spectrometer equipped with a self shielded z gradient triple resonance probe. The original sequence of Rinaldi (1983) was used, except that the

^{1}H and ^{13}C channels were reversed (figure 2.2). Broadband decoupling was not utilised during the aquisition period. Deuterium decoupling was not utilised since the effective resolution in the F_1 (^{13}C) dimension is very low, and the contribution of scalar relaxation of the second kind (Abragam, 1961; London, 1990) to the ^{13}C linewidth is very small for molecules with small rotational correlation times. Data were acquired with spectral widths of 6000 Hz and 1000 Hz in the F1 (^{13}C) and F2 (^{1}H) dimensions respectively, with 128 increments in the t_1 dimension and 64 transients per increment. A relaxation delay of 8 s was utilised between acquisitions with a mixing time (τ_m) of 1 s. The total acquisition time was 45 h. Prior to two-dimensional Fourier transformation, data were apodised in the t_2 dimension by an exponential function corresponding to a line-broadening of 3 Hz, and in the t_1 dimension by a cosine-bell window function followed by zero-filling once in the t_1 dimension.

2.5 Results and discussion

Figure 2.4 is a section from the $^{1}H\{^{13}C\}$ HOESY spectrum of Galβ1-4[U-^{13}C, ^{2}H]Glc illustrating connectivities from Glc C-4, C-5/C-3 and C-6 to Gal H-1. The NOE from Glc C-6 is particularly useful as a conformational restraint since, as an exocyclic atom, the distance from Glc C-6 to Gal-H1 is very sensitive to torsional fluctuations about the glycosidic linkage. In conventional homonuclear NOE measurements, NOEs are observed from Gal H-1 - Glc H-6 (H-6'), and to Glc OH-6 in studies in H_2O at low temperature (Chapter 4). However their use as conformational restraints is limited by the fact that they are dependent upon the

orientation of the hydroxymethyl group of the aglycon. In contrast, the heteronuclear NOE is, to first order, independent of the orientation of pendant groups.

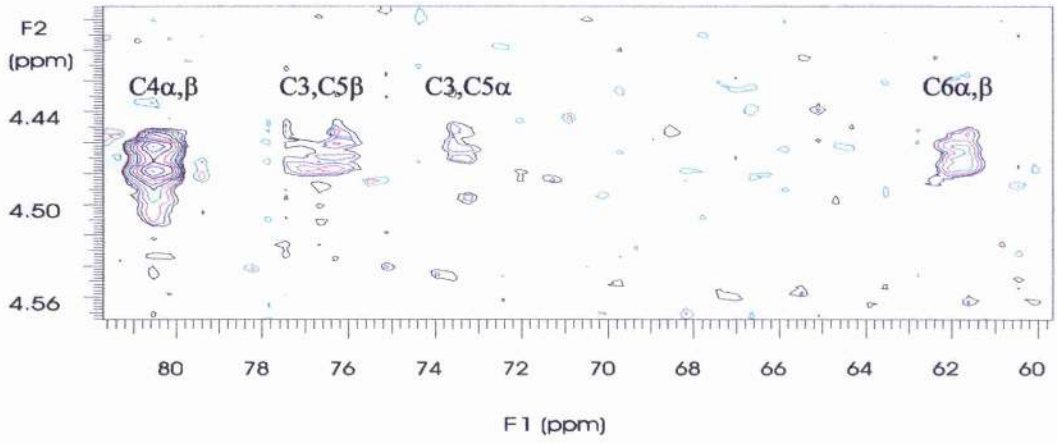

Figure 2.4. Section from $^{1}H^{13}C$ HOESY spectrum of Galβ1-4[U-^{13}C, ^{2}H-Glc], illustrating trans-glycosidic NOEs to GalH-1.

2.5.1 Quantitation of heteronuclear NOEs

Determination of the absolute magnitudes of heteronuclear NOEs in Galβ1-4[U-^{13}C, ^{2}H]Glc is not trivial since there is no intra-residue ^{13}C-^{1}H vector in a given molecule that can be used as a reference distance. One approach to the problem is to utilise the fact that ^{2}H isotopic enrichment of the commercially available U-^{13}C, ^{2}H glucose utilised in this study is not 100%. Although the percentage of protons in the aglycon of Galβ1-4[U-^{13}C, ^{2}HGlc)] is low (~3%), this is nevertheless sufficient to generate

cross peaks in the 2D HOESY spectrum arising from one-bond ^{13}C-^{1}H heteronuclear NOEs in protonated isotopomers. Since the magnitudes of these NOEs are independent of the conformation about the glycosidic linkage to first order, theoretical simulations of their magnitudes can be used to calibrate the observed heteronuclear trans-glycosidic NOEs. For this purpose, it is necessary in principle to correct the measured intensities for the longer T_1 relaxation times of the ^{13}C spins that are directly bonded to ^{2}H compared with ^{1}H, which result in differential recovery of z magnetisation during the relaxation delay. However, the T_1 values of the ^{13}C spins directly bonded to ^{2}H in the disaccharide, measured by conventional inversion-recovery experiments, are all less than 3.2 s. As a result, the z magnetisations of deuterated carbons under the experimental conditions employed here have relaxed to >95% of their equilibrium values between successive transients, and no correction is required within experimental error. The resulting ^{1}H ^{13}C intensities are shown in table 2.1. These are all of lower intensity than predicted from the relevant simulation (Figure2.3E and table 2.1). However, these simulations were computed with the geometry about the glycosidic linkage fixed in a single orientation corresponding to the global minimum energy conformation of the glycan ($\varphi,\psi \sim +60^{\circ}, 0^{\circ}$). Simulations obtained from a 500ps *in vacuo* free dynamics simulation of the glycan (Table 2.1), which is more representative of the dynamic behaviour of oligosaccharides in solution (Rutherford et al., 1993) are in better agreement with experimental values (Table 2.1).

Table 2.1 - Experimental and theoretical inter-glycosidic Heteronuclear NOEs for Galβ1-4Glc

Conectivity	$^1H\{^{13}C\}$ NOE (%)[a]		
	Experimental	Theoretical (global)	Theoretical (dynamic)
Glcα H-1 - Glcα C-1 [b]	0.21	-	-
Gal H-1 - Glc C-4	0.28	0.37	0.26
Gal H-1 - Glc C-5[c]	0.06	0.07	0.04
Gal H-1 - Glc C-3[c]		0.03	0.04
Gal H-1 - Glc C-6	0.05	0.13	0.05

[a] Trans-glycosidic NOEs were quantified indirectly with respect to the $^1H^{13}C$ NOE between Glcα H-1 and Glcα C-1, and represent the sum of the NOE intensities in each anomer of the disaccharide.

[b] The reported value is the theoretical intensity of the $^1H^{13}C$ NOE between Glcα H-1 and Glcα C-1 (10.87%) using a rotational correlation time of the molecule of 0.15ns, followed by correction for the percentage of isotopomers bearing Glcα H-1 (3.9%) and the anomeric ratio in the disaccharide.

[c] Resonance overlap of C-3 and C-5 for both anomers prevents independent experimental measurement of these NOEs.

2.6 Conclusions

It has been demonstrated that trans-glycosidic heteronuclear NOEs can be observed in oligosaccharides appropriately enriched with ^{13}C and ^{2}H. Heteronuclear full-relaxation matrix calculations of steady state $^{13}C\{^{1}H\}$ and transient $^{1}H\{^{13}C\}$ NOEs indicate that while the latter have smaller maximum intensities, proton detection results in a similar absolute sensitivity. Although the observed trans-glycosidic NOEs are of low intensity (<1%), they can readily be detected with conventional 2D HOESY experiments. Three trans-glycosidic heteronuclear NOEs were experimentally detectable in Galβ1-4[U-^{13}C, ^{2}H]Glc.

Chapter 3

Direct Measurement of Angles in a dilute liquid crystalline medium

Abstract

Molecular alignment was conferred on a series of oligosaccharides by dissolving them in a dilute liquid crystalline medium. Due to the resulting anisotropic alignment tensor, it was possible to measure residual dipole-dipole coupling constants using a $^{1}J_{CH}$ modulated HSQC and hence long-range angular information was obtained. These restraints were incorporated into dynamical simulated annealing calculations for several oligosaccharides in order to verify their usefulness in structural calculations.

3.1 Introduction

3.1.1 Traditional NMR Restraints

There are three principle sources of geometric information used in NMR: NOEs, three bond scalar couplings, and chemical shifts (Wüthrich, 1986; Case, D. E., 1994; Gronenborn, A. M., 1995; Cavanagh, J., 1996). Although many successful conformational studies have been carried out using only these restraints, there are inherent problems with them all. NOEs, on which many studies heavily rely, are only semi-quantitative and can only be measured for distances of ~5Å or less. Three bond scalar (J) couplings are highly accurate reporters on the intervening dihedral angle (Wang, 1996), but measurement is often difficult particularly in larger systems where the natural resonance line width exceeds that of the small J couplings. In addition, translating the J coupling information into geometric information depends on calibration of empirical Karplus relationships. Chemical shifts are easily measured with high accuracy and are extremely sensitive to local geometry (Osapay, 1996). Unfortunately, knowledge of the various factors determining chemical shifts, in particular those of ^{13}C and ^{15}N, remains incomplete and therefore they can only be interpreted in a qualitative way.

The success of structure determination by NMR, has been largely due to the presence of 'long-range' NOEs corresponding to short inter-proton distances between residues far apart in the primary sequence: Such restraints are highly restrictive of conformation. However there are generally not enough 'long-range' NOEs and there

is therefore clearly a weakness in NMR for determining structures of molecules which lack these long-range constraints.

3.1.2 Summary

In view of the limited amount of long range NMR information for use in structural calculations, the need for a generally applicable method for gaining such long-range information is clear. The relationship between dipole-dipole couplings and angular information has long been understood (Gayathri, 1982; Bothner-By, 1985; Bothner-By, 1995). Although this relationship has been utilised in solid state NMR, until recently the measurement of dipolar couplings has not generally been possible in solution-state NMR because of motional averaging.

A method for measuring these dipolar couplings has recently been developed by Tjandra and Bax (Tjandra and Bax, 1997). In a dilute, diamagnetic liquid crystalline medium that aligns with the magnetic field, the alignment of the liquid crystal medium is partially conferred to the solute molecule. As a result the solute molecule no longer tumbles completely isotropically. This allows dipolar coupling constants to be measured with high accuracy. The measurement of dipolar coupling constants using a dilute liquid crystalline medium has been demonstrated recently for biological macromolecules (Tjandra and Bax, 1997). This chapter shows that the dilute liquid crystal approach is not restricted to biological macromolecules alone, but is readily applicable to the smaller carbohydrates.

3.2 Direct Measurement of Distances and Angles in Oligosaccharides by NMR in Dilute Liquid Crystalline Medium

3.2.1 Origin of Dipole-Dipole Interactions

If a molecule is placed in a magnetic field, a magnetic moment is induced that is proportional to the field strength and the magnetic susceptibility. As most molecules are not spherically symmetric, magnetic susceptibility is a tensor, rather than a scalar, giving different moments for different orientations. The induced magnetic moment will in turn interact with the field, and molecules with an anisotropic magnetic susceptibility tensor will have an energetically preferred alignment with respect to the magnetic field (Lohman, 1978; Bastiaan, 1987). If departures from isotropic alignment are sufficiently large, measurement of the dipolar contribution is possible. The dipolar interaction between two spin 1/2 nuclei in the high field limit can be represented by (Tolman, 1995):

$$H_D = -[\gamma_i\gamma_j h / (2\pi^2 r^3)] \langle(3\cos^2\theta-1)/2\rangle I_{zi}I_{zj} \qquad [3.1]$$

where $\gamma_{i/j}$ refer to the magnetogyric ratios of the two nuclei, h is Planks constant, r is the distance between nuclei, θ is the angle between the inter-nuclear vector and the applied magnetic field and $I_{zi/j}$ are the spin operators for the two nuclei.

3.2.2 Reasons for measuring dipole-dipole interactions

From equation [3.1], the dipolar interaction is dependent on both the bond vector angle relative to the alignment tensor, and the distance between the two nuclei in question. It is therefore a potentially useful property, as the dipolar couplings provide direct information on the orientations of the corresponding bond vectors relative to the molecule's magnetic susceptibility. The major advantage of such restraints is that all orientations are calculated relative to the same axis system. As a result, the orientation of a bond vector at one end of a molecule can be correlated with the orientation of a bond vector at the other end of the molecule, effectively providing long range restraints. These restraints are therefore fundamentally different from the strictly local NOE and J coupling restraints.

If a molecule is tumbling with a degree of anisotropy, then a splitting to the quadrupolar resonance of ^{2}H will be observed, due to incomplete averaging of the quadrupole coupling. In such a case a dipolar coupling will manifest itself as a splitting of a NMR resonance. In the case where a nuclear pair are directly bonded (e.g. ^{13}C-^{1}H), the dipolar interaction will add to the scalar coupling and because the sign and magnitude of $^{1}J_{CH}$ is well known, both the sign and the magnitude of the dipolar coupling can be easily obtained. Although the measurement of dipolar couplings potentially leads to valuable conformational information, until recently such restraints have not been fully exploited in solution NMR. This is because dipolar effects are not normally observed in high resolution spectra due to motional averaging. In the liquid state the magnetic field induced alignment is in competition

with Brownian motion. All motions occurring on time scales short compared to the reciprocal of the dipolar interaction in Hz ($<10^{-3}$s for ^{1}H-^{15}N) contribute to the averaging, including molecular tumbling in solution. For diamagnetic molecules at moderate field strengths, there is little preference in orientation: In terms of equation 3.1, $\langle(3\cos^2\theta-1)/2\rangle$ tends to zero. With a large applied magnetic field and an anisotropic magnetic susceptibility tensor it is sometimes possible to measure residual dipolar couplings. Bothner-By and co-workers demonstrated that in solution the dipolar couplings in molecules with an anisotropic susceptibility tensor no longer average to exactly zero but exhibit a residual splitting, which scales with the square of the magnetic field (Gayathri, 1982; Bothner-By, 1985; Bothner-By, 1995). More recently, Prestegard and co-workers demonstrated that such residual dipolar couplings, on the order of a few Hz, can also be observed in paramagnetic cyanometmyoglobin (Tolman, 1995), and Bax and co-workers measured residual dipolar splittings in human ubiquitin (Tjandra, 1996).

Although dipolar couplings could be extremely useful parameters in structural calculations, unfortunately, only in favourable systems and with considerable effort, can these dipolar couplings be measured with sufficient accuracy from their magnetic susceptibilities. What is required therefore, is a simple and general method for inducing alignment of bio-molecules with the magnetic field. Various ways for increasing the degree of molecular alignment have been suggested previously, including the use of strong electric fields and polarised light (Tjandra, 1997). Tjandra and Bax recently demonstrated a technically much simpler method for achieving an

adjustable degree of solute alignment (Tjandra, 1997). A degree of alignment is transferred to a non-spherically symmetric molecule dissolved in a solvent containing particles that are oriented relative to the magnetic field. The use of an aqueous, dilute, liquid crystalline (LC) phase for the alignment of proteins, allowed the measurement of ^{1}H-^{15}N dipolar couplings (Tjandra, 1997). Here we demonstrate the general applicability of this method by demonstrating its use for the measurement of ^{1}H-^{13}C dipolar couplings in a series of carbohydrates.

3.2.3 Bicellar Systems

Liquid crystalline media were first used some time ago for orienting solutes in order to aid structural studies (Saupe, 1963; Emsley, 1975; Diehl, 1985). The problem has generally been that the degree of solute orientation typically obtained in LC solvents is so large that the NMR spectra of even small molecules become too complex to interpret. Recently, a number of compounds which form LC arrays at low concentrations in water have been identified (Boden, 1987; Sanders, 1992; Harrison, 1996). Mixtures of dihexanoyl phosphatidylcholine (DHPC) and dimyristoyl phosphatidylcholine (DMPC) that form discotic phospholipid micelles, have been shown to be maintainable at low concentrations (3% w/v), and offer a high degree of magnetic alignment (Bax, 1997).

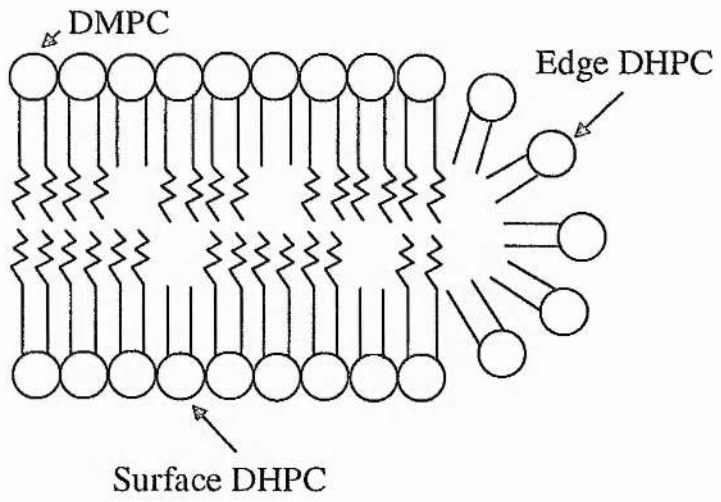

Figure 3.1 - 2D cross section of the edge of a discoid (bicelle)

At a DHPC:DMPC ratio of 1:2.9, below the liquid crystalline phase transition temperature (T_m) the lipid mixture is in an isotropic liquid phase (Sanders, 1995). On heating the lipids up to above T_m, they form a liquid crystal phase, or more specifically disc shaped particles, often referred to as bicelles, with diameters of several hundred angstroms and a thickness of ~4nm (Sanders, 1992; Harrison, 1996; Vold, 1996). Figure 3.1 shows a highly idealised model for a 2D cross section of the edge of a discoid. The lipids are diamagnetic, and as a result, the bicelles orient with their normal orthogonal to the magnetic field. NMR spectra of DHPC/DMPC mixtures were shown to be consistent with the notion of disc-shaped phospholipid aggregates in which DMPC forms a bi-layered section surrounded by a rim of DHPC, which excludes the myristic acid chains from contact with water (Sanders, 1992). The DHPC/DMPC molar ratio is believed to determine the size of the discs (Vold, 1996).

A 1:2.9 molar ratio then corresponds to discs with a thickness of ~4nm, and a diameter of ~40nm.

At the bicelle concentrations used, the average spacing between bicelles exceeds 40nm. As this spacing is much larger than the size of any of the carbohydrates used, the rotational diffusion of the carbohydrates in such a medium is expected to be little affected by the bicelles. This is an observation derived from relaxation measurements carried out by Bax and Tjandra (Bax, 1997) who showed that for ubiquitin the T_1 relaxation rates of ^{15}N were not affected by the presence of bicelles.

3.2.4 Measurement of Dipolar Contributions to $^1J_{CH}$ Splittings

By using a standard HSQC method without proton decoupling it is a simple task to measure a $^1J_{CH}$ carbon-proton splitting. In order to obtain the dipolar contribution to $^1J_{CH}$ in the presence of lipid bicelles it is necessary to run one such experiment at 35°C (*i.e.* above T_m) and another at 22°C (*i.e.* below T_m). The splittings at 35°C include both scalar and dipolar contributions, whereas those in the unaligned state (22°C) contain only scalar contributions. The dipolar coupling is thus given by equation 3.2:

$$D_{CH} = J_{35} - J_{22} \qquad [3.2]$$

where J_{35} and J_{22} are the splittings at 35°C and 22°C respectively. Although this is a simple and convenient way to assess the magnitude of dipolar couplings present at a

particular lipid concentration, the dipolar contribution to the overall coupling observed may be relatively small, and therefore difficult to measure accurately by these means. A further problem is one of increased spectral overlap because of the coupled protons. Therefore although this method is useful for preliminary studies, it is desirable to use a different method for their determination.

3.2.5 $^1J_{CH}$-modulated 2D HSQC

Tjandra and Bax presented a method for accurate measurement of the field dependence of $^1J_{CH}$ in proteins uniformly enriched with ^{13}C (Tjandra and Bax, 1997). They were able to refine their method to an accuracy of about 0.3 Hz. The advantage of using such a method, as well as an increased accuracy, is that ^1H-^{13}C decoupling can be utilised, reducing the problem of spectral overlap. This scheme was therefore adopted as the most suitable method for the accurate measurement of dipolar contributions in oligosaccharides. Figure 3.2 shows the pulse sequence used, which is essentially a variation on the CT-HSQC experiment (Santoro, 1992). By altering the time point at which the ^1H 180^o pulse is applied during the constant-time evolution period, the intensity in the correlation spectrum becomes a simple function of $^1J_{CH}$ and permits this coupling to be calculated from the observed intensities (Santoro, 1992; Vuister, 1993).

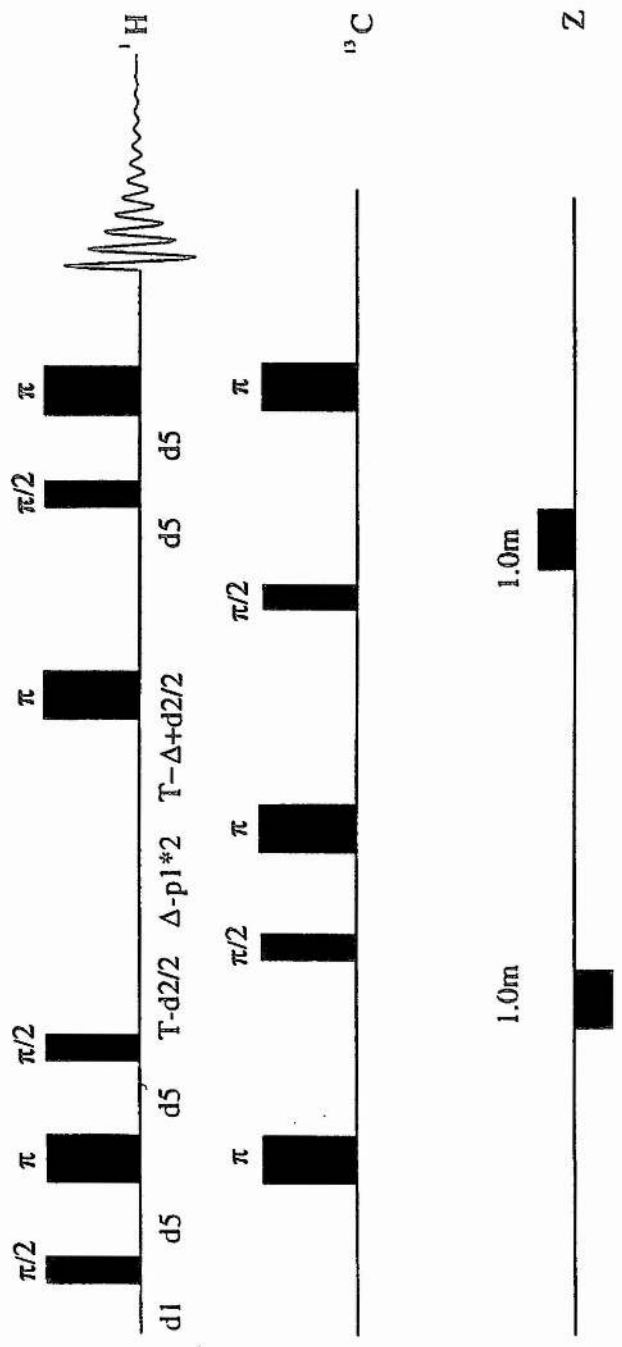

Figure 3.2 - $^1J_{CH}$-modulated 2D HSQC

Figure 3.2 is essentially a regular HSQC with an additional $^1J_{CH}$ evolution period. Although the measurement can be performed as a regular 3D experiment by systematically incrementing the de-phasing delay, 2(T-Δ), we took the approach of recording a limited set of 2D spectra, centred around durations of 2(T-Δ), which maximised the dependence of resonance intensity on $^1J_{CH}$. To a first approximation, the intensity of a 2D ^1H-^{13}C correlation in a spectrum recorded with the scheme of figure 3.2 is given by equation 3.3:

$$I(2(T-\Delta)) \quad = \quad C\cos(2\pi J_{CH}(T-\Delta)\exp(-2\Delta/T_2^*) \qquad [3.3]$$

where T_2^* is the inverse of the decay rate of the ^{13}C magnetisation as a result of transverse relaxation and unresolved long-range ^1H-^{13}C couplings.

The intensity of a ^{13}C-^1H correlation in the 2D CT-HSQC spectrum is thus proportional to $\cos[2\pi^1J_{CH}(T-\Delta)]$. $^1J_{CH}$ is then determined by optimising the fit between $\cos[2\pi^1J_{CH}(T-\Delta)]$ C and the intensities observed for different Δ durations. In order to obtain accurate results a range of Δ values were selected which allowed the 'turn over' of the curve (*i.e.* such that the factor $\sin[2\pi\ ^1J_{CH}(T-\Delta)]$ changes sign).

3.2.6 Direct Structure refinement against Residual Dipolar Couplings

Having measured the dipolar coupling constants, we wished to incorporate them in dynamical simulated annealing calculations in order to derive a solution conformation. As we were using dilute aqueous liquid crystalline medium of oriented bicelles to produce alignment of oligosaccharides, axial symmetry of the solute could not be assumed *a priori*. Since any assumption of axial symmetry in the presence of significant rhombicity would clearly affect the accuracy of the resulting coordinates, it was important to determine the degree of rhombicity from the experimental residual dipolar coupling data, without reference to a previously known structure.

The geometric content of the residual dipolar couplings was incorporated into the simulated annealing protocol (Homans, 1992) used for structure determination by minimising the term $E_{dipolar}$ (Tjandra, Omichinski, 1997):

$$E_{dipolar} = k_{dipolar}(\delta_{calc} - \delta_{obs})^2 \qquad [3.4]$$

where $k_{dipolar}$ is a force constant, and δ_{calc} and δ_{obs} are the observed and calculated values of the residual dipolar couplings, respectively. The expression for the residual dipolar coupling $\delta(\theta,\phi)$ between two directly coupled nuclei can be simplified to the form (Gayathri, 1982; Bothner-By, 1995):

$$\delta(\theta,\phi) = K\{D_a(3\cos^2\theta - 1) + 3/2\, D_r(\sin^2\theta \cos 2\phi)\} \qquad [3.5]$$

where D_a and D_r are the axial and rhombic components of the tensor given by $1/3[D_{zz}-(D_{xx}+D_{yy})/2]$ and $1/3(D_{xx}-D_{yy})$ respectively; θ is the angle between the inter-atomic vector and the z axis of the tensor; and ϕ is the angle which describes the position of the projection of the inter-atomic vector on the x-y plane, relative to the x axis. In this case the tensor D is the molecular alignment tensor for molecules aligned in anisotropic liquid crystals. K is given by equation 3.6.

$$K = S\mu_o / 4\pi \quad \gamma_P\gamma_Q h / 4\pi^2 r_{PQ}^3 \qquad [3.6]$$

S is the generalised order parameter for internal motion of the vector PQ, μ_o is the magnetic permeability of a vacuum, γ_P and γ_Q are the magnetogyric ratios of P and Q respectively, h is Planck's constant, and r_{PQ} is the distance between P and Q.

$E_{dipolar}$ was evaluated by calculating the θ and ϕ angles between the C-H bond vectors and an external arbitrary axis system. As the orientation of the axis system was not known *a priori* it was allowed to float during the simulated annealing calculations. The external axis was represented by an artificial tetra-atomic molecule comprising four atoms, X, Y, Z and 0, with three mutually perpendicular bonds, X-0, Y-0, and Z-0), representing the x, y, and z axes of the tensor, respectively. The value for $k_{dipolar}$ was chosen such that the agreement between observed and calculated values of the residual dipolar couplings was approximately equal to the experimental error.

3.2.7 Derivation of components of the alignment tensor

In order to make use of equations [3.4] and [3.5] for structure refinement, the values of D_a and the rhombicity R (defined as D_r/D_a) must be determined directly from the experimental data. The minimum value of the residual dipolar coupling, δ_{min}, occurs at $\theta = \phi = 90^\circ$, such that D_a is given by:

$$D_a = -\delta_{min} / (1 + 1.5R) \qquad [3.7]$$

As a first approximation the most negative (smallest) residual dipolar coupling, as the minimum value, was taken to be aligned perpendicular to the principal axis of the alignment tensor, giving rise to a starting value for the axial component of the alignment tensor. The maximum value of the residual dipolar coupling, δ_{max}, which occurs at $\theta = 0^\circ$, is given by $2D_a$. Unfortunately, a reliable estimate of δ_{max} is more difficult to obtain from the experimental data. This is because the probability of finding a bond vector that makes an angle θ to the z axis of the tensor is proportional to sin θ, and hence the probability of finding a bond vector with $\theta \sim 0^\circ$ is very low (Tjandra, Omichinski, 1997). Since δ_{min} can be accurately determined experimentally, but D_R cannot be obtained independently of R (unless an accurate value of δ_{max} is known), the strategy that was used involved calculating a series of structure ensembles for different estimates of R. Using the calculated value for the axial component of the alignment tensor, the rhombic component of the alignment tensor was determined from a series of trial dynamical simulated annealing calculations incorporating dipolar restraints. Since the relative geometries of the endocyclic bond

vectors of any residue are to first order independent of the overall conformation of the molecule. The rhombic component of the alignment tensor was thus obtained by simple optimisation of this parameter with respect to the best fit between experimental and theoretical residual dipolar couplings.

3.3 Materials and methods

In order to demonstrate the suitability of this method for the measurement of dipolar couplings and moreover, to demonstrate the applicability of these parameters in structural calculations, NMR and modelling studies were carried out on a series of oligosaccharides (figure 3.3). Each oligosaccharide was uniformly ^{13}C labelled in order that dipolar interactions involving the carbons could be measured.

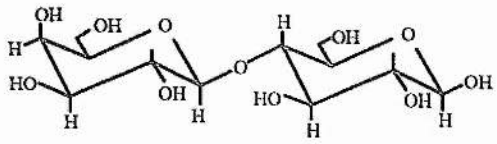

Lactose

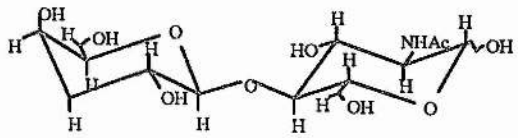

LacNAc

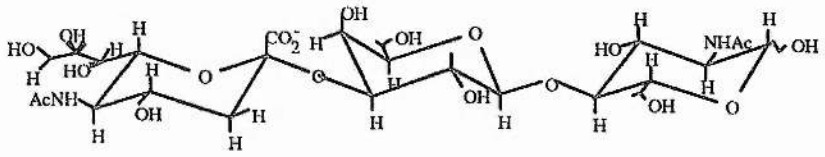

SialylLac Nac

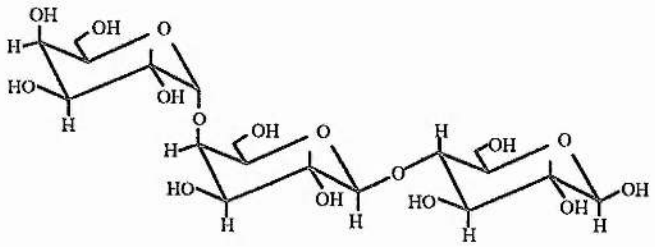

Gb3

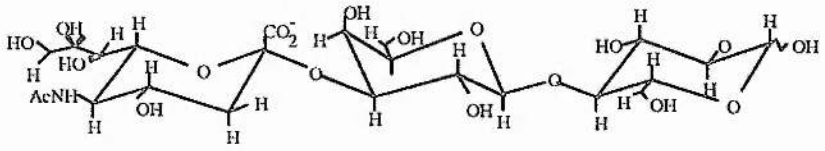

Gm3

Figure 3.3 - Oligosaccharides used for dipole-dipole experiments

3.3.1 Sample preparation

NMR samples were prepared by dissolution of 2mg of ^{13}C-enriched (97%) oligosaccharide in a solution of dihexanoylphosphatidylcholine (DHPC): dimyristoylphosphatidylcholine (DMPC) (1:2.9 w/w) in D_2O, pD 7.2. DHPC and DMPC were purchased from Avanti Polar Lipids (Alabama, USA). The sugars were dissolved by repeatedly heating to 35°C and cooling to 4°C, sonicating and centrifuging. In order to stabilise the liquid crystalline phase, we found the addition of 100mM KCl to the DHPC:DMPC mixture to be helpful.

3.3.2 Optimisation of lipid concentration

The concentration of the lipid solution varied depending on the oligosaccharide to be studied. For a given lipid concentration, the amount of conferred alignment and hence the size of the residual dipolar couplings, is dependent on the asymmetry of the solute molecule. The greater the degree of asymmetry that a molecule has, the lower the lipid concentration required for a certain amount of alignment. It is important that the dipolar couplings should be of a size, which are simple to measure accurately. However, if there is too high a degree of alignment, spectral complexity will increase dramatically as many unwanted dipolar couplings become measurable, resulting in very broad spectra, making the measurement of the residual dipolar couplings of interest difficult. One of the advantages of using a liquid crystalline medium for alignment is that the lipid concentration can in principle be varied to give optimum residual dipolar couplings of a size that are most easily measured (*i.e.* 3-15Hz) for

any sugar. Therefore as might be expected trisaccharides require a lipid concentration (w/v) which is lower than that required by a less asymmetric dissacharide.

A table of the sugars studied and the optimised lipid concentrations along with the references for how these labelled sugars were synthesised is given in table 3.1.

Table 3.1: Summary of lipid concentrations for oligosaccharides

Oligosaccharide	DHPC:DMPC Conc^{n} (w/v)	Reference
lactose (Galβ1-4Glc)	33%	(Kiddle, 1998)
Gb_3 (Galα1-4Galβ1-4Glcβ)	10%	(Shimitzu, 1998)
Gm_3 (Neu5Acα2-3Galβ1-4Glc)	7.5%	(Probert, 1997)
LacNAc (Galβ1-4GlcNAc)	20%	(Harris, 1997)
Sialyl LacNAc (Neu5Acα2-3Galβ1-4GlcNAc)	7.5%	(Harris, 1997)

3.3.3 NMR experiments

All NMR spectra were recorded on a Varian Unity^{+} 500.12 MHz spectrometer. Initial experiments for the determination of optimum lipid concentrations were carried out using a standard HSQC without ^{1}H decoupling. Alignment of a sample above the liquid crystalline phase transition temperature was checked by 1-dimensional ^{2}H and ^{31}P NMR experiments. Residual dipolar couplings were obtained as the difference between the one-bond ^{13}C-^{1}H splittings measured at 35^{o}C and 22^{o}C using the

modified J-modulated HSQC experiment shown in figure 3.2. Each 2D spectrum consisted of 128 complex t_1 points and 1024 complex t_2 points, with 8 scans per t_1 increment and with spectral widths of 13000 Hz and 3000 Hz in F1 and F2 respectively.

3.3.4 Structure calculations

Dynamical simulated annealing calculations were performed using ten random geometries of the appropriate oligosaccharide as input, and with the application of residual dipolar restraints. The geometric content of these restraints was incorporated into the simulated annealing protocol (Homans, 1992) as described (Clore, 1998), using the program XPLOR (Brünger, 1993) modified to incorporate dipolar coupling restraints (Clore, 1998). A uniform value for the force constant $k_{dipolar}$ of 1 kcal Hz^{-2} was utilised throughout the simulated annealing protocol.

3.4 Results and Discussion

3.4.1 ^2H and ^{31}P NMR

^2H and ^{31}P NMR experiments were used to check the behaviour and concentration of the liquid crystalline media. Figure 3.4 shows the ^{31}P NMR spectra of a DHPC/DMPC solution at a concentration of 20% w/v at various temperatures. The up-field shift of the DMPC ^{31}P resonance in the liquid crystalline phase reflects the orientation of the phosphate group CSA tensor relative to the bicelle normal, and this up-field change in ^{31}P shift also indicates that the bilayers are oriented parallel to the magnetic field (Seelig, 1985). In the aligned state (35°C) the ^2H solvent signal shows

a well resolved doublet splitting, reflecting incomplete averaging of the large ^2H quadrupole coupling in this liquid crystalline medium (figure 3.5). The ^2H splitting is, to a good approximation, proportional to the concentration of bicelles, ranging from 24.0 Hz at 20% w/v, to 11.3 Hz at 7.5% and 8.7 Hz at 5%.

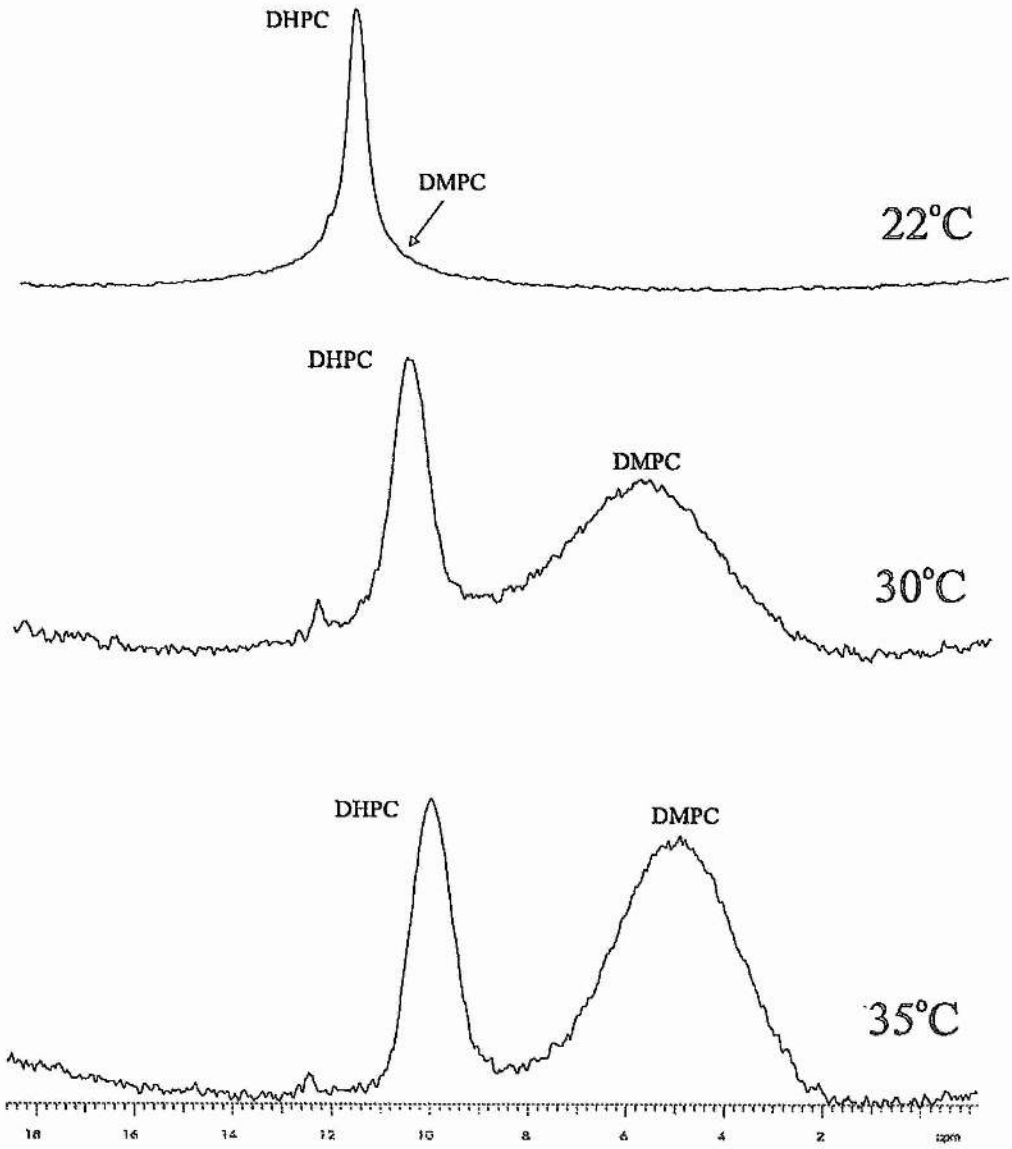

Figure 3.4 – Variation of ^{31}P NMR with temperature for a 20% w/v concentration of DHPC/DMPC

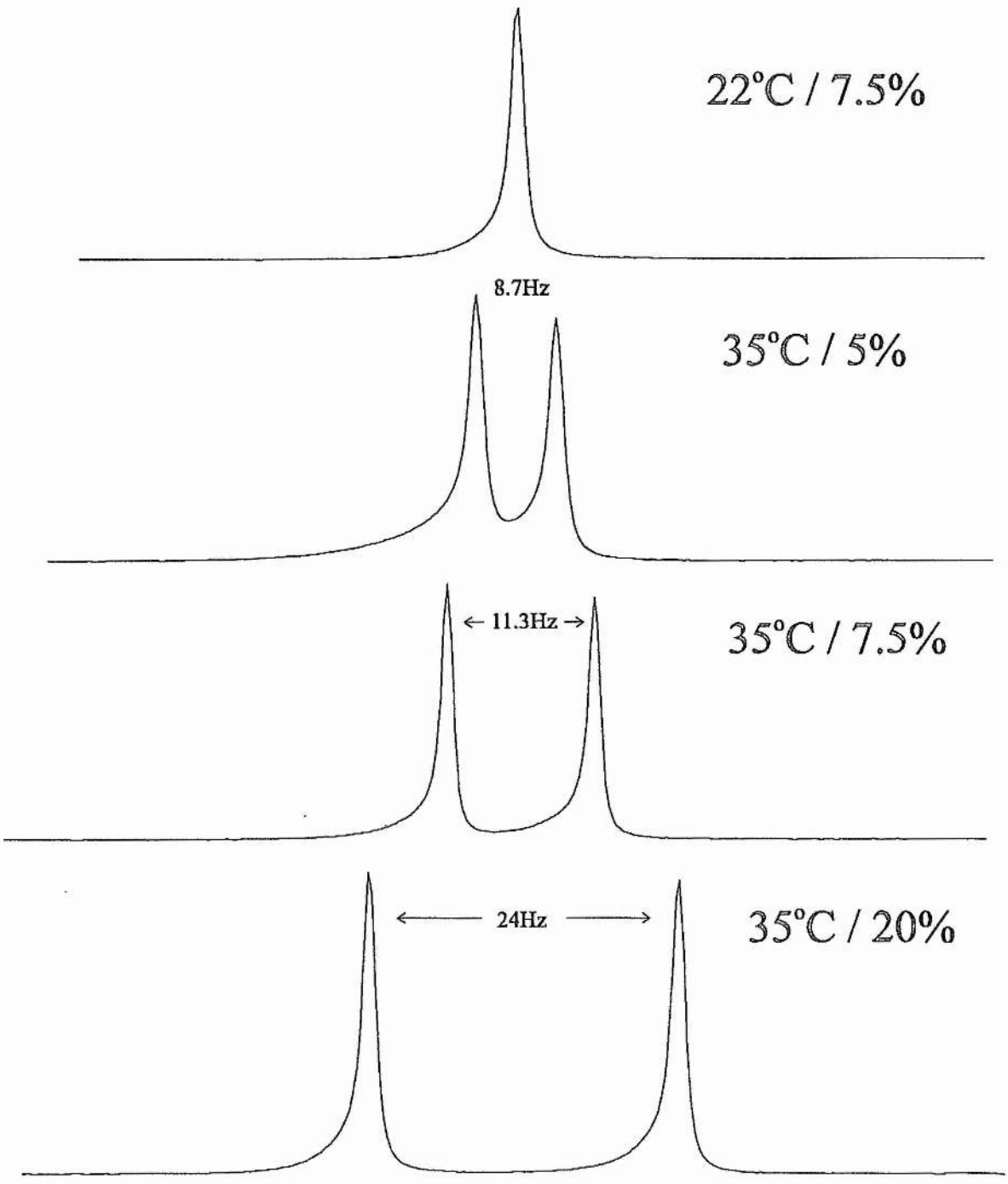

Figure 3.5 – ^{2}H splitting at various DHPC/DMPC concentrations

3.4.2 Measurement of dipolar couplings

It was found for all sugars that collecting between nine and twelve J-modulated HSQC spectra, at both 22°C and 35°C, incremented in 500ms steps from 500ms upwards was sufficient for producing curves that 'turned over' (*i.e.* such that sin $2\pi^1J_{CH}$ (T-Δ) changes sign) while at the same time giving enough points for good coverage of the curve. A summary of the HSQC experiments carried out for each sugar can be seen in table 3.2.

Table 3.2: J-modulated HSQC experiments acquired

Oligosaccharide	Number of experiments 22°C	35°C	initial delay (Δ) (ms)	Increment (ms)
lactose (Galβ1-4Glc)	12	12	500	500
Gb_3 (Galα1-4Galβ1-4Glcβ)	10	10	500	500
Gm_3 (Neu5Acα2-3Galβ1-4Glc)	9	9	500	500
LacNAc (Galβ1-4GlcNAc)	9	9	500	500
Sialyl LacNAc (Neu5Acα2-3Galβ1-4GlcNAc)	9	9	500	500

For all sugars, there were a total of 98 J-modulated HSQC spectra acquired. Figure 3.6 shows sections from four of these HSQC spectra recorded with different values of Δ for lactose. The spectra demonstrate the change in peak intensity observed with increasing values of Δ.

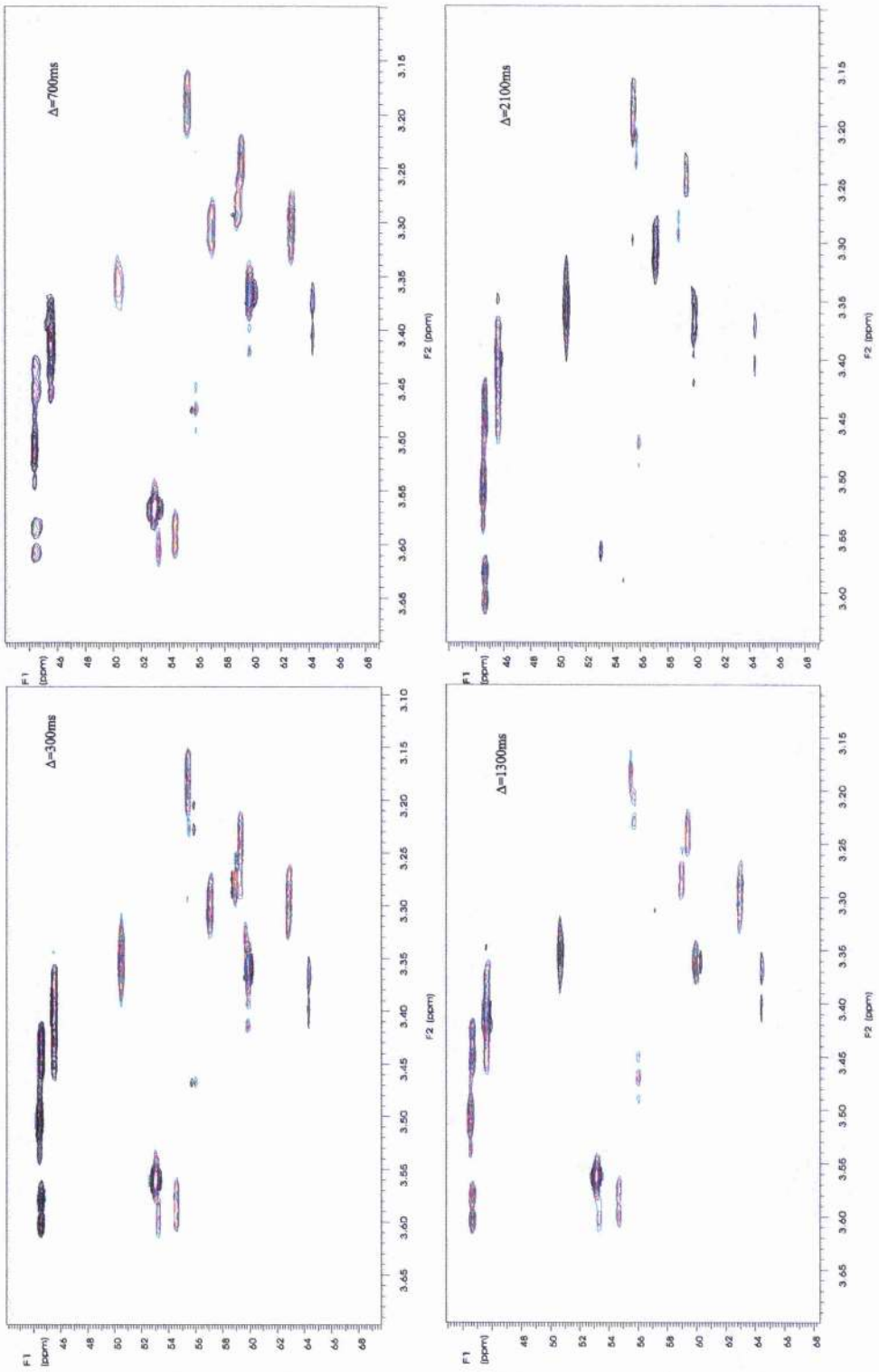

Figure 3.6 - J-modulated HSQC spectra for lactose

In order to extract the dipolar coupling constants, the variation in peak intensity was plotted against 2(T-Δ). To obtain coupling constants from the curves, a non-linear least-squares fitting procedure was carried out using the Origin program (Microcal software Inc.). The values of the peak intensities for Gal H1-C1, Glcβ H1-C1 and Gal H3-C3 of lactose at both 22°C and 35°C can be seen in table 3.3, these values were plotted to produce curves which can be seen in figure 3.7 a, b and c.

On obtaining a coupling constant for a particular resonance at 35°C and 22°C the dipolar coupling constants could be calculated from the difference (equation 3.2). The above procedure was repeated for each resonance of the five oligosaccharides; tables 3.4 –3.8 give the measured coupling constants at 35°C and 22°C for each sugar as well as the calculated residual dipolar coupling constants.

Table 3.3: Measured values of peak intensity for selected resonances of lactose

2(T-Δ)	I(Gal H1-C1)		I(Gal H3-C3)		I(Glcβ H1-C1)	
	35°C	22°C	35°C	22°C	35°C	22°C
0.026	0.31	1.09	-1.49	-0.54	0.49	0.86
0.025	0.87	1.47	-0.74	0.62	0.75	1.04
0.024	1.12	1.36	0.16	1.74	0.79	0.93
0.023	1.13	0.97	1.01	2.51	0.67	0.62
0.022	0.82	0.31	1.63	2.76	0.35	0.18
0.021	0.29	-0.36	2.00	2.63	-0.08	-0.34
0.020	-0.37	-1.03	1.98	1.91	-0.47	-0.77
0.019	-0.90	-1.38	1.45	0.95	-0.72	-1.00
0.018	-1.10	-1.45	0.69	-0.28	-0.77	-0.94
0.017	-1.12	-1.04	-0.18	-1.45	-0.68	-0.71
0.016	-0.73	-0.42	-1.12	-2.43	-0.38	-0.29
0.015	-0.19	0.23	-1.75	-2.90	0.02	0.19

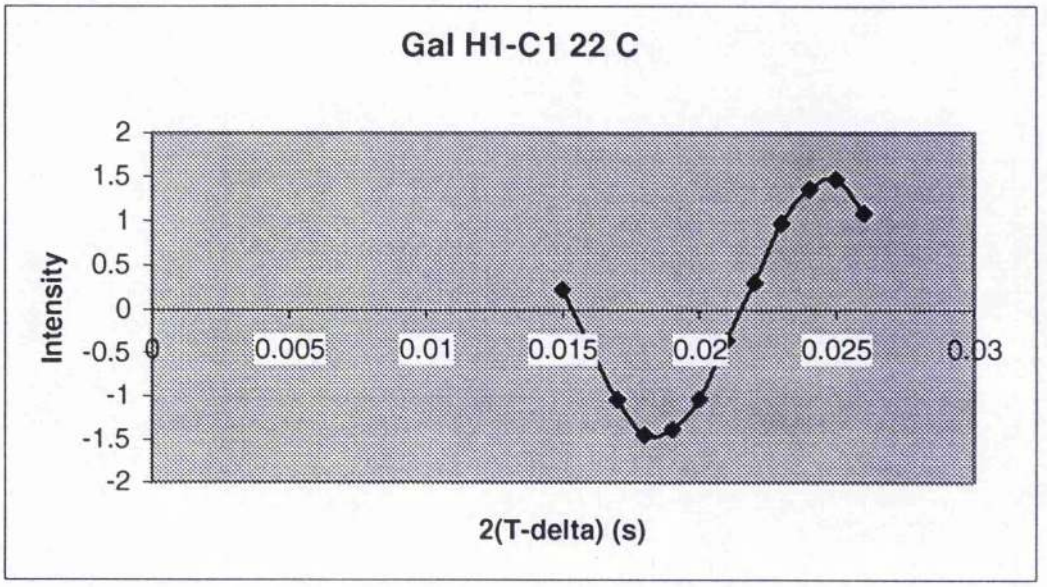

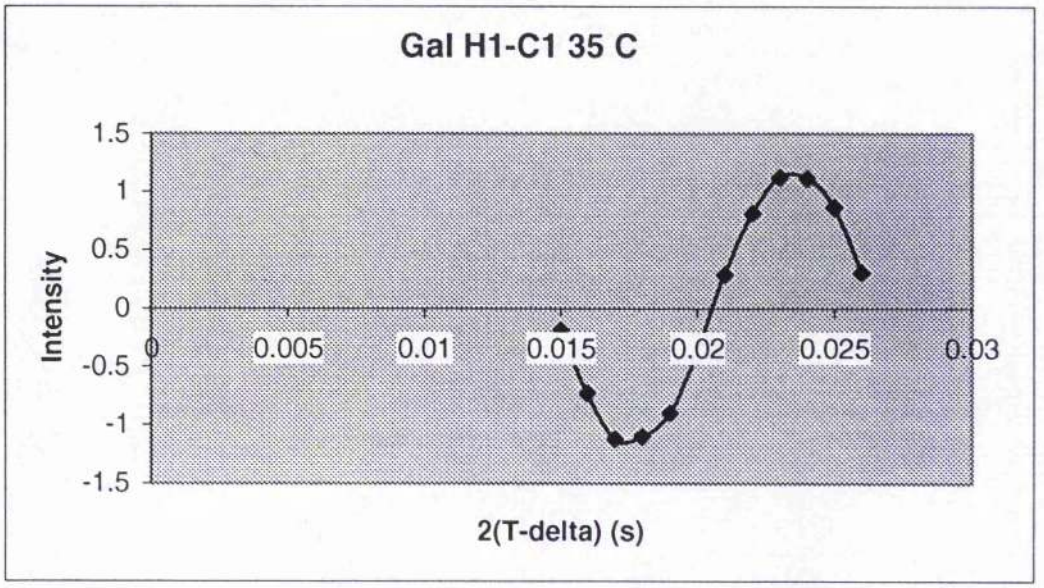

Figure 3.7a – Plots of Intensity vs 2(T-Δ) For Gal H1 – C1 of Lactose

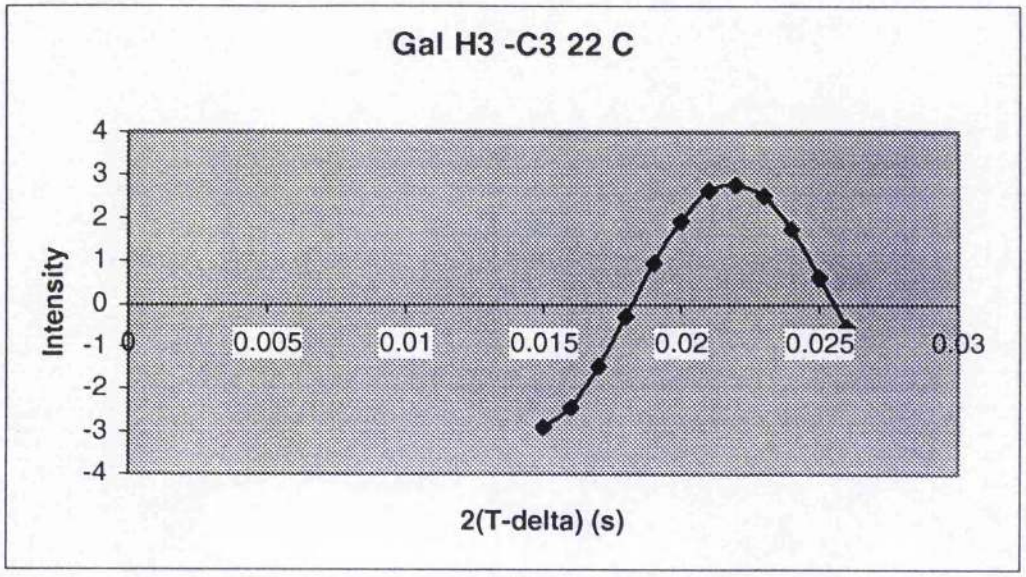

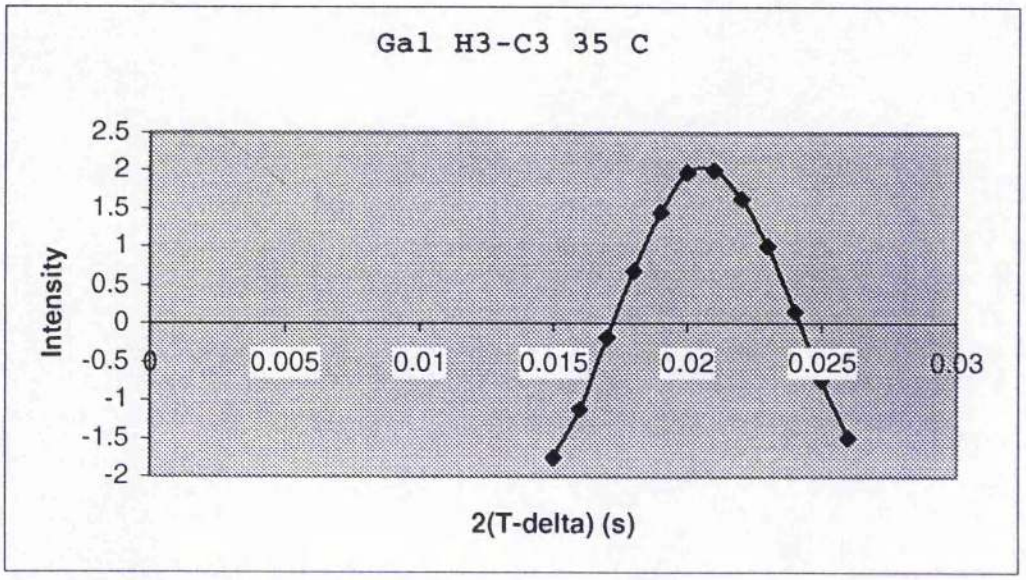

Figure 3.7b – Plots of Intensity vs 2(T-Δ) For Gal H3 – C3 of Lactose

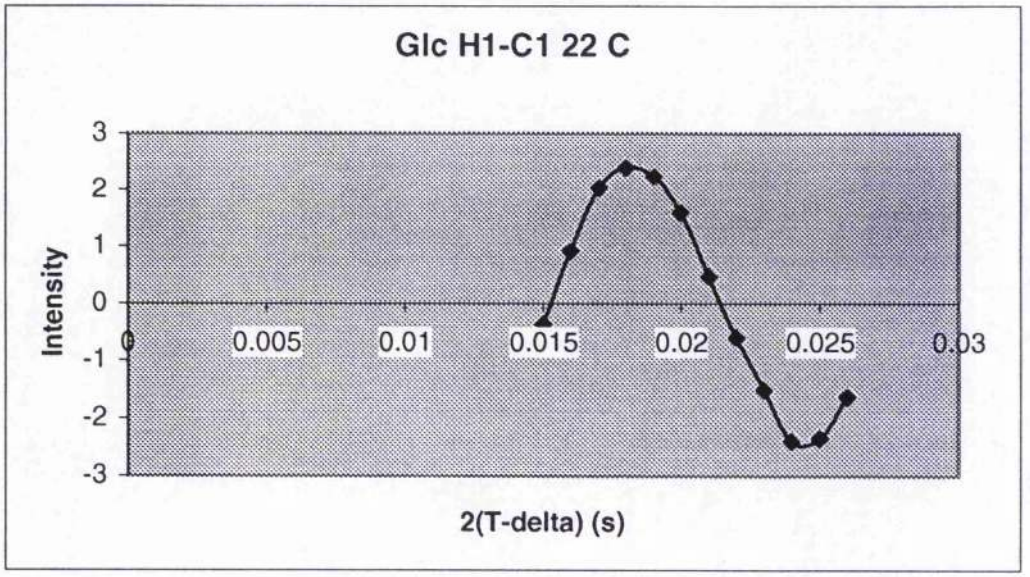

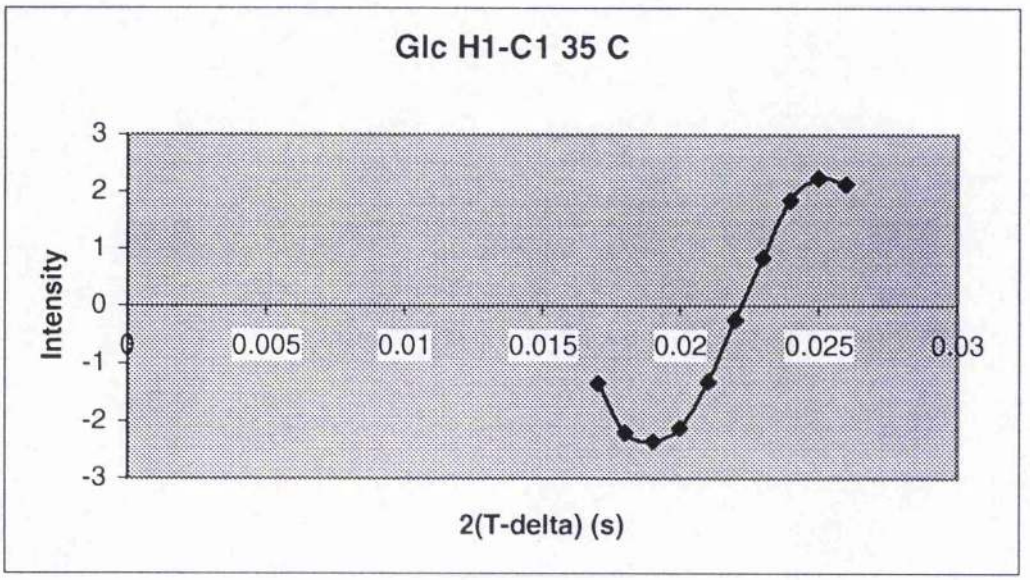

Figure 3.7c – Plots of Intensity vs 2(T-Δ) For Glc H1 – C1 of Lactose

Table 3.4. Residual ^{1}H-^{13}C Dipolar couplings for Galβ1-4Glc in a 33% (w/v) solution of DHPC:DMPC (1:2.9 w/w) in D_2O, pD 7.2

Bond Vector	J_{CH} (35°C)	J_{CH} (22°C)	Residual dipolar coupling (Hz)*
Glcβ H1-C1	165.4	161.5	+3.9
Glcβ H3-C3	152.3	148.4	+3.9
Glcβ H5-C5	146.7	142.0	+4.7
Galβ H1-C1	170.0	162.5	+7.5
Galβ H3-C3	144.9	137.0	+7.9
Galβ H4-C4	142.0	146.0	-4.0
Galβ H5-C5	148.9	140.9	+8.0

*Values obtained by non-linear least-squares fitting of experimental intensities from J-modulated HSQC experiments. Estimated average error in the measurements is ±0.5 Hz.

Table 3.5. Residual ^{1}H-^{13}C Dipolar couplings for LacNAc (Galβ1-4GlcNAc) in a 20% (w/v) solution of DHPC:DMPC (1:2.9 w/w) in D_2O pD 7.2, containing 100mM KCl.

Bond Vector	J_{CH}(35°C)	J_{CH}(22°C)	**Residual dipolar coupling (Hz)***
GlcNAcα H1-C1	157.2	171.5	-14.3
GlcNAcα H2-C2	154.8	138.0	+16.8
GlcNAcα H3-C3	159.9	146.4	+13.5
GlcNAcα H5-C5	161.3	146.0	+15.3
Gal H1-C1	173.4	162.5	+10.9
Gal H2-C2	148.7	138.5	+10.2
Gal H4-C4	149.0	146.8	+2.2
Gal H5-C5	150.4	140.8	+9.6

*Values obtained by non-linear least-squares fitting of experimental intensities from J-modulated HSQC experiments. Estimated average erro in the measurements is ±0.5 Hz

Table 3.6. Residual ^{1}H-^{13}C Dipolar couplings for Neu5Acα2-3Galβ1-4Glc in a 7.5% (w/v) solution of DHPC:DMPC (1:2.9 w/w) in D_2O, pD 7.2, containing 100 mM KCl.

Bond Vector	J_{CH}(35°C)	J_{CH}(22°C)	**Residual dipolar coupling (Hz)***
Glcβ H1-C1	168.3	160.9	+7.4
Glcβ H2-C2	154.5	145.0	+9.5
Glcβ H3-C3	154.3	144.7	+9.6
Glcβ H4-C4	149.8	142.1	+7.7
Galβ H1-C1	174.6	163.1	+11.5
Galβ H2-C2	160.3	148.4	+11.9
Galβ H3-C3	152.0	142.8	+9.2
Galβ H4-C4	146.4	147.8	-1.4
Galβ H5-C5	150.8	141.3	+9.5
Neu5Acα H4-C4	146.8	143.6	+3.2
Neu5Acα H5-C5	149.6	144.8	+4.8
Neu5Acα H7-C7	128.9	142.3	-13.4
Neu5Acα H8-C8	133.3	144.4	-11.1

* Values obtained by non-linear least-squares fitting of experimental intensities from J-modulated HSQC experiments (Tjandra and Bax 1997). Estimated average error in the measurements is ±0.5 Hz.

Table 3.7. Residual dipolar ^{1}H-^{13}C Dipolar couplings for Galα1-4Galβ1-4Glcβ in a 7.5% (w/v) solution of DHPC:DMPC (1:2.9 w/w) in D_2O, pD 7.2, containing 100 mM KCl.

Bond Vector	J_{CH}(35°C)	J_{CH}(22°C)	**Residual dipolar coupling (Hz)***
Galα H1-C1	165.6	169.9	-4.3
Galα H2-C2	161.5	150.4	+11.1
Galα H3-C3	144.1	143.2	+0.9
Galα H4-C4	140.8	152.0	-11.2
Galα H5-C5	153.5	143.5	+10.0
Galβ H1-C1	157.8	163.4	-5.6
Galβ H2-C2	127.0	132.3	-5.3
Galβ H3-C3	130.4	136.5	-6.1
Galβ H4-C4	152.9	145.7	+7.2
Galβ H5-C5	135.1	140.1	-5.0
Glcβ H1-C1	156.6	161.4	-5.8
Glcβ H2-C2	134.3	140.1	-5.8
Glcβ H3-C3	132.4	139.1	-6.7
Glcβ H4-C4	140.0	146.2	-6.2
Glcβ H5-C5	135.9	141.9	-6.0

* Values obtained by non-linear least-squares fitting of experimental intensities from J-modulated HSQC experiments. Estimated average error in the measurements is ±0.5 Hz.

Table 3.8. Residual dipolar ^{1}H-^{13}C Dipolar couplings for Neu5Acα2-3Galβ1-4GlcNAc in a 7.5% (w/v) solution of DHPC:DMPC (1:2.9 w/w) in D_2O, pD 7.2, containing 100 mM KCl.

Bond Vector	J_{CH}(35°C)	J_{CH}(22°C)	**Residual dipolar coupling (Hz)***
Gal H2-C2	156.0	150.0	+6.0
Gal H3-C3	149.0	143.8	+5.2
Gal H4-C4	145.2	148.2	-3.0
Gal H5-C5	150.8	140.0	+10.8
GlcNAcβ H5-C5	147.9	140.9	+7.0
Sia H4-C4	145.0	142.8	+2.2
Sia H5-C5	151.1	145.5	+5.6
Sia H6-C6	148.1	143.1	+5.0
Sia H8-C8	131.1	145.5	-14.4

* Values obtained by non-linear least-squares fitting of experimental intensities from J-modulated HSQC experiments. Estimated average error in the measurements is ±0.5 Hz.

3.4.3 Comparison of residual dipolar coupling constants, with ring geometry

Since the ring geometry of the constituent monosaccharide residues in the oligosaccharides are essentially fixed on the NMR time scale, the relative magnitudes of the intra-residue residual dipolar couplings would be expected to reflect the stereochemistry at each carbon centre. By comparison of the ring geometry of the Galactose in Galβ1-4Glc (figure 3.3) with the residual dipolar coupling (table 3.4), it can be seen that the residual dipolar couplings for Galβ H1 - C1, H3 - C3 and H5 - C5 are comparable, reflecting a similar (axial) orientation of the methine protons. In contrast, the residual dipolar coupling for the H4 - C4 bond vector is different in magnitude and negative, reflecting a completely different (equatorial) orientaion of the methine proton. Similar relationships can be seen between the residual dipolar couplings and the ring geometries for all the sugars.

3.5 Structural Calculations

3.5.1 Derivation of components of the alignment tensor

Values for the axial and rhombic component of the alignment tensor were determined directly from the experimental data, as described in section (3.2.7). Values for the axial and rhombic components as well as the rhombicity were calculated using equations 3.4 and 3.5. The bond distance r_{PQ} was taken to be 0.109 nm and it was assumed that the most negative dipolar coupling for each sugar was proportional to the axial component of the alignment tensor (D_a). The values obtained for each sugar can be found in table 3.9.

Table 3.9: Experimentally determined values for Da, Dr and rhombicity

Oligosaccharide	$S.A_a$	$S.A_r$	R
lactose (Galβ1-4Glc)	4.33×10^{-4}	8.67×10^{-5}	0.2
Gb_3 (Galα1-4Galβ1-4Glcβ)	4.81×10^{-4}	9.61×10^{-5}	0.2
Gm_3 (Neu5Acα2-3Galβ1-4Glc)	5.75×10^{-4}	1.15×10^{-4}	0.2
LacNAc (Galβ1-4GlcNAc)	6.14×10^{-4}	1.23×10^{-4}	0.2
Sialyl lacNAc (Neu5Acα2-3Galβ1-4GlcNAc)	6.18×10^{-4}	1.24×10^{-4}	0.2

3.5.2 Dynamical simulated annealing calculations

In order to examine the conformational properties of the oligosaccharides that gave rise to the residual dipolar couplings given in tables 3.4 – 3.6, the latter were incorporated in a restrained dynamical simulated annealing protocol for each oligosaccharide giving a series of low energy structures. (figure 3.8). Table 3.10 gives details of the low energy stuctures for each oligosaccharide.

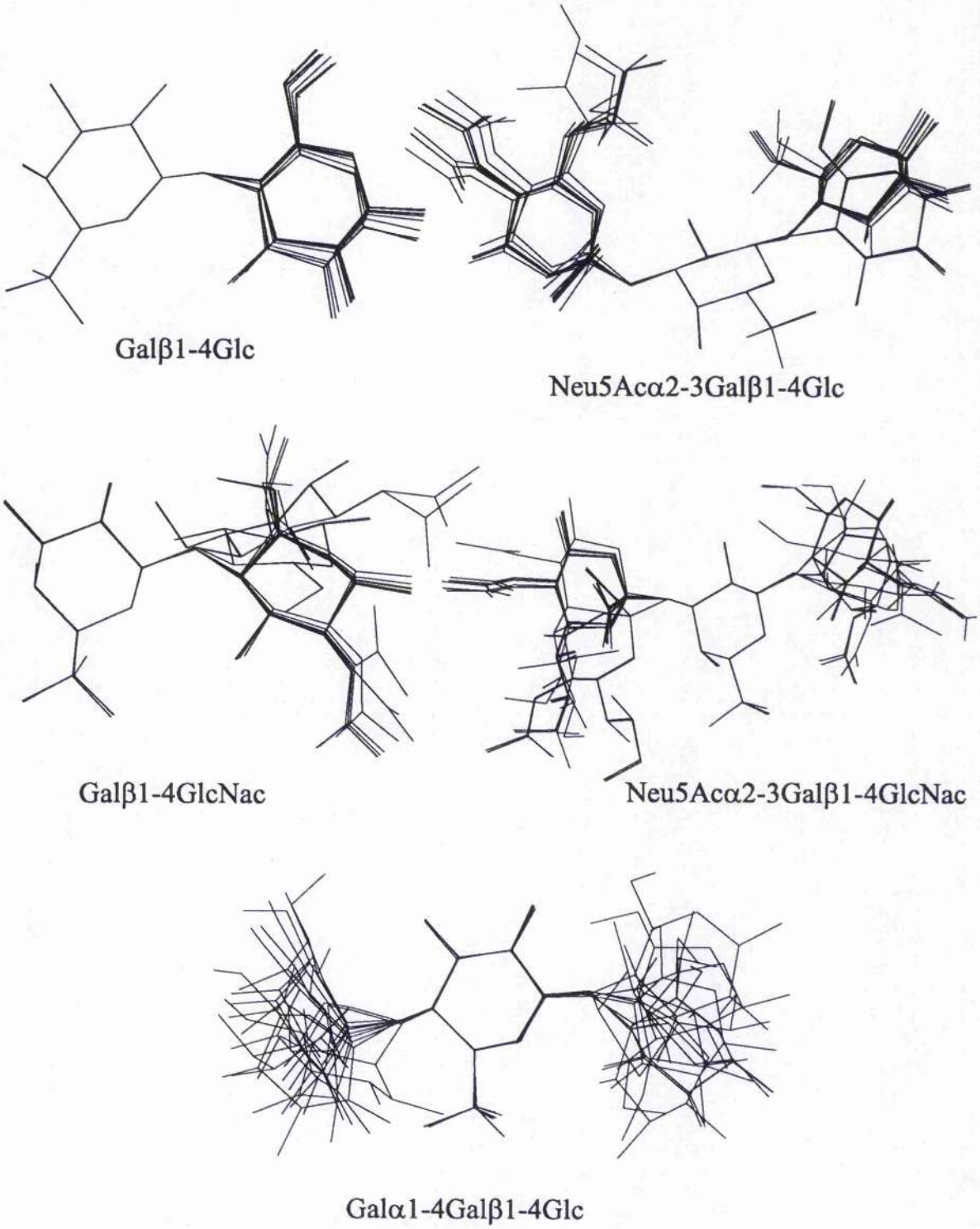

Figure 3.8 Low energy conformations

Table 3.10: Results of restrained dynamical simulated annealing.

Oligosaccharide	Glycosidic linkage	Number of families	dihedral angles (φ, ψ)
lactose	Galβ1-4Glc	2	~+10°, -21° ~-5°, +30°
lacNAc	Galβ1-4GlcNAc	3	~+30°, -11° ~+118°, -26° ~+4°, +64.39°
Gb_3	Galα1-4Gal Galβ1-4Glc	several	
Gm_3	Neu5Acα2-3Gal	1	~+72°, +5°
	Galβ1-4Glc	2	~+15°, -18° ~+62°, +15°
Sialyl LacNAc	Neu5Acα2-3Gal	2	~-153°, -24° ~+169°, -63°
	Galβ1-4GlcNAc	several	~+15°, -14°

3.5.3 Galβ1-4Glc (lactose)

The restrained dynamical simulated annealing for lactose, using dipolar restraints only, gave two possible families about the glycosidic linkage. There were no deviations from experimental dipolar couplings greater than 0.1 Hz for any of the structures obtained. This indicates that each conformation is essentially consistent with all of the measured dipolar couplings. By comparison with the structure and dynamics observed for lactose in chapter 4 of this thesis, it can be concluded that the conformations about the glycosidic linkages implied from the dipolar restraints map to accessible regions of conformational space.

3.5.4 Neu5Acα2-3Galβ1-4Glc (Gm_3)

There were no deviations from experimental dipolar couplings greater than 0.1Hz for any of the conformations. By comparison with a previous study on the structure and dynamics of Gm_3-OS (Milton, 1998), the conformations about the glycosidic linkages implied from the dipolar restraints map to accessible regions of conformational space defined in that study. The measured dipolar restraints are consistent with a model involving relatively small torsional oscillations about the minimum energy conformation of each glycosidic linkage.

The orientation of the z axis of the external axis system used in the simulated annealing calculations, which indicates the direction of the principle axis of the alignment tensor, is approximately collinear (within 20^{o}) of the C5 - C6 bond vector of Neu5Acα. The large negative couplings for the C7 - H7 and C8 - H8 bond vectors

of the sidechain of Neu5Acα indicate that these vectors are fixed in an orientation perpendicular to the C5 - C6 bond. This observation is again consistent with earlier observations (Milton, 1998), and supporting the hypothesis (Poppe, 1991) that this side chain is stabilised by a hydrogen bond in solution from OH-8 to the carboxyl group of Neu5Ac.

3.5.5 Galβ1-4GlcNAc (LacNAc)

A majority of the structures adopt one conformation (~+30°, -11°), however there are departures from this as indicated in table 3.10. The deviations from experimental dipolar couplings are again <0.1Hz, indicating that all the conformations are consistent with the experimental dipolar couplings. Previous studies (Harris, 1997; Ichikawa, 1992) indicate the existence of torsional fluxionality that is consistent with the observation of more than one conformation in the presence of dipolar restraints.

3.5.6 Neu5Acα2-3Galβ1-4GlcNAc (Sialyl LacNAc)

About the Neu5Acα2-3Gal linkage there were two conformations that were consistent with the dipolar couplings, however, for the Galβ1-4GlcNAc linkage, there were several conformations which were consistent with the dipolar couplings. This is again consistent with a dynamic situation as suggested in other studies (Harris, 1997; Ichikawa, 1992). As there were once again no departures from experimental dipolar couplings of greater than <0.1Hz, it can be concluded that these conformations are consistent with the dipolar couplings. The fact that these restraints fit for several conformations about the Galβ1-4GlcNac linkage, is again probably due

to the dynamic nature of the molecule, yielding only average values for the dipolar couplings.

3.5.7 Galα1-4Galβ1-4Glc (Gb_3)

The modelling study for this sugar gave no coherent information for this carbohydrate. This was the only case studied where there were departures from theoretical dipolar couplings greater than 0.1 Hz, there were in fact some differences of up to 0.7 Hz. This indicates that not all the calculated conformations are in as good agreement with the experimentally determined dipolar couplings as is the case with the other carbohydrates studied. There is no single conformation that agrees with the measured dipole-dipole coupling constants. The reasons for this are unclear, however again the problem for this type of restraint is that in a dynamic system only an average dipolar coupling can be measured. In the case of Gb_3 it would appear that a range of conformations come close to fitting the average dipolar restraints, but none of these conformations fit them accurately.

3.6 Conclusions

It has been demonstrated that small oligosaccharides exhibit sufficient anisotropy in solution to obtain a degree of orientation in dilute liquid-crystalline solvents. This alignment is sufficient to allow the measurement of substantial residual dipolar couplings from C-H bond vectors. These dipolar couplings contain long-range information that has been incorporated in dynamic simulated annealing calculations of several sugars with varying success. In the case of lactose and Gm_3, the proposed

models are consistent with previously suggested solution behaviour based on short-range structural information from ^{1}H-^{1}H nuclear Overhauser effects and three-bond transglycosidic ^{1}H-^{1}H and ^{13}C-^{1}H coupling constant measurements. Clearly there are problems in the models of some of the other sugars, most notably Gb_3. These studies perhaps highlight once again the problems often encountered in the study of free solution state conformations of oligossacharides, where the dynamic nature of many such sugars, reduces the usefulness of what effectively become average restraints. It may thus be concluded that where the measurement of residual dipolar coupling constants may be of most use, is in conformational studies of oligosaccharides in their bound state conformations.

Chapter 4

Heteronuclear NMR investigation of the Solution Structure and Dynamics of the carbohydrate moiety Galβ1-4 Glc

Abstract

The three-dimensional structure and dynamics of Galβ1-4Glc are investigated using the additional NMR-derived restraints discussed in the previous chapters. Heteronuclear NMR experiments on ^{13}C and ^{13}C, ^{2}H enriched Galβ1-4Glc have allowed additional structural information to be obtained. These include ^{13}C-^{13}C trans-glycosidic long-range coupling constants, and the unambiguous measurement of inter-glycosidic NOEs that were previously overlapped. Experiments at low temperature have also allowed the measurement of NOEs to exchangeable protons. With the inclusion of the ^{1}H-^{13}C inter-glycosidic NOEs (chapter 2) and the residual dipolar couplings (chapter 3) in a molecular dynamics protocol, it is shown that the conformation cannot be represented by a single structure, but is best represented by a dynamical model with significant torsional fluctuations confirming the flexibility of carbohydrates in solution.

4.1 Introduction

The determination of the solution structures of carbohydrates is not trivial due to the presence of substantial torsional motions about the glycosidic linkages. These motions give rise to time-averaged values of trans-glycosidic NMR parameters such as nuclear Overhauser effects and long-range spin-coupling constant measurements, and the extraction of meaningful structural and dynamic information from these parameters requires a suitable model of the internal motion. In principle a suitable model can be derived by computation of a molecular dynamics trajectory for the glycan, the authenticity of which can be assessed by back-calculation of relevant NMR parameters from the simulation, for comparison with experimentally derived values. A problem with this approach is that current molecular mechanical forcefield parameterisations for carbohydrates are of insufficient accuracy over the total potential surface to generate motional models of sufficient accuracy. In order to overcome this limitation, molecular dynamics simulations have been performed in the presence of weak NOE restraints that modify the potential surface, and give rise to molecular dynamics trajectories that can predict with accuracy additional conformation-dependent parameters such as transglycosidic ^{13}C-^{13}C coupling constant measurements. However, with the application of NOE restraints, albeit weak, it is difficult to ensure that the true motional behaviour of the glycan is not masked by their presence. For example, the use of conventional biharmonic restraints may prevent torsional excursions to other regions of conformational space when such excursions exceed the upper or lower bounds of the restraining condition. This problem is not restricted to studies on carbohydrates, and indeed has been addressed

in the context of side chain motions in proteins by application of protocols that include time averaging (Torda, 1989). In these protocols, relevant distance averaging over the time course of the simulation is required to satisfy the relevant restraining condition. A fundamental barrier to the use of protocols of this type, in application to carbohydrates is that the number of conformational restraints that are conventionally available is insufficient, and the trajectory computed with time-averaged restraints becomes essentially indistinguishable from a free dynamics simulation (Torda, 1990). In order to overcome this limitation, in this chapter it is demonstrated that additional conformational parameters can be obtained from isotopically ^{13}C and $^{13}C,^{2}H$-enriched Galβ1-4Glc including $^{1}H\{^{13}C\}$ nuclear Overhauser effects (chapter 2), ^{13}C-^{13}C transglycosidic long-range couplings and residual dipolar couplings in liquid crystalline media (chapter 3). With a well defined structure, Galβ1-4Glc represents a good model system for demonstrating the value of combining these new parameters.

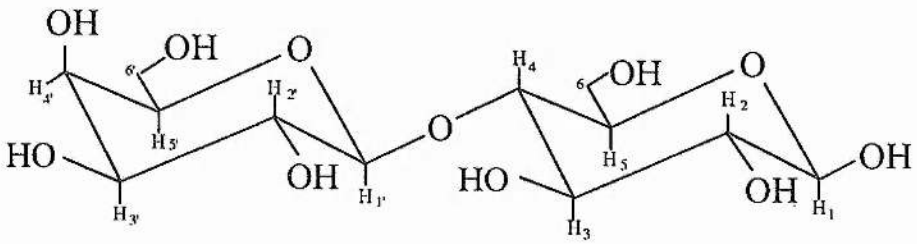

Figure 4.1: Schematic representation of Galβ1-4Glc

4.2 Materials and Methods

4.2.1 Sample Preparation

Galβ1-4[U-^{13}C, ^{2}H]Glc was prepared by chemoenzymatic synthesis performed in a 2.5 ml solution containing 10mM UDP-galactose and 10mM U-^{13}C, ^{2}H glucose (from Martek Biosciences) in 50mM phosphate buffer (pH 7.4). One unit of galactosyltransferase was added with 1mM lactalbumin and Mn^{2+} to a concentration of 5mM, and the mixture was incubated at 37°C overnight.

U-^{13}C-Galβ1-4Glc was prepared by chemoenzymatic synthesis performed in 2.5 ml solution of 50mM Tris (pH 7.8), 5mM $MgCl_2$, 50mM ATP and 50mM ^{13}C Galactose. One unit of Galactokinase was added and the mixture was incubated at 37°C for 24 hours. To this was added 1 unit of Uridylyl transferase and 10mM UDP-glucose, this was incubated at 37°C for 24 hours. After this time 50mM ^{13}C glucose, 1 unit of galactosyltransferase and 1mM lactalbumin was added. The solution was left for a further 24 hours at 37°C.

[^{13}C]Galβ1-4[^{2}H,^{13}C]Glc was prepared in the same way as above, except in the final stage 50mM [^{13}C, ^{2}H,] glucose was added instead of ^{13}C glucose.

The disaccharide products were purified by Biogel P-2 column (2.5 cm * 100cm) chromatography, with H_2O eluant.

Samples for experiments at 30°C were dissolved and lyophilised into 99.96% D_2O three times followed by dissolution into 700µL D_2O. For the observation of the exchangeable protons samples were dissolved in 750µL of H_2O containing 15% 99.96% Acetone-d_6 (Cambridge Isotopes). The pH was adjusted to ~5.7 by careful step-wise addition of dilute HCl or NaOH and transferred to a 5mm NMR tube. The sample was degassed by sonication for about one minute.

4.2.2 NMR Experiments

NMR spectra were obtained at 300K with a ^1H reference frequency of 500.12MHz on a Varian Unity$^+$ spectrometer equipped with a self shielded z gradient triple resonance probe. All spectra were recorded in the phase-sensitive mode with use of the States (States *et al.*, 1982) method for quadrature detection.

Two-dimensional {^{13}C}^1H heteronuclear Overhauser effect (HOESY) experiments were recorded on Galβ1-4[U-^{13}C, ^2H]Glc as described [chapter 2].

Two-dimensional homonuclear ^1H ROESY experiments for the measurement of ROEs to and from exchangeable hydroxyl protons were recorded on Galβ1-4Glc at 258 K in H_2O/acetone solution (85:15 v/v) with a conventional ROESY pulse sequence appended with a double pulsed-field gradient echo sequence. Spectra were acquired with spectral widths of 3600 Hz in each dimension, 1024 complex points in t_2, 256 complex points in t_1 and with 16 transients per t_1 increment. The spin-lock time was 100ms using a weak (~3 kHz) continuous-wave rf field whose carrier was

shifted to low-field of the spectrum for the duration of the spin-lock. Prior to Fourier transformation time-domain data were apodised with cosine-bell functions in each dimension. Hydroxyl exchange rates were measured using the method described by Adams and Lerner (Adams, 1992) incorporating a double pulsed-field gradient echo sequence (Hwang, 1995).

Three-dimensional NOESY-HSQC experiments were recorded with spectral widths of 1100Hz in the t_1 and t_2 (^{1}H) dimensions, 6000Hz in the t_3 dimension, and 128, 32, and 512 complex points in the t_1, t_2 and t_3 dimensions, respectively. A mixing time of 500 ms was used. Prior to Fourier transformation, each dimension was apodised with cosine-bell weighting functions followed by zero filling to 256, 64, and 1024 complex points, respectively.

Two-dimensional gradient-enhanced long range carbon-carbon correlation (LRCC) experiments (Bax *et al.* 1992) were recorded on U-^{13}C-Galβ1-4Glc with a proton sweep width of 1.1 kHz, a ^{13}C sweep-width of 6.5kHz, and 1024 complex points in t_2 and 256 complex points in t_1. A total of 64 scans were acquired per t_1 increment. ^{13}C-^{13}C couplings evolve and are re-focussed during the delay (2T) of 22.2ms. The values of the long range coupling constants are derived from the ratios of cross-peaks obtained in the spectrum in the manner described by Bax (Bax *et al.*, 1992).

Residual ^{13}C-^{1}H dipolar couplings were measured in U-^{13}C-Galβ1-4Glc in D_2O containing 33% w/v of a mixture (1:2.9) of dihexanoyl phosphatidylcholine and dimyristoylphosphatidylcholine as described in chapter 3.

4.2.3 Molecular Modelling

Dynamical simulated annealing calculations and molecular dynamics (MD) simulations were computed *in vacuo* as described (Homans & Forster, 1992; Rutherford & Homans, 1994). Random structures were generated by dynamical quenching. An initial structure was built with pyranose rings in the $^{4}C_{1}$ chair conformation with trial values of phi (φ) and psi (ψ), and subjected to 200ps of unrestrained molecular dynamics at 750K. A random structure was saved every 10ps. Energy minimisation by restrained simulated annealing was achieved as follows: Models were equilibrated for 10ps with a thermal bath at temperatures 500K, 450K, 350K, 300K, and then successively for 1ps in decreasing steps of 10K, followed by a further 1ps at 5K. The system was minimised using a steepest descents algorithm until the maximum derivative was less than 0.04 K J mol^{-1} $Å^{-1}$. Restraints were applied as a biharmonic function. NOE contacts were arbitrarily assigned as strong (1.8Å - 2.7Å), medium (1.8Å - 3.3Å), and weak (1.8Å - 5.0Å). Residual dipolar restraints were incorporated into the molecular dynamics simulation as described (Homans, 1992; Clore, 1998), using the program XPLOR modified to incorporate dipolar restraints. Values for the axial and rhombic components of the alignment tensor were determined as described in section 3.2.7.

The MD simulations incorporated homonuclear ^{1}H NOE restraints, including those to and from hydroxyl protons, in the form of time-averaged restraints as described by Torda (Torda, 1989 and 1990), with a memory time τ of 5ps. Theoretical NOE intensities and spin-coupling constants were computed from molecular dynamics simulations using in-house written software. Computation of NOE intensities incorporated a full relaxation matrix approach including a formalism appropriate for the computation of NOE and ROE data due to fluctuating inter-nuclear distances arising from internal motions which are fast with respect to the rate of molecular tumbling (Tropp, 1980; Homans and Forster, 1992). A single overall isotropic correlation time for the molecule was assumed, and was obtained by fitting the ratio of the theoretical diagonal peak to cross-peak intensities for a known, fixed distance (intra-residue NOE) to the experimentally measured values.

4.3 Results and Discussion

4.3.1 Spectral Assignments

Spectral assignments for the non-exchangeable protons and carbons were made using COSY, TOCSY and HSQC spectra acquired at 30°C and are given in table 4.1 and on the HSQC spectrum in figure 4.2. In order to assign the hydroxyl proton chemical shifts, COSY and TOCSY experiments with excitation sculpting for water suppression (Harris, 1997) were carried out at 258 K. These assignments along with the exchange rates for the hydroxyl protons are given in table 4.2 and the TOCSY experiment is shown in figure 4.3.

Table 4.1 - ^{1}H and ^{13}C chemical shift assignments for Galβ1-4Glc at 303K.

	Galactose		Glcβ		Glcα	
	^{1}H	^{13}C	^{1}H	^{13}C	^{1}H	^{13}C
1	4.47	103.0	4.68	95.7	5.24	91.8
2	3.57	70.9	3.30	73.7	3.60	71.2
3	3.68	72.6	3.67	74.5	3.85	71.5
4	3.95	68.5	3.67	78.3	3.67	78.3
5	3.68	75.3	3.62	74.9	3.97	70.0
6	3.79	61.0	3.97/3.82	59.9	3.88/3.90	59.9

Chemical shifts are referenced to $\delta_{TSP} = 0.00$ppm

Table 4.2 - Chemical shifts and exchange rates for exchangeable protons in H_2O/Acetone-d_6 (85:15) at 258K.

Proton	Chemical Shift (ppm)	Exchange Rate (s^{-1})
GlcβOH1	8.05	19.6
GlcβOH2	6.67	15.5
GlcβOH3	6.14	10.4
GlcαOH1	7.33	15.7
GlcαOH2	6.30	20.2
GlcαOH3	6.02	-----
GlcαOH6	5.97	-----
GalOH2	6.63	13.2
GalOH3	6.22	20.2
GalOH4	6.05	10.6

Chemical shifts are referenced to $\delta_{TSP} = 0.00$ppm

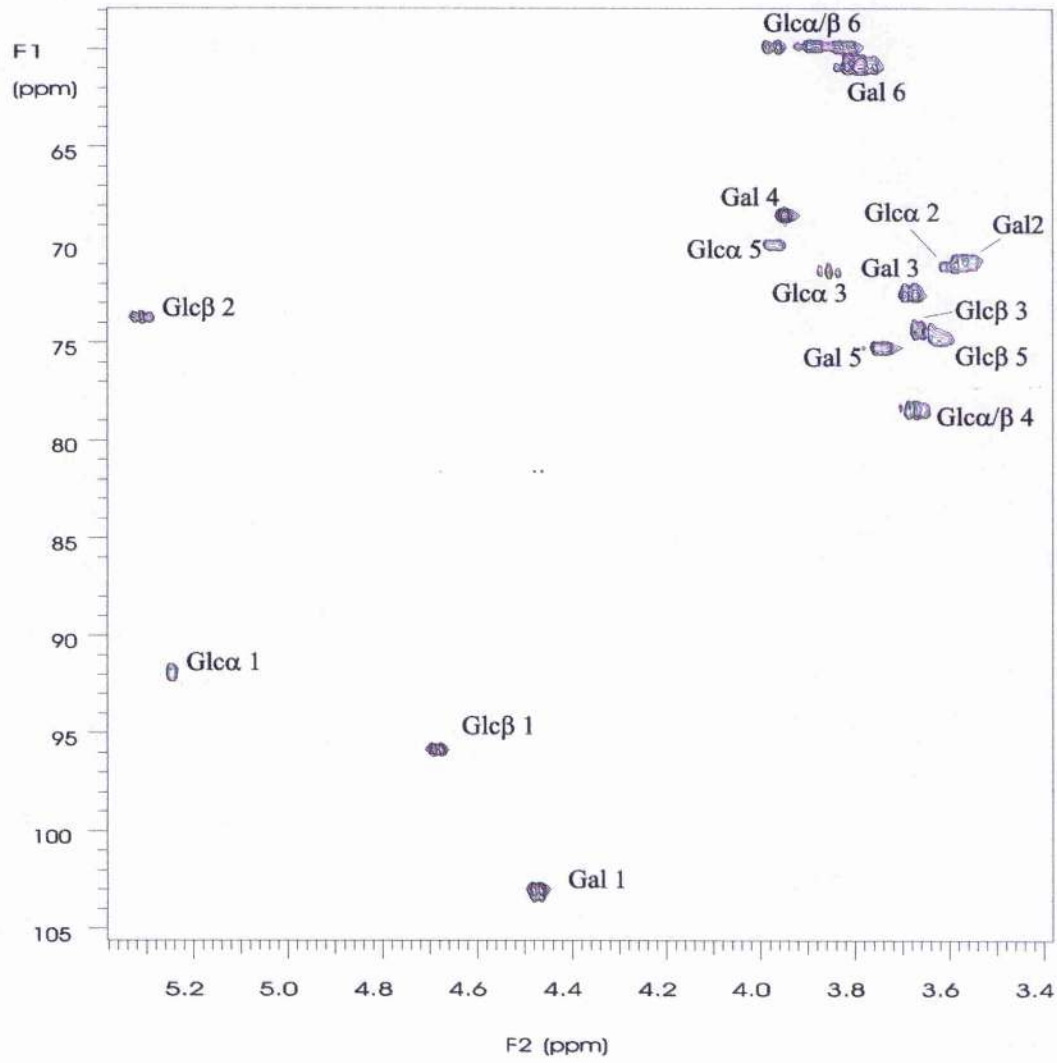

Figure 4.2 – HSQC spectrum of Lactose

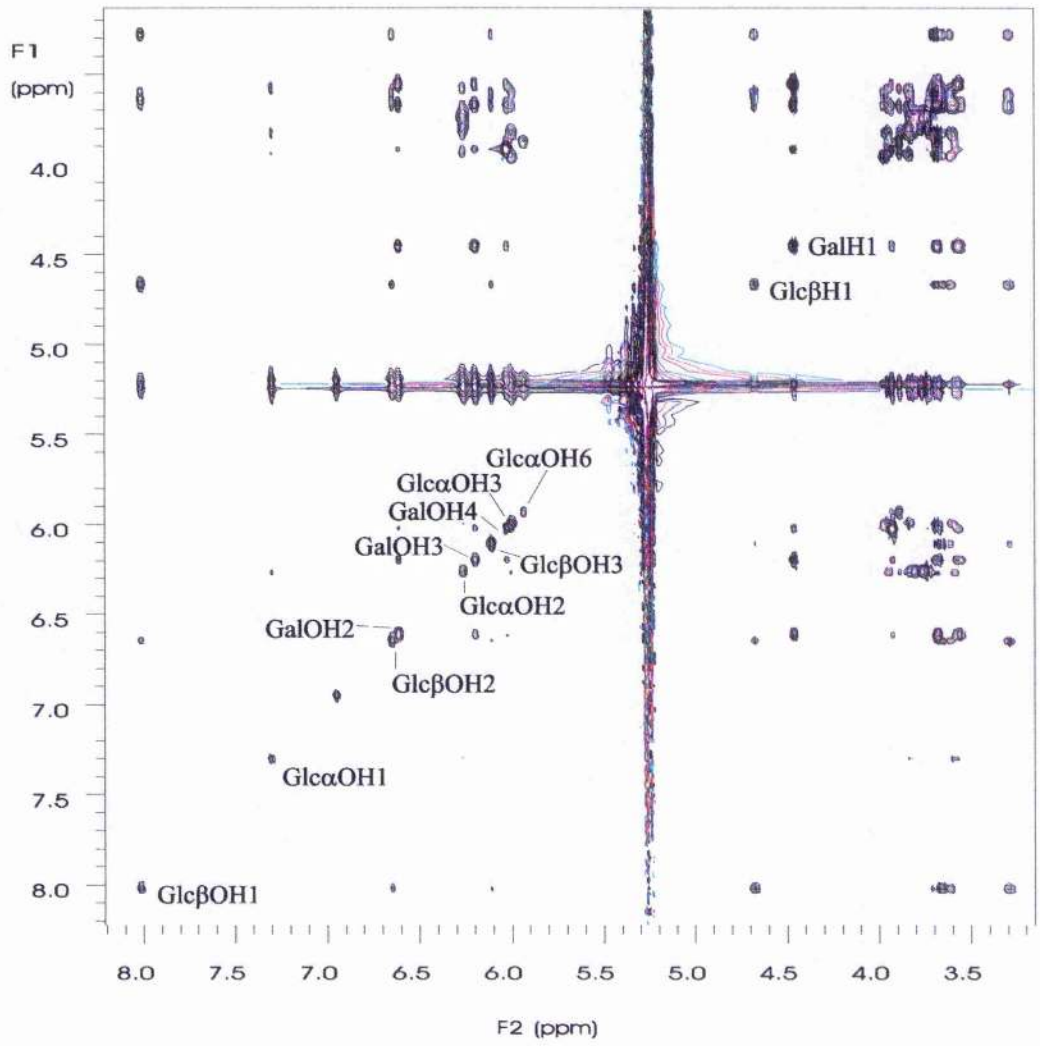

Figure 4.3 – TOCSY spectrum of lactose run at 258 K.

4.3.2 Inter-glycosidic NOEs

4.3.2.1 Non-exchangeable ^1H-^1H Homonuclear NOEs

Three homonuclear ^1H NOE connectivities are detectable across the glycosidic linkage of Galβ1-4Glc, namely Gal H-1 to Glc H-4, H6 and H6'. It can be seen from the 2D NOESY experiment in figure 4.4, that these NOEs cannot be readily quantified due to substantial resonance overlap. Thus, three-dimensional NOESY-HSQC experiments were utilised on [U-^{13}C] Galβ1-4Glc, from which well resolved NOE cross-peaks could be obtained in F1/F3 ($^1H/^1H$) planes (figure 4.5). The NOE cross-peak volumes were summed over all planes where the NOE was present. The three inter-glycosidic NOEs observed were normalised to an intra-residue cross-peak volume, and were used in molecular modelling simulations (Table 4.3)

The measurement of only three inter-glycosidic NOEs is indicative of the problem in determining the solution conformation of oligosaccharides. The linkages are the primary source of conformational flexibility, therefore the overall three-dimensional structure is under defined by these NOEs alone. This results in a reliance on molecular mechanics calculations to restrict the number of possible conformations that are consistent with the NMR data, and it has been shown that this can give results which are not reliable (Rutherford, 1993).

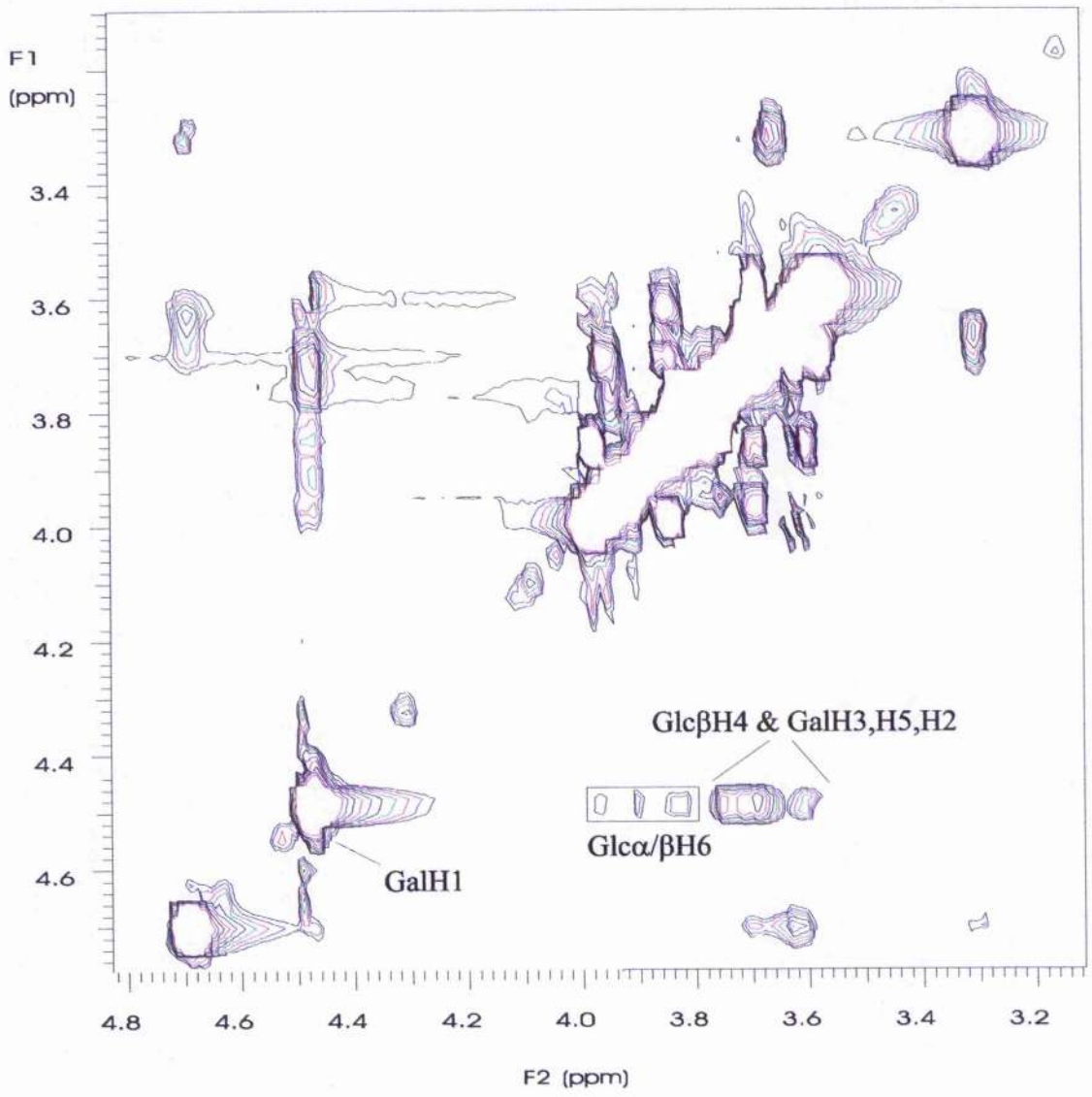

Figure 4.4 – 2D NOESY experiment for lactose

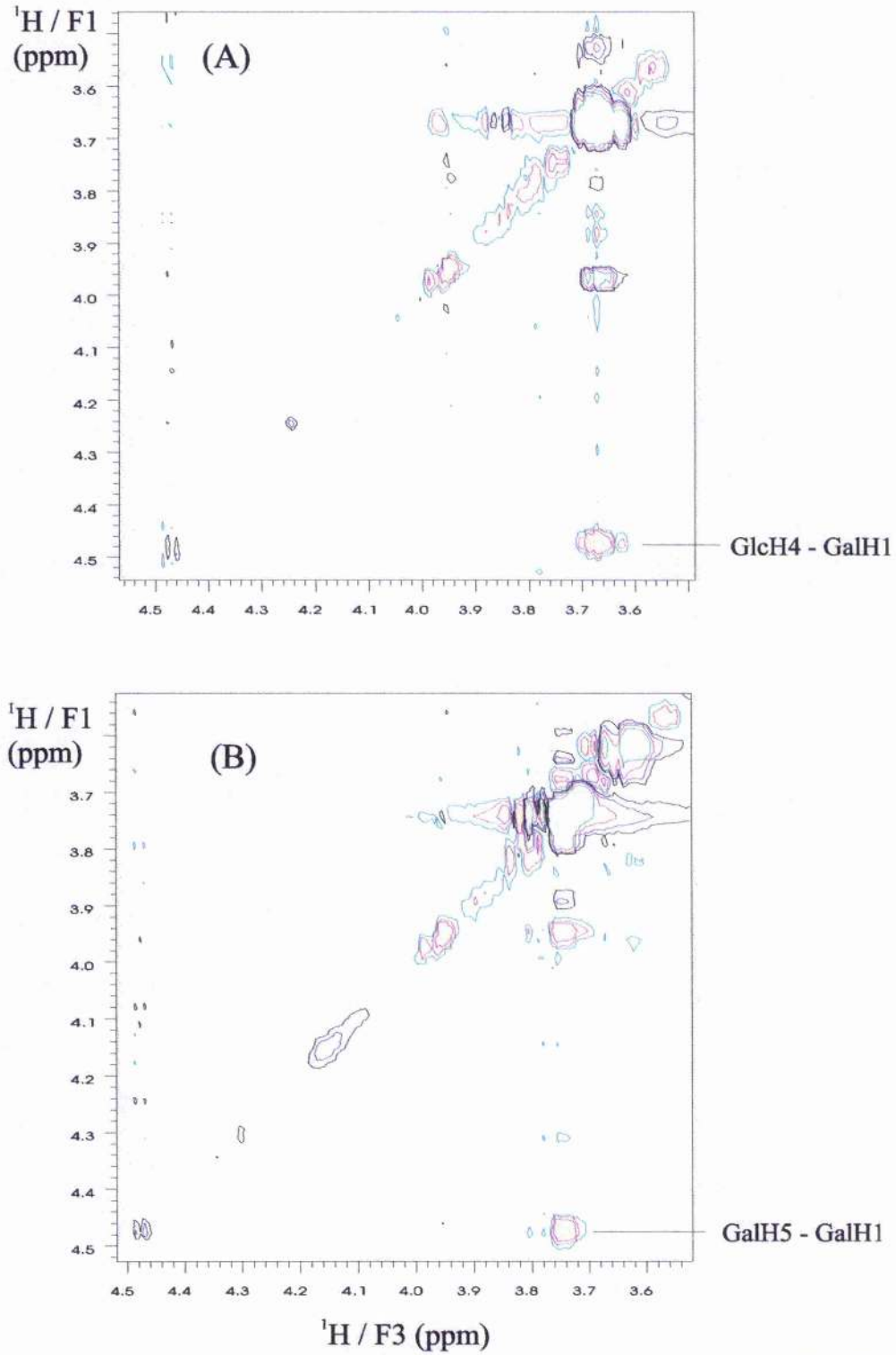

Figure 4.5 – F1F3 planes from the 3D NOESY – HSQC spectrum of [U-^{13}C] lactose at 303K at the ^{1}H chemical shifts of (A) Glc α/β C4 and (B) GalC5

4.3.2.2 ROEs involving Exchangeable Protons

Exchangeable protons in carbohydrates have been observed and used in conformational analysis for a long time. The majority of this work has been in the solvent DMSO-d_6 (Dabrowski, 1989, 1993), in which the exchangeable protons (OHs and NHs) do not exchange with the bulk solvent and therefore are observable at ambient temperature. More recently, work pioneered by Poppe and van Halbeek (Poppe, 1991), and Adams and Lerner (Adams, 1992), have allowed hydroxyl protons to be observed in a mixture of water and acetone-d_6. Harris *et al.* demonstrated that this fact allowed the measurement of proton NOEs to the hydroxyl protons (Harris, 1997).

Three additional transglycosidic homonuclear ^{1}H ROEs involving hydroxyl protons were measurable in Galβ1-4Glc at 258K. In these cases it was not necessary to resort to three-dimensional methods since the relevant hydroxyl protons were well resolved in conventional two-dimensional spectra. A section of the two dimensional ROESY spectrum of Galβ1-4Glc at pH 5.7 corresponding to the non-exchangeable region in F2 and the exchangeable proton resonances in F1, acquired using the excitation sculpting ROESY sequence, is shown in figure 4.6.

4.3.3 Quantitation of ROE data involving exchangeable protons

The extraction of quantitative distance information from cross-peak intensities is not straightforward. First, as discussed by James and co-workers (Liu, 1993), a loss of cross-peak intensity arises from exchange of magnetisation with solvent water. This is effectively a leakage process that affects only the diagonal elements of the relaxation matrix, and can be accounted for in a full relaxation matrix calculation of NOESY or ROESY intensities. A second problem concerns the saturation of the water magnetisation. If the water magnetisation is saturated prior to acquisition, substantial saturation transfer can occur from bulk solvent (which is in vast excess) to the solute during the acquisition period and relaxation delay. This can result in a substantial reduction in resonance intensity of exchangeable protons (Grzesiek, 1993; Li, 1993; Stonehouse, 1994).

Harris *et al.* showed that no compensation is needed for the degree of saturation, the 'effective' longitudinal relaxation of water (Harris, 1997). The exchange rates must be known as the exchange of hydroxyl protons with bulk water leads to a decrease in the observed NOE intensity. This effect must be taken into account. The exchange rates can be measured using a modified Adams and Lerner pulse sequence (Adams, 1992), and were measured for lactose (Table 4.2). The longitudinal relaxation rate of the hydroxyl protons can only be estimated since it cannot be readily separated from the exchange rate, which is usually much larger. Conventional T_1 measurements for the ^{13}C enriched disaccharide in dimethylsulfoxide suggest that the relaxation rate is

in the region 1.3 - 1.6s^{-1} for all the hydroxyl protons. The experimental and theoretical hydroxyl NOEs can be found in table 4.3.

4.3.4 Trans-glycosidic ^{13}C-^{13}C Coupling Constants

Carbon-carbon coupling constants have been measured using the quantitative J correlation method described by Bax (1992). Figure 4.7 shows F1 strips of the LRCC spectrum corresponding to the proton chemical frequencies of Gal-H1 and Gal-H2, with the one-bond correlations (reference peaks) and long range correlations corresponding to trans-glycosidic couplings indicated. The coupling constants were measured by taking a ratio of these correlations and the values obtained using this method are recorded in table 4.4.

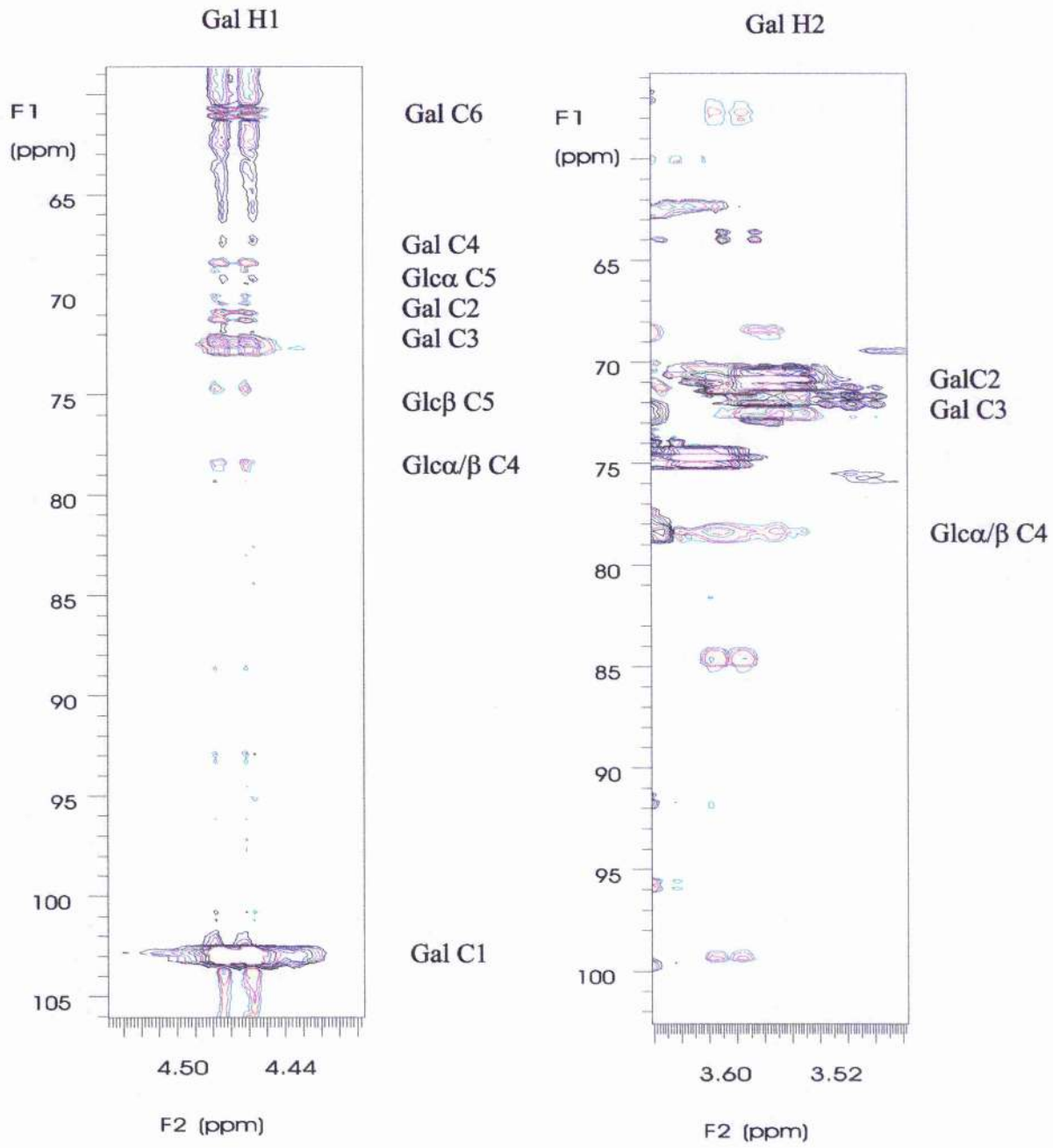

Figure 4.7 – F1 strips of the 2D ^{1}H-^{13}C LRCC spectrum at the ^{1}H chemical frequencies of Gal H1 and Gal H2

Table 4.3 – Summary of NOE results

NOE	Theoretical (%)	Experimental (%)[1]
GalH1-GalH3	1.78	2.02
GalH1-GlcH4	3.77	3.67
GalH1-GlcH6	0.08	0.18
GalH1-GlcH6'	0.17	0.37
GalH1-GalH5	4.82	5.24
GalH1-GlcHO3	0.14	0.50
GalH1-GlcHO6	0.15	0.27
GalOH2-GlcH6	0.84	0.81
GlcH1-GlcC1	-	0.21
GalH1-GlcC4	0.26	0.28
GalH1-GlcC6	0.05	0.05
GalH1-GlcC5	0.04	0.06
GalH1-GlcC3	0.04	

1) Estimated error ±10% of percentage NOE.

Table 4.4 – Summary of carbon-carbon Coupling

Coupling	Theoretical (Hz)	Experimental[1](Hz)
GalC2-GlcC4	2.3	2.5
GalC1-GlcC3	0.6	<1
GalC1-GlcC5	2.5	2.0

1) Estimated average error ± 0.5 Hz

Table 4.5 – Summary of Dipolar restraints

Dipolar coupling	Theoretical (Hz)	Experimental[1](Hz)
GalH1- GalC1	8.3	7.5
GalH3 – GalC3	6.9	7.9
GalH4 – GalC4	-4.6	-4.0
GalH5 – GalC5	7.7	8.0
GlcH1 – GlcC1	3.9	3.9
GlcH3 – GlcC3	3.9	3.9
GlcH5 – GlcC5	4.7	4.7

1) Estimated average error ±0.5Hz

4.3.5 Modelling

The NOE restraints summarised in table 4.3 were utilised as distance restraints in a dynamical simulated annealing protocol with ten random geometries of Galβ1-4Glc as input. A 5ns restrained MD simulation was computed, with restraints derived from the NOEs, and for the residual dipolar couplings for the glucose moiety only. The time-averaged inter-glycosidic NOEs involving exchangeable protons were calculated over the course of the simulation, using a full relaxation matrix analysis appropriate for fluctuating inter-nuclear distances due to internal motions which are rapid with respect to overall isotropic tumbling (Tropp, 1980; Homans and Forster, 1992).

The rotation about the C5-C6 bond of oligosaccharides is slow with respect to overall tumbling (Nishida, 1984). This becomes important as one of the NOE restraints involves the OH6 of glucose which is affected by the slow rotation. In order to account for this it is necessary to carry out two simulations with the dihedral angle ω about C5-C6 bond constrained to two conformations, gg (180°) and gt (-60°) that are observed to exist in the disaccharide (Nishida, 1984). The in house written program, MDNOE2 was used to back calculate the NOEs for each simulation and a weighted average [gg (66%) and gt(34%)] was then taken over the two simulations. The resulting torsional fluctuations about φ and ψ lie within a global energy minimum region (figure 4.8).

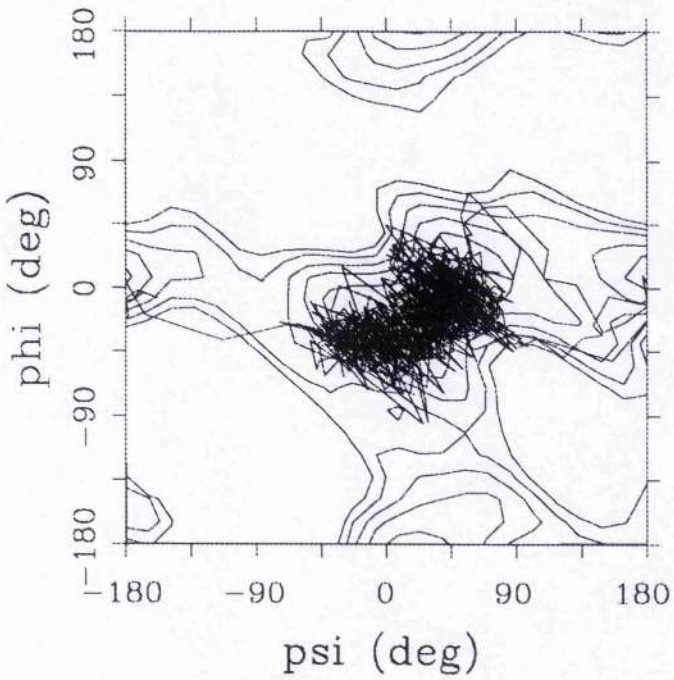

Figure 4.8 – Instantaneous values of the glycosidic torsion angles φ and ψ over the 5ns restrained molecular dynamics simulation *in vacuo* for Galβ1-4Glc

4.3.6 Assessment of model

Long range spin-coupling constants and residual dipolar coupling constants were back calculated in order to assess the model proposed from the molecular dynamics simulation. Tables 4.4 and 4.5 list the experimental and theoretically back calculated values for these parameters. As can be seen the theoretical values are in good agreement with the experimental values, indicating that the model is consistent with both parameters.

4.4 Conclusions

The three-dimensional structure and dynamics of Galβ1-4Glc have been investigated using time-averaged NOE restraints between ^{1}H, ^{1}H; ^{1}H, $O^{1}H$; and interglycosidic ^{1}H, ^{13}C. A molecular dynamics simulation was carried out incorporating these as well as residual dipolar restraints. Long range spin-coupling constants as well as the remaining residual dipolar couplings were used to assess the model. The additional NOEs provided by the low temperature studies are much more sensitive to conformation than the NOEs involving non-exchangable protons alone. The latter, by their nature, involve protons close to the glycosidic linkage, where as NOEs involving OH protons in oligosaccharides are not necessarily close to the glycosidic linkage. The residual dipolar coupling restraints prove useful for purposes of back calculation and agree quite well with the proposed model.

Heteronuclear NMR investigations of the solution behaviour of lactose have distinct advantages over purely homonuclear methods. In particular complete unambiguous assignment of NOE cross-peaks was possible using a three-dimensional NOESY-HSQC. The additional restraints obtained from NOE spectra at low temperature between protons and hydroxyl protons along with the interglycosidc ^{1}H-^{13}C NOEs (chapter 2) allowed the use of time-averaged restrained molecular dynamics simulations. This is more appropriate than conventional modelling strategies for simulating oligosaccharides that are known to undergo significant conformational fluctuations between two or more low energy structures.

Using all the distance restraints in a restrained molecular dynamics simulation, the torsional fluctuations predicted lie within the global minimum energy region of the glycan. The agreement of the back calculated data are sufficient to suggest that the flexible model is consistent with the experimental data.

Chapter 5

Other NMR techniques being developed for probing the Conformation of Oligosaccharides

Abstract

The first part of the chapter describes the measurement of three-bond ^{1}H-^{13}C scalar coupling constants between ring carbons and hydroxyl protons to probe the existence of an intra-molecular hydrogen bond in Galβ1-4Glc. Two pulse sequences were compared; firstly a Heteronuclear Single Quantum coherence (HSQC) experiment with gradient tailored water suppression, and secondly a gradient refocused Heteronuclear Multiple Quantum Coherence (HMQC) experiment. Experiments were carried out in mixed solvent and at 258 K in order to observe the hydroxyl protons. Under those conditions the results indicated the existence of a hydrogen bond.

The second part of the chapter describes the direct measurement of angles between bond vectors using relaxation via cross-correlated dipolar couplings. Angles can be determined directly by using the effects of dipole-dipole cross-correlated relaxation of double quantum and zero quantum coherences. This approach leads to angular information without the need for calibration of a Karplus-type curve, as is the case for scalar coupling measurements. A proton detected INADEQUATE experiment was used for the measurement of the projection angles between the C-H vectors in fully ^{13}C labelled lactose, in order to assess the viability of this method for oligosaccharides. It was demonstrated that the measurement of cross-correlated relaxation effects is potentially useful for the characterisation of oligosaccharides.

5.1 Measurement of three-bond ^{1}H-^{13}C J coupling constants to probe the existence of intramolecular hydrogen bonds.

5.1.1 Introduction

The presence of intramolecular hydrogen bonds in crystals has been well documented (Jeffrey and Saenger, 1991). However their importance in contributing to the shape of carbohydrate molecules in water has not as yet been satisfactorily demonstrated experimentally. Although hydrogen bonding of labile NH protons in aqueous solutions of proteins and nucleic acids has been thoroughly investigated (Wuthrich, 1986), under normal conditions in carbohydrates, hydroxyl protons are in fast chemical exchange with water which severely limits their use as conformational probes (Dabrowski and Poppe, 1989).

Various approaches have been adopted in an effort to confirm or deny the existence of hydrogen bonds. It has been observed, in studies carried out on model compounds such as alcohols, that hydrogen bonding causes a downfield change in chemical shift of the involved protons, and that an increase in temperature causes an up-field change (Pople *et.al.*, 1959). Coupling constants and nuclear Overhauser enhancement (NOE) measurements have been used to establish whether or not a particular hydrogen bond is sterically possible. Correlation times of ^{13}C nuclei may vary, if intramolecular hydrogen bonds restrict their motions (McCain and Markley, 1986, 1987). Changes in chemical shift and relaxation time are merely suggestive of hydrogen bonding and therefore these parameters cannot be relied upon as definite evidence. A hydrogen bond may be responsible for decreasing the temperature

sensitivity of the chemical shift, or for restricting rotation about the C-O bond and reducing the exchange rate with water for such a nuclei, however other factors may be involved in producing any of these observations.

More direct evidence for the existence of hydrogen bonding comes from NMR parameters for the hydroxyl protons involved. A study was carried out for sucrose (Sheng, 1995), which included the comparison of hydroxyl proton chemical shifts, temperature coefficients and vicinal coupling constants of the hydroxyl protons. A two-dimensional ROESY experiment was used to seek evidence for any direct chemical exchange between hydroxyl protons possibly involved in intra-molecular hydrogen bonds. This study showed the transient existence of an inter-residue hydrogen bond in sucrose in aqueous solution, which was in conflict with the findings of a previous study (Adams and Lerner, 1991).

It has often been speculated that intra-molecular hydrogen bonds are overwhelmed by solvation of OH protons with solvent water. Williams and co-workers calculated the energetics of a hydroxyl to hydroxyl hydrogen bond to be virtually the same as that for a hydroxyl to water bond (Cox, 1991). From this it is questionable whether the intra-residue hydrogen bond could in fact supply the needed stabilisation.

5.1.2 Three-bond ^{1}H-^{13}C coupling constants as probes for the existence of hydrogen bonds

The measurement of three-bond ^{1}H-^{13}C coupling constants is another possible means of gaining evidence as to the existence of inter-residue hydrogen bonding.

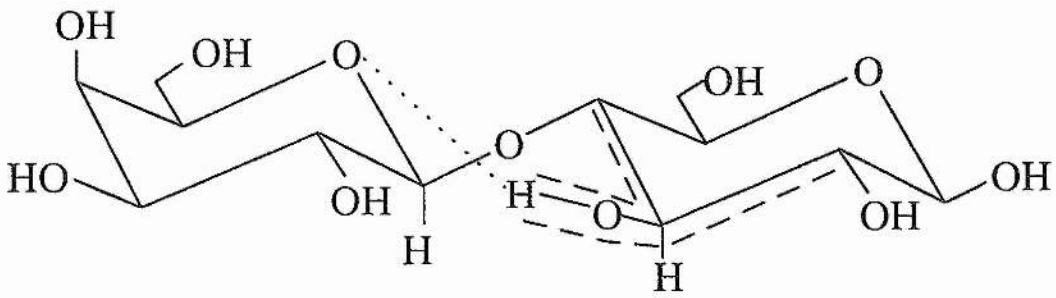

Figure 5.1: Galβ1-4[U^{13}C, ^{2}H Glc]; the dashed line represents a hydrogen bond, and the broken lines represent three bond coupling constants.

In the presence of a hydrogen bond between OH3 of the glucose and the ring oxygen of the galactose (dashed line, figure 5.1), the probability of the three bond coupling constants between C2 → OH3 and C4 → OH3 (indicated by the broken lines) being different is very high. If however there is no hydrogen bond, the hydroxyl proton will be able to freely rotate and therefore the coupling constants between C2 → OH3 and C4 → OH3 will be average values.

5.1.3 Observation of Hydroxyl protons

The application of exchangeable protons in conformational studies of carbohydrates is well documented (Dabrowski, 1989; Acquotii, 1990; Poppe, 1991; Poppe, 1992; Sicinska, 1993; Poppe, 1994; Lynch, 1996). Unfortunately, at room temperature in aqueous solutions, hydroxyl protons are in fast exchange, resulting in hydroxyl proton signals occurring under the water resonance. Using DMSO-d_6 as solvent allows hydroxyl proton resonances to be readily observable at room temperature. However there are problems with the use of DMSO-d_6; first, and of particular relevance for this study, DMSO-d_6 is well known for assisting in the formation of hydrogen bonds, yielding conformations about the glycosidic linkage not seen in aqueous solutions (Dabrowski and Poppe, 1989; Acquotti, 1990; Ejchart and von der Lieth, 1992; Dabrowski *et.al.*, 1993). An example of this can be seen with Galβ1-3GlcOMe. A hydrogen bond is observed between Gal-OH2 and Glc-OH4 that helps drive the conformation into the anti-configuration about the glycosidic linkage, where the two glycosidic C-H bonds are turned from each other by approximately 180° (Dabrowski, 1995). Second, only small oligosaccharides are soluble in DMSO-d_6 limiting the application of this approach.

In order to measure parameters involving the hydroxyl protons, the sample was dissolved in a mixed solvent of water and acetone, this enabling experiments to be carried out at a lower temperature (258 K), overcoming the problem of fast exchange (Poppe, 1991; Poppe, 1994; Harris, 1997). At this temperature, the

hydroxyl proton resonances are readily observable with exchange rates around $10s^{-1}$ or less, which is sufficiently slow that narrow line widths are obtained.

5.2 Choice of experimental scheme

5.2.1 Water Suppression

A pre-requisite for the observation of the exchangeable proton resonances is an efficient method of suppressing the water signal. Several approaches to water suppression can be taken. The most conventional approach involves on-resonance pre-saturation of the water resonance with the ^1H carrier set to the water frequency. To gain digital resolution in the acquisition domain, the carrier may be positioned in the centre of the hydroxyl region and off-resonance DANTE pre-saturation applied (Kay, 1989). However pre-saturation can lead to severe attenuation of the hydroxyl resonances. This problem is avoided by adopting pulse schemes which do not perturb the spin population of water during the relaxation delay such as jump and return (Griffey, 1985) or 11-echo (Sklenar and Bax, 1987) selective excitation schemes. Alternatively, a spin-lock purge pulse may be used to de-phase the transverse component of the water magnetisation in the inhomogeneous radio-frequency field (Messerle, 1989). These methods however suffer from low water suppression in a single acquisition. Phase cycling can be used to remove the residual water effectively, but its signal amplitude restricts the receiver gain and consequently the attainable S/N ratio. The use of pulsed gradients of static magnetic field (Knuttel, 1990; Davis, 1992), allows efficient selection of coherence pathway and removes the need for phase cycling. Such a method however suffers from a two-fold reduction in

sensitivity because only one of two symmetrical coherence transfer pathways contribute to the observed signal.

5.2.2 Gradient Tailored Water Suppression in ^{1}H-^{13}C HSQC

The scheme shown in figure 5.2 is based on a gradient tailored water suppression technique for ^{1}H - ^{15}N HSQC experiments (Sklenar, 1993). Indirect detection provides substantial improvement in sensitivity due to the difference in magnetogyric ratio and faster relaxation of protons compared to carbons. The Heteronuclear Single Quantum Coherence experiment (HSQC) offers increased resolution in the carbon dimension as the heteronuclear dipolar broadening is smaller than the broadening of multiple quantum coherence in the HMQC and also in the HSQC ^{1}H - ^{13}C scalar coupling is removed. The pulse sequence of figure 4.2 has the advantages that the carrier frequency can be placed in the hydroxyl region which maximises digital resolution in the acquisition domain, also the excitation scheme gives uniform excitation across the hydroxyl region and therefore full sensitivity is retained. Rather than using gradient pulses to select the appropriate coherence transfer pathway, the gradient pulses are exploited to remove the unwanted coherences. In the Water Suppression by Gradient Tailored Excitation (WATERGATE) scheme (Grzesiek, 1993), all coherences uniformly excited by a $\pi/2$ non-selective pulse are de-phased by the first field gradient. Only coherences that experience selective π rotation by the selective sandwich, are rephased by the second gradient. Therefore by setting the selective π sandwich to rotate the resonances of interest, all unwanted resonances are removed. As demonstrated for 2D NOE spectroscopy (Wang, 1987) a non-

selective π pulse flanked by two selective π/2 pulses can be used for efficient water suppression. The required frequency shift of the selective π/2 pulse pair can be obtained by simultaneous amplitude and phase modulation, however this experiment is rather problematic to adjust. Use of hard pulse sequences modified for off resonance water suppression offers a better alternative.

5.2.3 Gradient refocused multiple bond heteronuclear HMQC

An alternative approach for measuring three-bond coupling constants is to use the pulse sequence shown in figure 5.3. This pulse sequence is essentially a regular heteronuclear multiple quantum coherence experiment (HMQC) but with additional ^{13}C 180° pulses and gradients. This pulse sequence allows the use of field-gradient pulses and at the same time pure-absorption line shapes are retained. The basic requirement for retaining absorption-mode line shapes is that symmetrical pathways with coherence order $p = \pm n$ are retained during t_1 (Bodenhausen, 1984). In order to achieve this it is necessary to record two separate spectra. In the first spectrum, suitable field gradients are used to select the pathway which has coherence order $+n$ during t_1 and -1 during t_2, this is known as the echo or N-type spectrum (Nagayama, 1979). In the second spectrum $-n$ is selected in t_1 and -1 during t_2, this is known as the antiecho or P-type spetrum. It is then possible to combine these two spectra during data processing to yield an absorption-mode spectrum (Bachman, 1977; Keeler, 1985). In the case of the HMQC pulse sequence in figure 5.3, the P and N-type spectra can be recorded simply by inverting the sense of the final gradient (Davis, 1992). The gradient pulse that is used to select heteronuclear multiple

quantum coherence during t_1 is split into two equal parts, i.e. the first two gradients are applied in the same sense. The ^1H magnetisation experiences no net dephasing as the ^1H chemical shift is refocused by the ^1H 180° pulse. However the ^{13}C magnetisation is dephased during this period because there are two ^{13}C 180° pulses. As a result the final gradient rephases the ^{13}C magnetisation but dephases the ^1H magnetisation in t_1, which corresponds to the water resonance. This sequence therefore offers a suitable alternative to measuring long range ^1H-^{13}C couplings with water suppression.

Both the HSQC with WATERGATE suppression and the gradient-refocused multiple bond HMQC experiments were used to measure the three bond heteronuclear coupling constants in order to obtain a comparison.

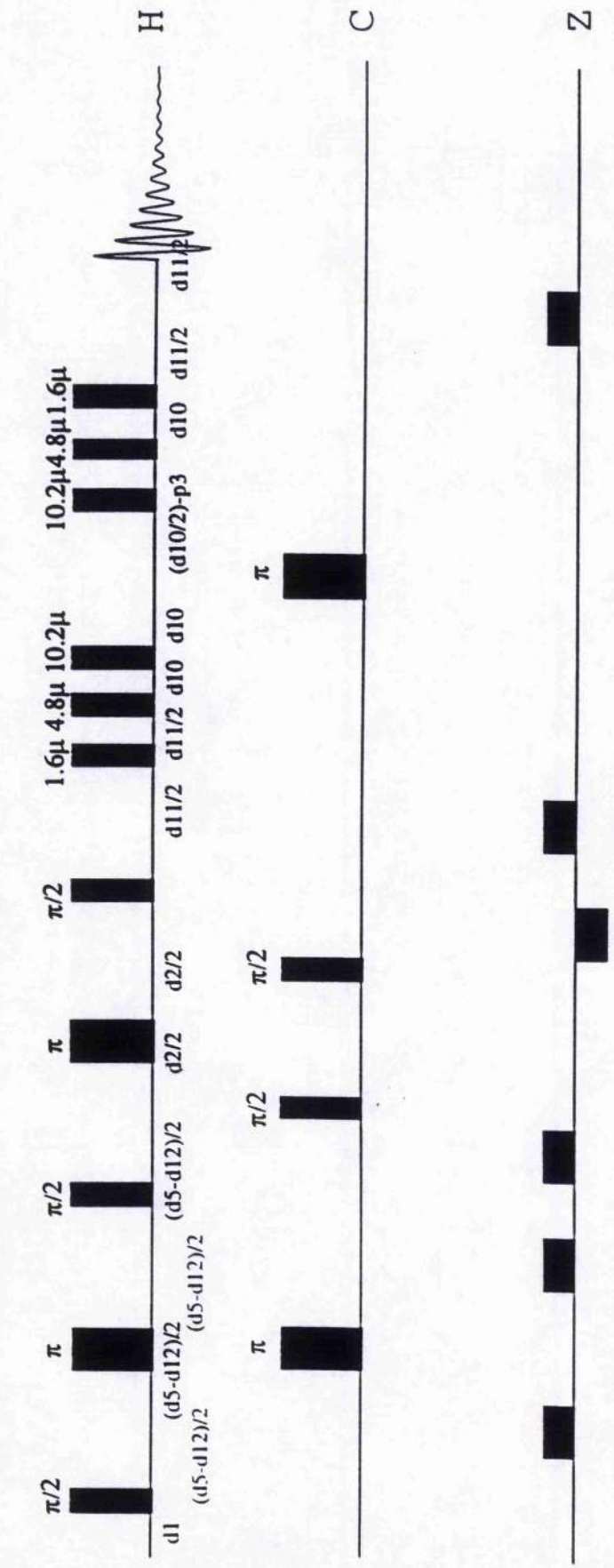

Figure 5.2 - HSQC with gradient tailored water suppression

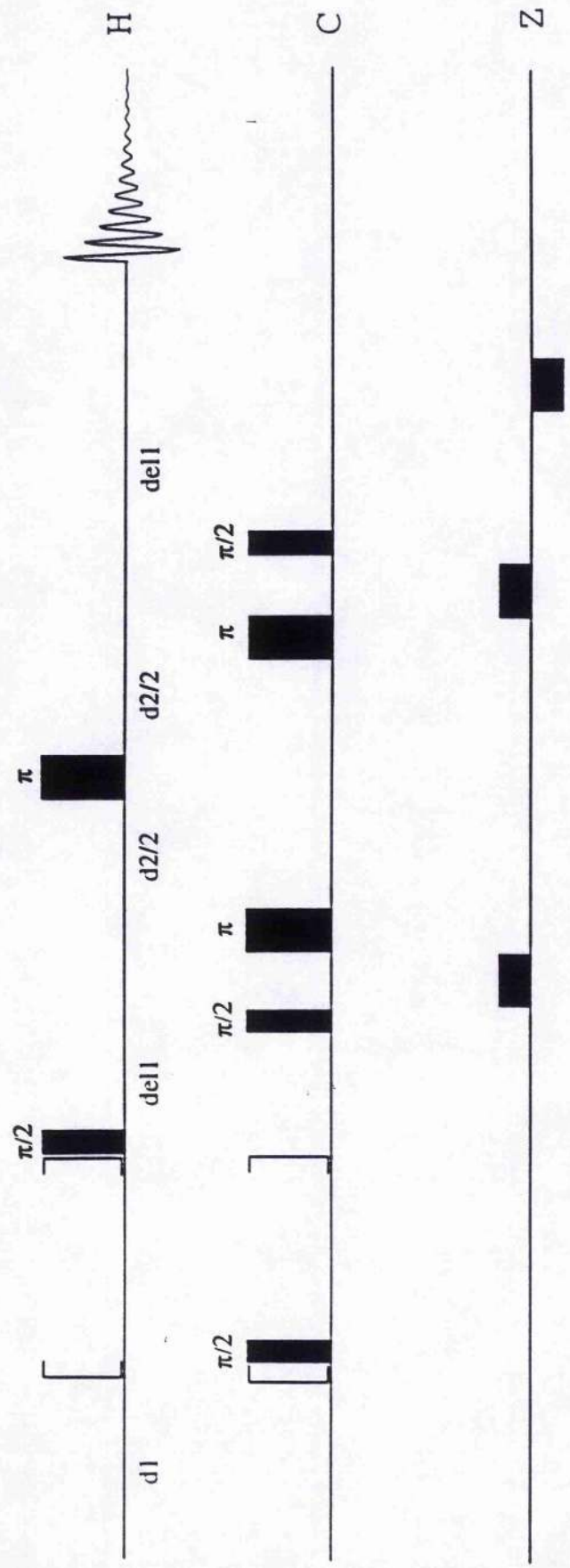

Figure 5.3 - Gradient refocused multiple bond HMQC

5.3 Materials and Methods

5.3.1 Sample Preparation

Preparation of Galβ1-4[U-^{13}C-^{2}H]Glc

Chemoenzymatic synthesis was performed in 2.5ml solution containing 10 mM UDP-galactose and 10 mM U-^{13}C, ^{2}H glucose in 50 mM phosphate buffer (pH 7.4). One unit of galactosyltransferase was added with 1 mM lactalbumin and Mn^{2+} to a concentration of 5 mM, and the mixture was incubated at 37°C overnight. The disaccharide product was purified by Biogel P-2 column (2.5 cm × 100cm) chromatography, with H_2O as eluant.

Preparation of samples for NMR

Samples were prepared using a shortened version of the method originally proposed by Adams and Lerner (Adams, 1992). Galβ1-4[U-^{13}C-^{2}H]Glc (~10mg) was dissolved in 625µl of HPLC grade water, and the pH was adjusted to ~5.6 by careful step-wise addition of dilute HCl or NaOH. This was transferred to an NMR tube and 125µl of Acetone-d_6 (Cambridge Isotopes), was added. The sample was degassed by sonication for about one minute. [U-^{13}C-^{2}H]Glc was prepared in the same way.

5.3.2 NMR Experiments

NMR spectra were obtained at 258K with a reference frequency of 500.12 MHz on a Varian Unity^{+} spectrometer equipped with a self shielding z gradient triple resonance probe. All NMR spectra were recorded using the schemes of figure 5.2 or 5.3. The probe temperature was 258K in all experiments. A total of 128 and 1024 complex

points were acquired in the t_1 and t_2 dimensions respectively, with spectral widths of 2000 Hz for both ^{13}C and ^{1}H dimensions. 64 scans were acquired per increment and the total experimental time was ~11 hours for the HSQC and 10hours for the HMQC experiments.

5.4 Results and Discussion

The hydroxyl region of the long-range gradient refocused HMQC spectra and the long-range HSQC with WATERGATE suppression is shown in figure 5.4. Both pulse sequences gave similar results, however the gradient refocused HMQC experiment gave a better signal to noise ratio and was slightly more effective in terms of water suppression. Using ^{13}C labelling increased the sensitivity of the experiment. Using ^{2}H labelling removed undesirable ^{1}H-^{1}H couplings.

A HMQC experiment was run for [U-^{13}C, ^{2}H] glucose, (figure 5.5) in order to compare the peak volumes of GlcOH3β-GlcC2β with GlcOH3β-GlcC4β in a system where no intra-molecular hydrogen bond could exist. As expected the peak volumes for the GlcOH3β-GlcC2β and GlcOH3β-GlcC4β for glucose are the same indicating an average value and hence the expected free rotation of the hydroxyl proton.
The results for lactose are ambiguous as a result of resonance overlap. The cross peak that corresponds to GlcOH3β-GlcC3β is overlapped with that for GlcOH3β-GlcC2β, the latter being of prime importance for the purposes of this study. The peaks show couplings to two carbons leading to a triplet-splitting pattern; these couplings are not easily removed when using either of the pulse sequences described.

However with a carbon chemical shift for C2β of 73.76ppm and for C3β of 74.5ppm, the outer part of the GlcOH3β-GlcC2β triplet would be expected to be visible. Close inspection of the GlcOH3β-GlcC2β region indicates that this cross peak is close to zero and is probably of a lower intensity than the GlcOH3β-GlcC4β cross peak which is clearly measurable (figure 5.4A). Unfortunately it is not possible to quantify accurately the cross peak for C2 as a result accurate values for the coupling constants cannot be obtained.

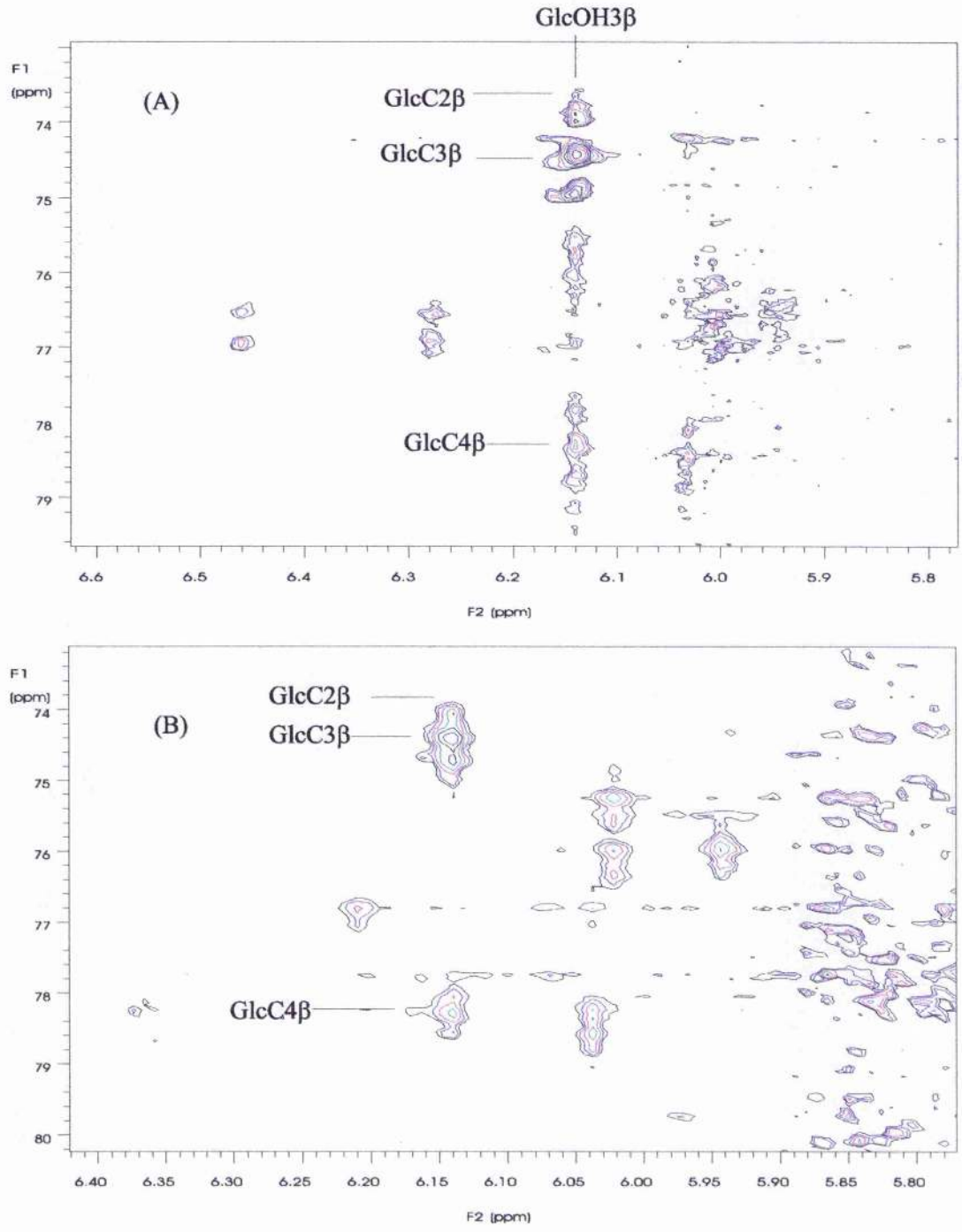

Figure 5.4 – Sections of (A) gradient refocused HMQC and (B) HSQC with WATERGATE suppression, for lactose

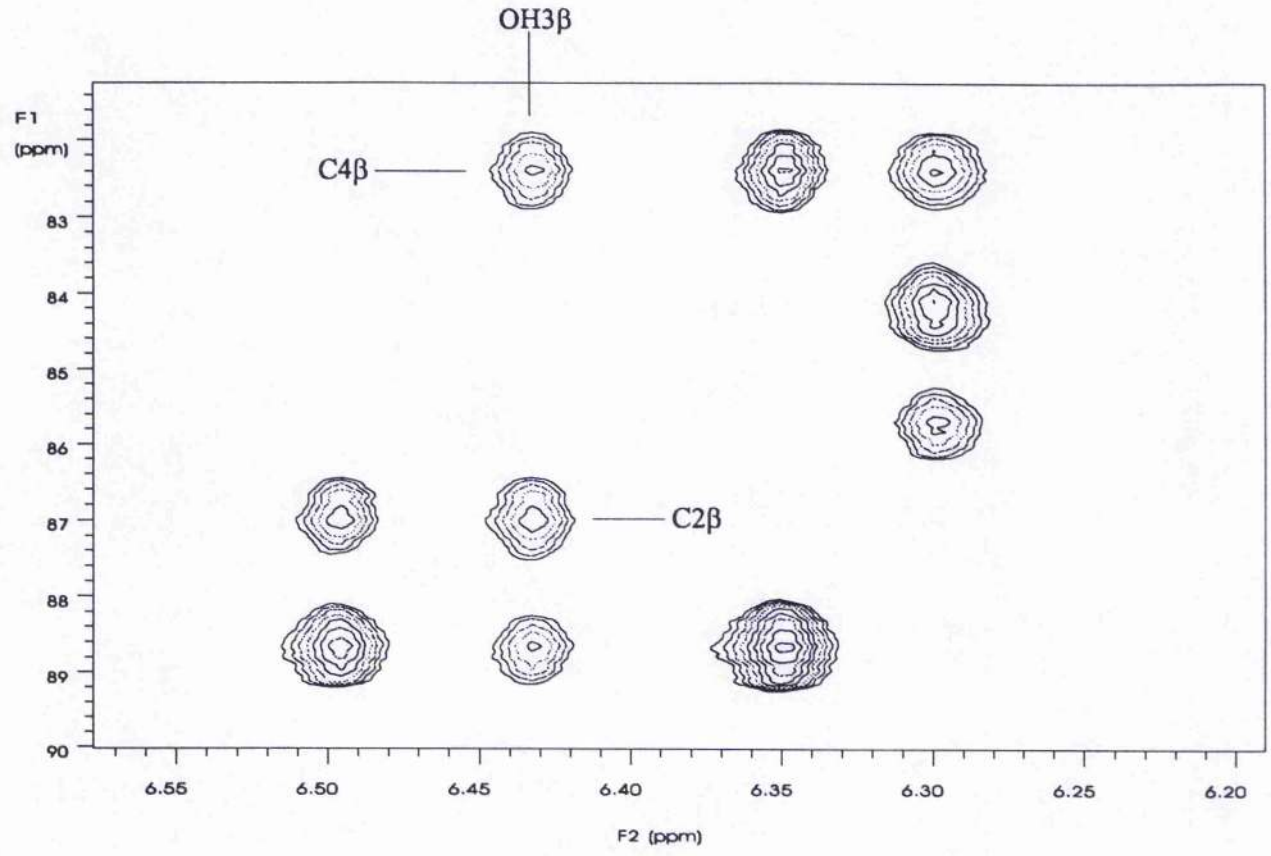

Figure 5.5 – Gradient refocused HMQC for glucose

5.5 Conclusions

Due to spectral overlap and the absence of a Karplus curve for this system, it is not possible to obtain definitive information as to the presence or not of a hydrogen bond in Galβ1-4Glc. However the chemical shift difference between GlcβC2 and GlcβC3 should be sufficient to observe some part of the GlcOH3β-GlcC2β multiplet and therefore the absence of such a peak indicates that this coupling constant is close to zero. This is in contrast to the GlcOH3β-GlcC4β coupling constant, where there is clearly a measurable peak. These results would therefore suggest that under these

conditions, there is a hydrogen bond from GlcOH3 to the ring oxygen of the Galactose. Clearly this conclusion is only of a qualitative nature and is thus limited. The principle limitations of the method as it stands is the requirement for >10mg of ^{2}H, ^{13}C labelled sugars due to a relatively low sensitivity, and the difficulty in either of the pulse sequences used to remove the ^{13}C-^{13}C coupling that exacerbates the overlap problem. Despite these problems it has been demonstrated that this approach could provide useful information as to the presence or not of intra-molecular hydrogen bonds.

5.6 Direct Measurement of Angles between Bond Vectors using relaxation via cross-correlated dipolar couplings

5.6.1 Introduction

Here a method is presented for determining the angles between two vectors connecting two pairs of nuclei within a carbohydrate molecule. The method relies on relaxation via cross-correlated dipolar couplings between the four nuclei that form the two inter-nuclear vectors under consideration. In solid-state NMR, dipolar couplings have been widely used to determine inter-tensorial angles (Linder, 1980; Feng, 1994; Schmidt-Rohr, 1996). However their use in solution NMR has been far less (Brüschweiler, 1989) as cross-correlation relaxation has generally been considered more of a disturbance to high-resolution NMR spectra than as a potentially valuable source of information. Dipolar couplings, which constitute the through space magnetic interaction between two nuclei are an effective source of relaxation of spin coherences. The efficiency of the relaxation depends on the time correlation of the dipolar coupling with itself (auto-correlation) or with another dipolar coupling (cross-correlation) (Werbelow, 1974). Here, we look at the interaction between carbon-proton pairs in glucose.

5.6.2 Theory

Longitudinal magnetisation is entirely due to population differences of the nuclear spin states. Longitudinal relaxation therefore involves population changes and it follows that the processes that bring it about are those that induce transitions between the spin states. The processes that cause relaxation are those of energy

exchange. Energy is directly exchanged between one set of energy levels (the nuclear spin system) and energy levels generally provided by the various translations, rotations, and internal motions of the molecules that constitute the sample. In order to mediate this energy transfer, the motion (or other change) that is to gain or lose the energy from the nuclear spin transition must itself cause a fluctuating magnetic field at the site of the nuclear spin involved. This fluctuating field must have a component fluctuating at the frequency corresponding to the transition to be relaxed.

The field experienced by a given nucleus is considered to be the vector sum of B_o, the applied static magnetic field, and the local field, B_{loc}.

$$B_{Total} = B_o + B_{loc} \qquad [5.1]$$

B_{loc} consists of the varying part of the total field, and it arises due to Brownian motion and other random changes within the lattice. Key properties of the local field are that it is incoherent across the sample, and that it has components at many frequencies reflecting the spectrum of frequencies present in the Brownian motion of the lattice. Several relaxation mechanisms contribute to B_{loc}, including dipole-dipole relaxation, quadrupolar relaxation and chemical shift anisotropy relaxation. Relaxation behaviour can be thought of as the pair-wise summation over all two-spin interactions of the various mechanisms acting to relax a particular spin. Treatment of relaxation in this way, overlooks the concept of cross-correlated relaxation. A qualitative explanation of what is meant by cross-correlated relaxation may be

achieved by considering the example of a $^{13}CH_2$ group: The motion of ^1H_A relative to ^{13}C, if considered independently, is of itself random (likewise ^1H_B relative to ^{13}C). However, these two motions are not completely random with respect to each other, since preservation of the molecular structure necessarily limits those relative motions of ^1H_A, ^1H_B, and ^{13}C that are possible. Such motions are said to be cross-correlated. The relaxation of the central carbon nucleus depends on the fluctuating field it experiences due to the two protons moving around it randomly, but in a cross-correlated fashion, as the molecule tumbles. A simple two-spin treatment tells you correctly what the influence of each proton is separately, but because of the cross-correlation, simple addition of their contributions will not give a totally complete picture. A more rigorous explanation of cross-correlation and its effects on relaxation can be found in a paper by Werbelow (Werbelow, 1974).

For a diamagnetic sample composed of spin ½ nuclei, there are two kinds of interactions between which cross-correlated induced relaxation can occur; dipole-dipole (DD) and chemical shift anisotropy (CSA), where CSA refers to the orientation dependence of the chemical shift. The two most frequently encountered cross-correlated relaxation effects, are either between two dipolar coupling (DD/DD), or between one dipolar coupling and CSA (CSA/DD).

Double quantum coherence involving the carbon transitions can be excited and indirectly detected which yields the scalar coupling between the proton and carbon. The relaxation rates $R_{\mu\nu}$ for the four transitions that are reflected in the line widths are given by the following equations (Abragam, 1961)

$$R_{\alpha\beta} = R^a - R_i^{CSA/DD} + R_j^{CSA/DD} - R_{i,j}^{C} \quad [5.2]$$

$$R_{\alpha\alpha} = R^a + R_i^{CSA/DD} + R_j^{CSA/DD} + R_{i,j}^{C} \quad [5.3]$$

$$R_{\beta\beta} = R^a - R_i^{CSA/DD} - R_j^{CSA/DD} + R_{i,j}^{C} \quad [5.4]$$

$$R_{\beta\alpha} = R^a + R_i^{CSA/DD} - R_j^{CSA/DD} - R_{i,j}^{C} \quad [5.5]$$

The indices i and j denote the two C-H vectors, R^a defines the contributions due to auto-correlated relaxation for the individual spectral lines. $R_i^{CSA/DD}$ and $R_j^{CSA/DD}$ describe the sum of all interactions due to dipole-CSA cross-correlated relaxation for the $C\text{-}H_i$ and $C\text{-}H_j$ vector, respectively, where CSA is the chemical shift (shielding) anisotropy that refers to the orientation dependence of chemical shifts. $R_{i,j}^{C}$ is the desired contribution resulting from dipole-dipole cross-correlated relaxation.

$R_{i,j}^{C}$, $R_i^{CSA/DD}$ and $R_j^{CSA/DD}$ can be determined from the intensities of the corresponding resonance lines in the INADEQUATE experiment (see experimental section), using the following equations.

$$R_{i,j}^{c} = \frac{1}{4}T * \ln\left[\frac{I(\alpha\beta) * I(\beta\alpha)}{I(\alpha\alpha) * I(\beta\beta)}\right] \quad [5.6]$$

$$R_i^{CSA/DD} = \frac{1}{4}T * \ln\left[\frac{I(\alpha\beta) * I(\beta\beta)}{I(\alpha\alpha) * I(\beta\alpha)}\right] \quad [5.7]$$

$$R_j^{CSA/DD} = \frac{1}{4}T * \ln\left[\frac{I(\beta\beta) * I(\beta\alpha)}{I(\alpha\alpha) * I(\alpha\beta)}\right] \quad [5.8]$$

where T is the delay in the experiment during which double-quantum coherence evolves. I(αα), I(αβ), I(βα), and I(ββ) are the intensities of the corresponding resonance lines in the spectrum (Reif, 1997).

If a molecule tumbles sufficiently slowly in solution, the cross-correlated dipolar relaxation depends on the angle θ between the two bond vectors (Werbelow, 1974; Cavanagh, 1996) according to

$$R_{i,j}^{C} = \left[\frac{\gamma_H \gamma_C}{(r_{CH})^3}\right]^2 \left(\frac{\eta\mu_0}{4\pi}\right)^2 * \frac{2}{5}\left(3\cos^2\theta - 1\right) * \tau_c \quad [5.9]$$

The gyromagnetic ratios γ_H and γ_C are nuclear properties, the one-bond distances are known, and the other constants are natural constants. The correlation time of the molecule (τ_c) can be determined from relaxation measurements and therefore θ can be calculated.

5.6.3 Proton Detected INADEQUATE experiment

The pulse sequence shown in figure 5.6 is a proton detected INADEQUATE experiment (Bax, 1980; Kiddle and Homans, unpublished). The pulse sequence results in a spectrum showing correlations for all pairs of covalently bound ^{13}C atoms. Although a natural abundance level experiment has advantages in terms of spectral simplicity, often there is a sensitivity problem. Various approaches have been take in order to improve the sensitivity of this experiment, including combinations with INEPT and DEPT type polarisation transfers from ^{1}H to ^{13}C (Sørensen, 1982; Sparks, 1985; Podkorytov, 1990). Also Keller and Vogele (Keller, 1986) detected ^{1}H magnetisation by doing the opposite polarisation transfer at the end of the INADEQUATE pulse sequence. However, it is the addition of pulsed-field gradients that greatly ease the suppression of the intense ^{1}H signals stemming from molecules with less than two ^{13}C atoms that has made the largest improvement to ^{1}H-detected INADEQUATE experiments (Gosser, 1993; Chung, 1993; Reif, 1996). The gradients provide gradient echo refocusing which utilises the fact that double quantum coherence is twice as sensitive to the gradients as the single quantum coherence in order to select the desired magnetisation. In order to get the required result the delays in this experiment were carefully adjusted. In period (1) the carbon chemical shift evolves during 2δ, J_{CH} is refocused by the ^{1}H π pulse, and J_{CC} evolves during 2T. Analysis of the sequence by the product operator formalism indicates that T is involved with both sine and cosine terms, as a result a compromise value of T=3ms was used. The $\pi_y/2$ pulse at the start of period (2) gives double quantum coherence, and double quantum coherence is modulated during d2. The additional π

pulse allows the gradients in period (2) to be split into two separate gradients of opposite sense to allow for the gradient refocusing. J_{CC} evolves during the constant time delay (2CTD) and is cosine modulated. Therefore setting $2CTD=1/J_{CC}$ gives an optimum value for CTD of 10ms or a whole number multiple thereof. Careful analysis of this section of the pulse sequence using the product operator formalism highlights a potential problem. Carbon atoms C2-C5 of glucose are coupled to two ^{13}C nuclei, C1 and C6 are coupled only to one ^{13}C. This fact becomes important because of the cosine modulation of the terms $2CTD\cos\pi J_{CC'}$ which refers to the cosine modulation of the first carbon coupling and $2CTD\cos\pi_{CC''}$ which refers to the cosine modulation of the second coupling. Due to the fact that $\cos\pi/2 = -1$, the carbons which experience two couplings (i.e. both terms) come out with opposite signs ($-1\times-1=+1$) to those which experience just one coupling.

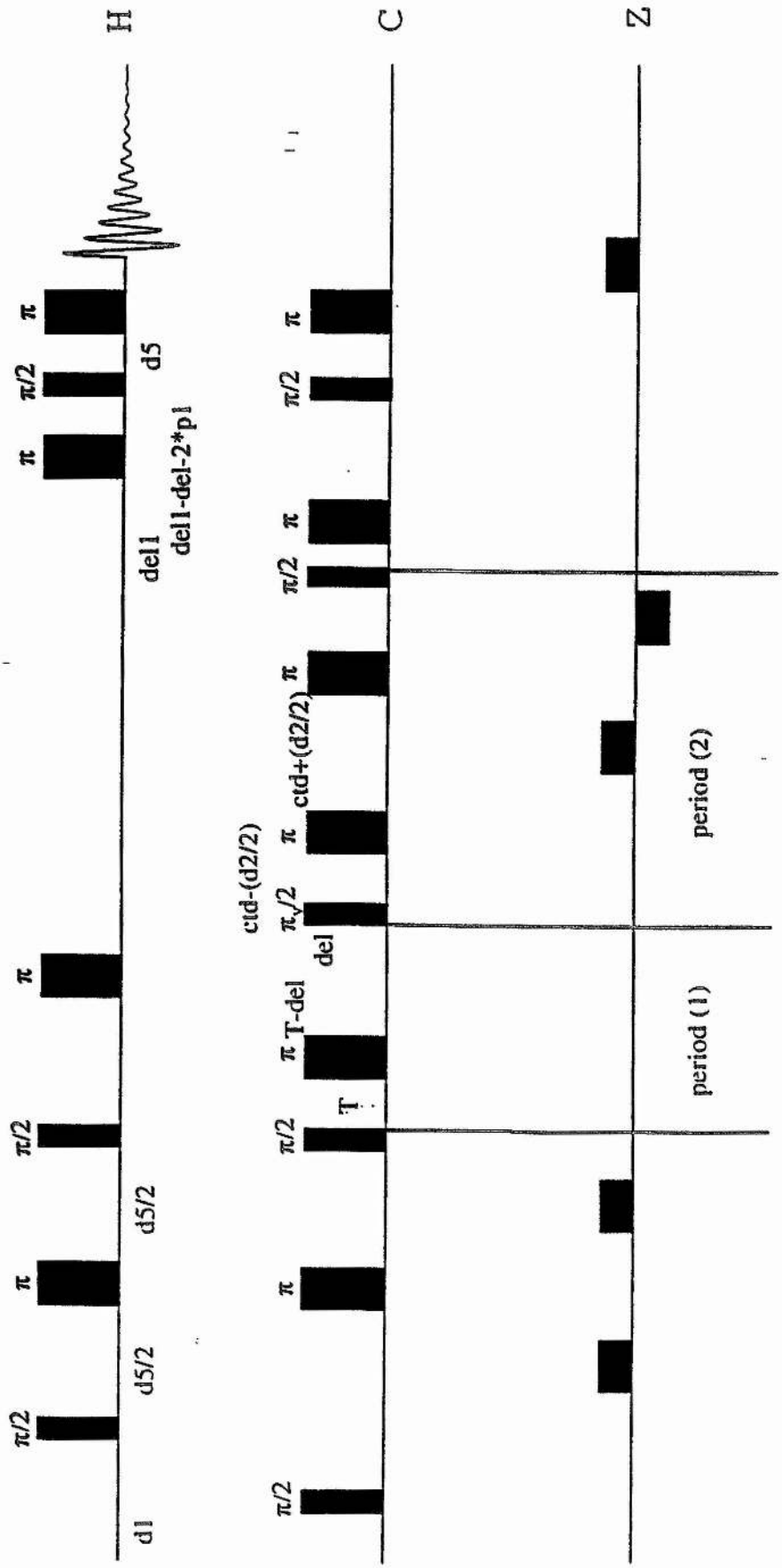

Figure 5.6 - Proton detected INADQUATE experiment

5.7 Materials and Methods

5.7.1 Sample preparation

In order to remove unwanted ^{13}C-^{13}C long-range couplings, while maintaining increased sensitivity compared to a natural abundance situation, experiments were carried out using 6% ^{13}C-labelled glucose. This was provided by Martek Biosciences (Columbia, MD). Samples were dissolved and lyophilised into 99.96% D_2O three times followed by dissolution into 700µL D_2O.

5.7.2 NMR Experiments

The NMR experiments were carried out at 277K with a ^1H reference frequency of 500.12 MHz on a Varian Unity$^+$ spectrometer equipped with a self shielded z gradient triple resonance probe. All experiments were acquired using the pulse sequence in figure 6.1. Data were acquired with spectral widths of 15000Hz and 1400Hz in the F1 (^{13}C) and F2(^1H) dimensions respectively, with 128 increments in the t_1 dimension and 64 transients per increment. T was set to 3ms and the constant time delay (CTD) was set to 100ms.

5.8 Results and Discussion

In order to observe the angular dependence of cross-correlated relaxation indicated in equation [5.9] it is necessary for the molecule to be tumbling sufficiently slowly (Werbelow, 1974). Initial experiments suggested that glucose tumbled too rapidly at room temperature for any cross-correlated relaxation effects to be measurable. Experiments were therefore carried out at 277K to reduce the tumbling time and a long constant time delay (ctd = 100ms) was used to maximise the amount of relaxation. The resulting spectrum for glucose can be seen in figure 5.7. From this it can be seen that the expected triplets result, with couplings due to J_{CH}. In relation to equations [5.6]-[5.8], the central peak of the triplet corresponds to the sum of $I(\alpha\beta)$ and $I(\beta\alpha)$ and the outer peaks correspond to $I(\beta\beta)$ and $I(\alpha\alpha)$ representing the four polarisation states proton nuclei can assume. Figure 5.8 shows the variation of the polarisation states as cross-correlated relaxation occurs due to the glucose tumbling more slowly at the lower temperature. This allowed the use of equations [5.6] and [5.9] to obtain values for θ. Although an accurate value of τ_c was not known for glucose at this temperature, an estimate was made using the Stokes-Einstein equation, giving a value of ~0.2. This is not accurate enough to give good quantitative information and indeed it was not possible to calculate an angle in every case using this estimate, however the values reported in table 5.1 are close to what might be expected from a qualitative examination of glucose structure.

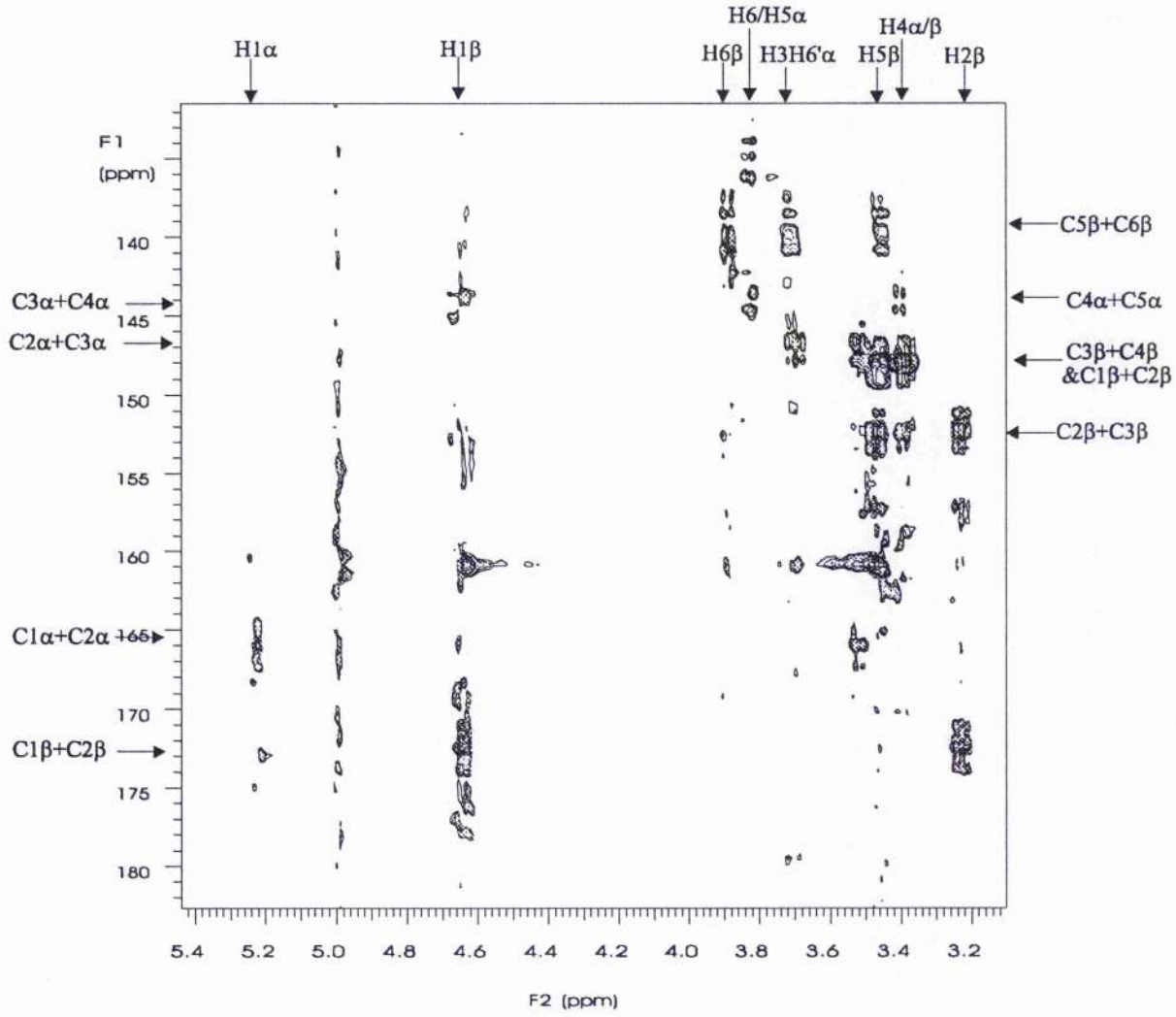

Figure 5.7 – Double quantum coherence experiment for glucose

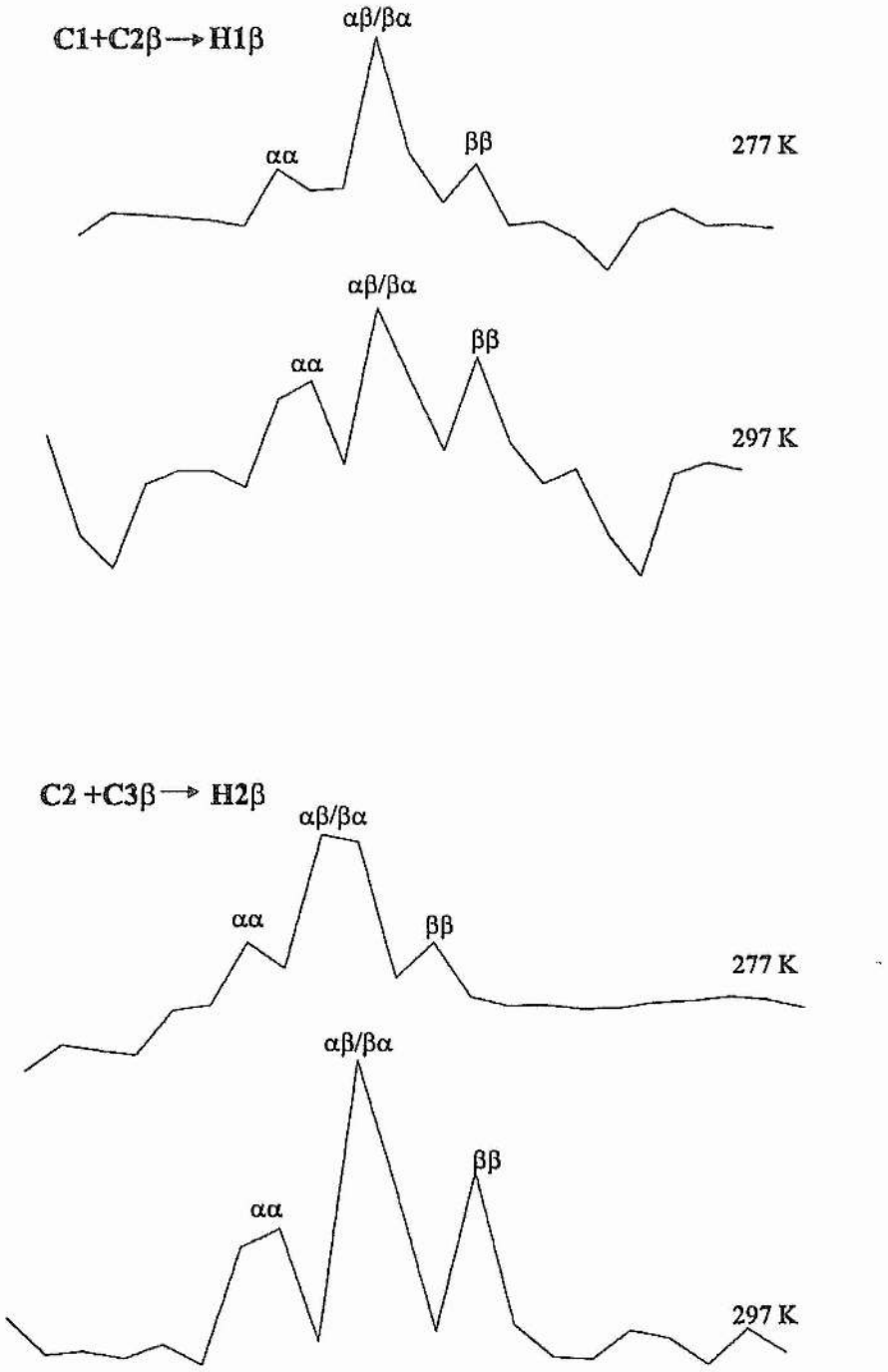

Figure 5.8 – Variation of the polarisation states as cross-correlated relaxation takes effect at the lower temperature

Table 5.1 – Calculated values of cross-correlated relaxation, and angles, using an estimated value of τ_C=0.2ms.

Resonance	$R_{I,J}^{C}$	Angle
C1C2α - H1α	-1.01	~68°
C1C2β - H2β	3.12	~14°
C2C3β - H2β	3.41	~4°
C3C4β - H4β	4.16	-----
C4C5β - Hβ5	3.31	~9°
C2C3β - Hβ3	3.33	~9°

The angles between the protons in β-glucose would be expected to be approximately the same in every case (i.e. ~0°) as they are all axially aligned. In fact the only significantly different angle for glucose would be to that between H1α (equatorial) and H2α (axial), this is consistent with the significantly different cross-correlated relaxation experienced by the C1C2α - H1α resonance.

5.9 Conclusions

It has been demonstrated that the measurement of cross-correlated relaxation effects is potentially useful for the characterisation of oligosaccharides. This method yields different information from the measurement of residual dipolar couplings demonstrated in chapter 3. The residual dipolar couplings provide projection information of bond vectors on molecular alignment tensors. Thus, they provide indirect information about the relative orientation of inter-atomic vectors with respect to each other. This method on the other hand, yields direct information about bond vector projections provided double or zero quantum coherence can be excited between them. A problem with the method as it stands, is the experiment is too insensitive for natural abundance sugars and unwanted ^{13}C-^{13}C couplings are present in the case of ~100% ^{13}C labelled sugars. This leads to the use of 6% ^{13}C labelled glucose that is clearly inconvenient if the method is to be used for other sugars.

This method may potentially be used to gain long-range structural information if two nuclei can be correlated in an efficient way. This could lead to studies of carbohydrates bound to proteins, particularly in view of the fact that the technique is dependent on a relatively large 90Hz (^{13}C-^{13}C) coupling, meaning that line broadening is not a serious problem.

Chapter 6

Transferred NOE studies on ^{13}C-Enriched Sialyl-Lewis-x Bound to E-selectin

Abstract

The bound-state conformation of ^{13}C-enriched Neu5Acα2-3Galβ1-4(Fucα1-3)GlcNAc (Sialyl Lewis-x, sLex) in association with E-selectin was investigated. The availability of ^{13}C-enriched material enabled the application of three-dimensional nuclear Overhauser effect ^{13}C-^{1}H heteronuclear single quantum correlation (NOESY-HSQC) experiments for the measurement of intra-molecular transferred nuclear Overhauser effects (TRNOEs). The additional dispersion afforded by the third (^{13}C) dimension permitted straightforward identification and quantitation of these TRNOEs, and several TRNOEs were identified that had not previously been reported. The bound-state conformation of the ligand, determined by use of a heteronuclear full-relaxation matrix analysis of the TRNOE data, differs significantly from that reported in previous studies.

6.1 Introduction

The tetrasaccharide Sialyl Lewis-x is known to play a role as a ligand for the selectin family of receptors, in the adhesion of leukocytes and neutrophils to vascular endothelial cells during an inflammatory response (reviewed by Lasky, 1995). A complete understanding of the molecular basis of recognition of Sialyl Lewis-x by the selectins ideally requires high-resolution structural data for the complex. Attempts to achieve this have focused on the use of transferred nuclear Overhauser effects (TRNOE) to probe the bound state conformation (Cooke, 1994; Hensley, 1994; Poppe et al., 1997; Scheffler, 1997; Scheffler, 1995).

6.1.1 The selectins

Sialyl Lewis-x antigen is the core carbohydrate moiety that is involved in the recognition of leukocytes by the endothelial cell wall through the interaction with a family of proteins namely the selectins. The selectins are a group of three proteins that enable adhesion between the endothelal cell wall and leukocytes. They are commonly referred to as E(endothelial)-, P(platelet)-, and L(leukocyte)-selectin. They are multi-domain proteins, with a unique overall structure. The primary sequence shows highly conserved regions in the lectin and EGF domains (~65%), and very high conservation between different mammalian species. The lectin domain is essential for the binding of carbohydrates, and is homologous to others found in mammalian proteins that require Ca^{2+} to bind carbohydrates. The EGF domain influences the lectin ability to mediate cell binding, possibly through stabilising the protein. The crystal structure of the lectin and EGF domains of E-

selectin (Graves, 1994) showed that these were distinct domains with little apparent association.

E-Selectin is expressed on the surface of endothelial cells. Its expression occurs via *de novo* protein synthesis, and is induced by the activation of the endothelium by certain cytokines, including interleukin 1 (1L-1), and tumour necrosis factor (TNF) (Bevilacqua, 1987). Maximum levels of E-selectin are found at the cell surface 3-6 hours after activation with cytokines, but this declines back to basal levels after 24 hours by shedding from the cell surface even in the constant presence of cytokines (Bevilacqua, 1989).

6.1.2 Carbohydrate Ligands

The identification of the physiological ligands for the selectins is complicated because, like most lectins, they bind to a wide variety of carbohydrate epitopes *in vivo*. The dependence of the selectins upon a carbohydrate ligand was illustrated in two patients with leukocyte adhesion deficiency type II disease, which is an inherent inability to recruit neutrophils to the sites of inflammation (Harlan, 1993). The inability to generate the ligands required for selectin mediated rolling is attributed to a defect in the fucose metabolism, and they are, therefore, unable to synthesise fucosylated carbohydrates. The observation that cell adhesion is sensitive to neuraminidase, indicates that fucose and sialic acid residues are essential for selectin binding, and a prototype carbohydrate ligand, sialyl Lewis-x, Neu5Acα2-3Galβ1-4[Fucα1-3]GlcNAc, was proposed as the minimal required

structure (figure 6.1). Although, recent advances have shown that sialyl Lewis-x is not the carbohydrate ligand presented *in vivo*, the actual ligands have structural variants of the sialyl Lewis-x core structure.

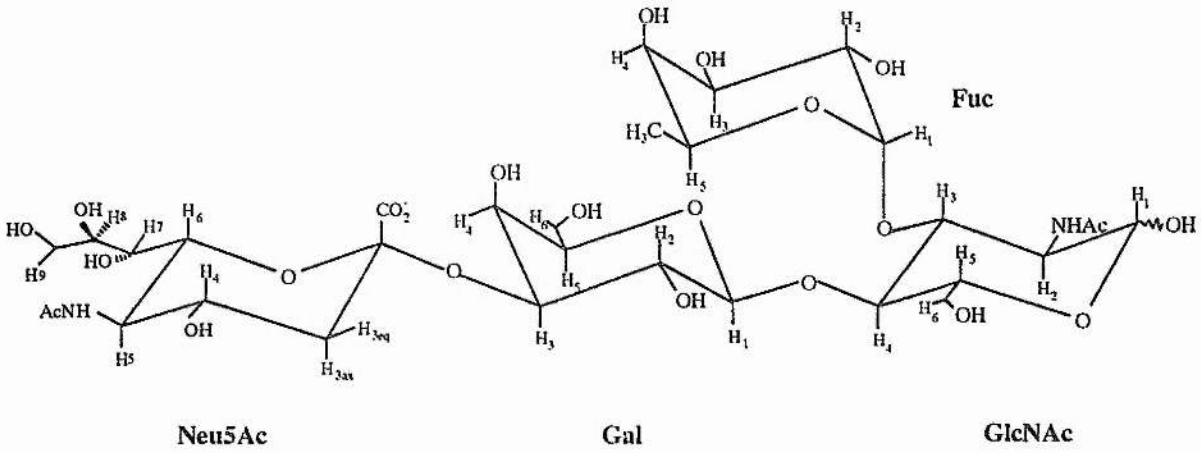

Figure 6.1 – Schematic representation of Sialyl LewisX (sLex)

6.1.3 NMR studies of sialyl Lewis-x

A complete understanding of the molecular basis of recognition of sialyl Lewis-x by the selectins ideally requires high-resolution three-dimensional structural data in free solution and when bound to the selectins. A study by Rutherford *et al.* (Rutherford, 1994) supported by a further study (Harris, 1998), proposed a three dimensional conformation of sialyl Lewis-x in the free state. Four studies have been carried out to date which report different bound-state conformations for the ligand (Cooke, 1994; Hensley, 1994; Poppe *et al.*, 1997; Scheffler, 1997;

Scheffler, 1995). Hensley *et al.* studied the bound conformation at 278K, and observed similar NOEs to those described for the Sialyl Lewis-x moiety in solution. This investigation only observed one NOE about the Gal-Neu5Ac linkage, between Gal-H3 and Neu5Ac-H3ax, and the authors therefore concluded that there was no conformational change upon binding. Cooke *et al*, studied the bound conformation at 298K, and under these conditions observed that the Gal-H3 - Neu5Ac-H3ax NOE was absent, indicating that conformational change upon binding had occurred. They predicted that sialyl Lewis-x selects a single conformation upon binding, with the most likely conformation being conformer 'A' which has a global minimum for the Neu5Ac-Gal linkage of –170°/-8° (Ichikawa, 1992). Scheffler *et al.* studied the bound conformation of sialyl Lewis-x at 310K and observed a disappearance of the Neu5Ac-H3ax -Gal-H3 NOE whilst observing an enhancement of the Neu5Ac-H8 - Gal-H3, over the solution studies. They therefore concluded that conformer 'B' is adopted upon binding, which has a global minimum for the Neu5Ac-Gal linkage of +163°/-57°. Confirmation of this has come from Poppe *et al.* who studied the bound conformation at 300K, and observed significant NOEs in a NOESY experiment.

A major difficulty with such studies is the severe resonance overlap of proton resonances in the ligand, which makes identification of all the available intra-ligand TRNOEs difficult, and severely compromises the measurement of TRNOE intensities. A possible solution to this problem would be to move from using 2D TRNOE experiments, to a heteronuclear three-dimensional NMR method (Kay,

1989) for the measurement of TRNOEs. For this ^{13}C-enriched sialyl Lewis-x bound to E-selectin is required. The additional spectral dispersion afforded by the third (^{13}C) dimension enables the determination of TRNOE intensities with good accuracy, and moreover several TRNOEs were observed that had not been reported previously.

6.2 Materials and methods

6.2.1 Sample preparation

The tetrasaccharide sialyl Lewis-x was obtained in ^{13}C-enriched form having been prepared as described (Probert, 1997). The E-selectin utilised in this study is a recombinant chimera of E-selectin and human IgG, in which the lectin, EDF and six CR domains of the E-selectin replace the antigen binding sites in IgG. For NMR analysis, 10mg of the chimera was dialysed against a D_2O buffer containing 50mM imidazole-d_4 with 1mM $CaCl_2$, pD 7.4. The sample was concentrated by use of a Centricon concentrator (YM-50, Amicon), to a final volume of 600 µl, and ^{13}C-enriched sialyl Lewis-x was added to a concentration 15 fold greater than the concentration of E-selectin binding sites in the chimera.

6.2.2 NMR experiments

Three-dimensional NOESY-HSQC experiments were recorded at 500.12MHz with a Varian Unity$^+$ spectrometer using a sample prepared as above. The probe temperature was 300 K in all experiments. A total of $128 \times 32 \times 512$ complex points were acquired in the F1, F2, F3 dimensions of the three-dimensional

spectrum, with proton (F1, F3) spectral widths of 2130 Hz and a carbon (F2) spectral width of 7000 Hz. The mixing time (τ_m) was 150 ms. Prior to three-dimensional Fourier transformation, time-domain data were apodised with cosine-bell weighting functions in each dimension.

6.2.3 TRNOE simulations

Experimental TRNOE intensities were measured directly as volume integrals from two-dimensional F1/F3 planes derived from three-dimensional NOESY-HSQC spectra, and integrals were summed for each plane that contained a contribution from the relevant cross-peak to give the three-dimensional volume integral. Transferred NOE simulations were computed with the in-house written software package MDNOE2. This package incorporates a full-relaxation matrix analysis of TRNOEs (London, 1992) and includes a formalism for computation of the relaxation matrix which accounts for internal motions which are fast with respect to the rotational tumbling time (Tropp, 1980). Simulations utilised the following parameters: Rotational correlation time of the ligand (τ_{cL}) = 0.24 ns; Rotational correlation time of the complex (τ_{cR}) = 110 ns; reduced rate constant (k) = 177 s^{-1} (corresponding to the literature value (Poppe, 1997) of k_{off} = 164 s^{-1}); dissociation constant (K_d) = 0.72 mM (Poppe, 1997); Concentration of E-selectin binding sites in the chimera ([R])=114 μM; Concentration of ^{13}C-sLex ([L]) = 1.7 mM; mixing time (τ_m) = 0.15 s.

6.3 Results and Discussion

6.3.1 Three-dimensional NOESY-HSQC

Previous studies of the bound state conformation have relied on two-dimensional methods and because of the problem of overlapping resonances, not all NOEs have been measurable. The advantages of moving into three dimensions can be readily seen in figure 6.2. This shows typical F2/F3 (^{13}C-^{1}H) planes derived from the complex of ^{13}C-sLex/E-selectin human IgG chimera (15:1, mole:mole). In comparison with two-dimensional NOESY experiments on this complex (Cooke, 1994; Hensley, 1994; Poppe, 1997; Scheffler, 1995), much greater spectral dispersion is afforded by the F2 (^{13}C) dimension. For example, the F2/F3 plane at the F1 resonance frequency of Fuc H-5 (panel A) shows clearly TRNOEs to both Fuc H-2 and Gal H-6. These TRNOEs have not been observed simultaneously in previous studies (Cooke, 1994; Hensley, 1994; Poppe, 1997; Scheffler, 1997; Scheffler, 1995). In addition, a weak but detectable TRNOE from Fuc H-5 to GlcNAc H-4 is observable in this plane, which has not been observed previously. In total, eleven inter-residue TRNOEs could be detected and quantified, and these are listed in table 6.1.

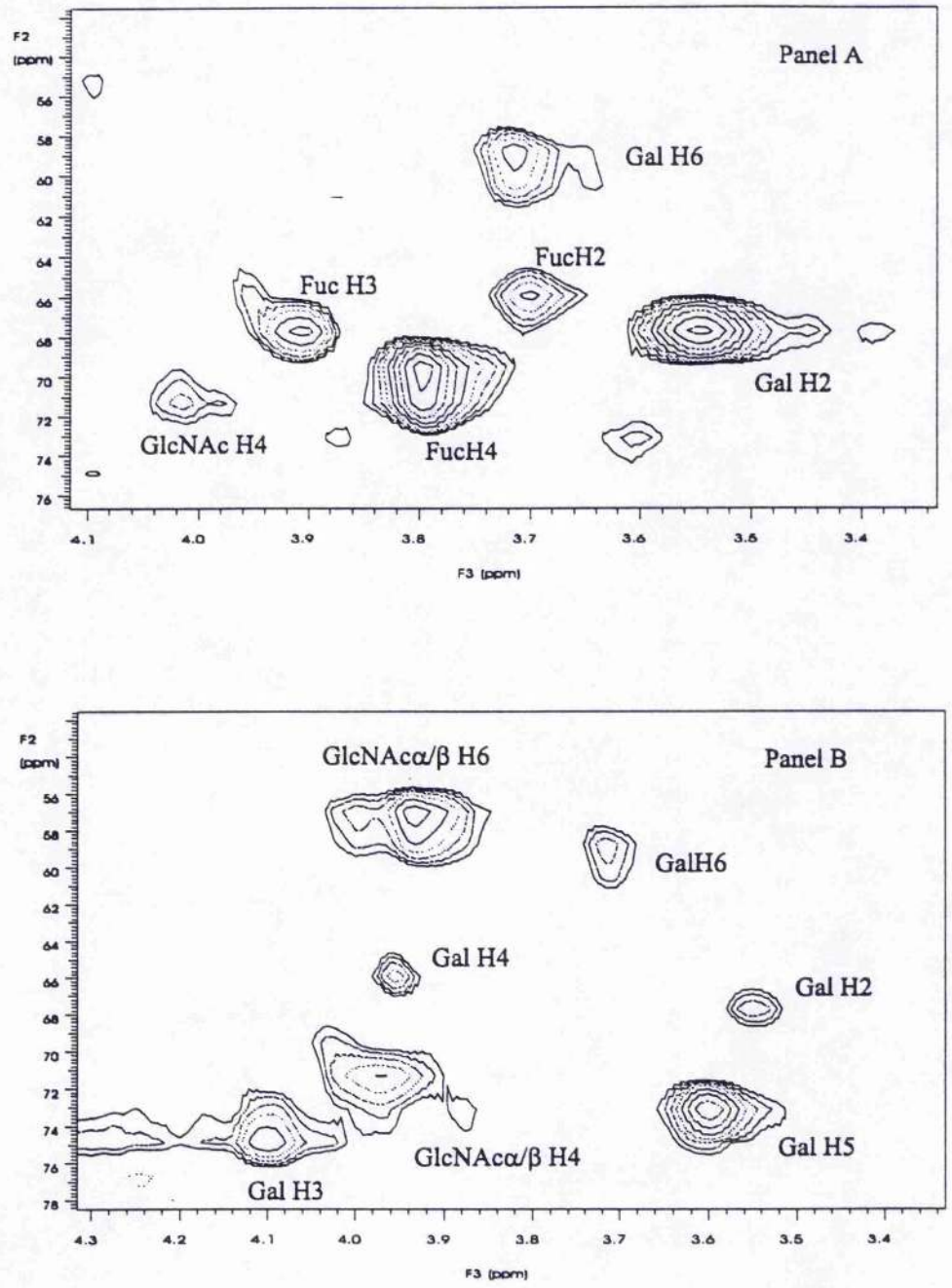

Figure 6.2 – F2/F3 (^{13}C-^{1}H) planes derived from the complex of ^{13}C-sLex/E-selectin, panels A and B

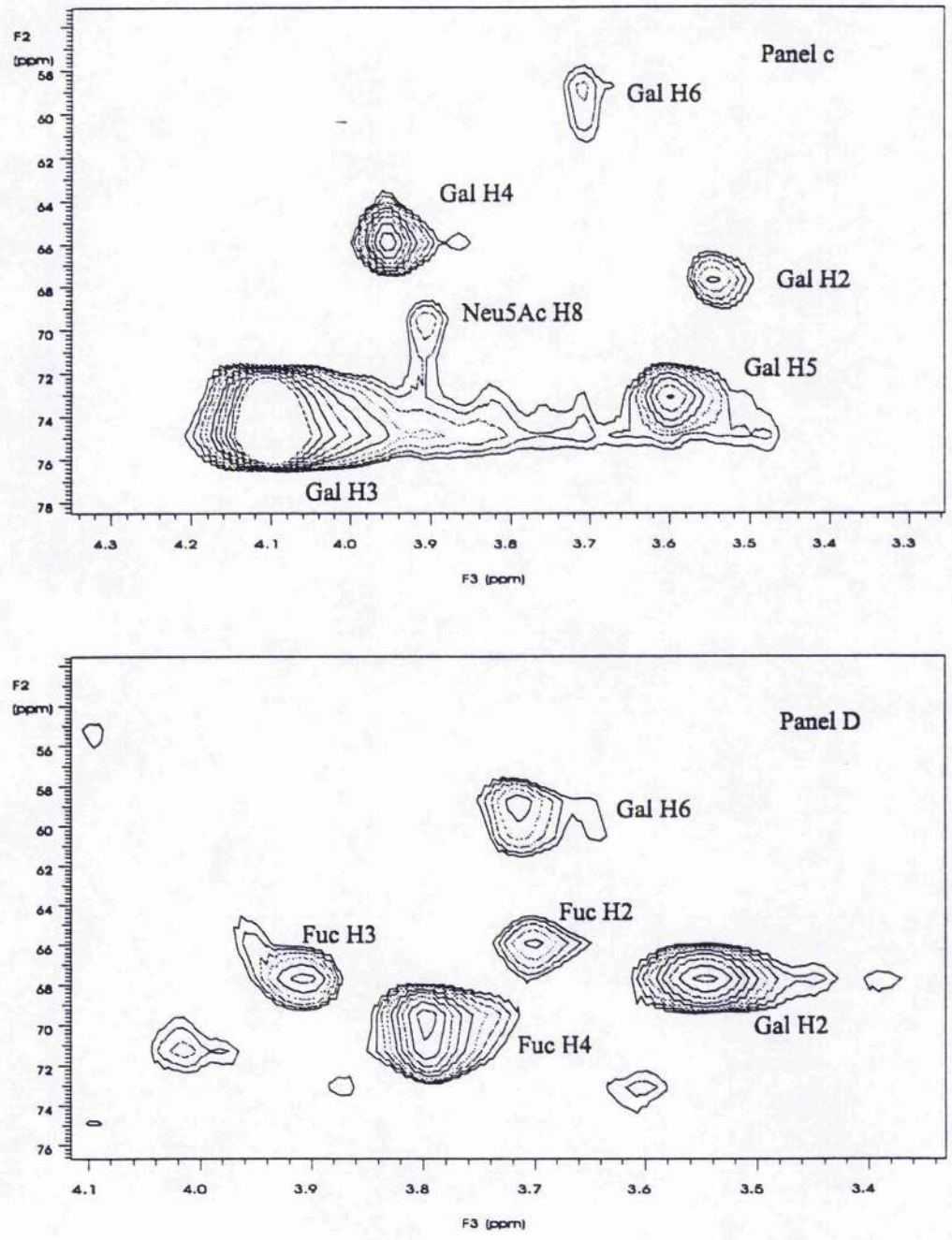

Figure 6.2 – F2/F3 (^{13}C-^{1}H) planes derived from the complex of ^{13}C-sLex/E-selectin Panels C and D

Table 6.1 Experimental TRNOEs observed in NOESY-HSQC experiments (τ_m = 150ms) on sLex/E-selectin IgG chimera (15:1 mole:mole), vs. theoretical values computed from full relaxation matrix simulations on the complex.

TRNOE connectivity	Experimental TRNOE (%)	Theoretical TRNOE (%)*
Fuc H5 - Gal H6	1.5	1.9
Fuc H5 - Gal H2	1.8	1.9
Fuc H5 - GlcNAc H4	0.6	0.5
Gal H1 – GlcNAc H6, 6'	6.7	11.1
Gal H1 – GlcNAc H4	4.4	4.9
Gal H3 – Neu5Ac H8	1.0	1.1
Fuc CH_3 – Gal H2	4.2	3.6
Fuc CH_3 – Gal H6	1.6	2.1
Fuc H1 – GlcNAc H3	4.6	5.2
GlcNAc CH_3 – Fuc H1	1.6	2.2
GlcNAc CH_3 – Fuc H2	2.4	1.1

* Full relaxation matrix simulations computed for sLex in a conformation that results from best-fitting theoretical TRNOEs to experimental values. Parameters that were used in this simulation were: Rotational correlation time of the ligand (τ_{CL}) = 0.24ns; Rotational correlation time of the ligand (τ_{CR}) =110ns; Reduced rate constant (k) = $177s^{-1}$; Dissociation constant (K_d) = 0.72 mM (Poppe, 1997); Concentration of E-selectin binding sites in the chimera ([R]) = 114μM; Concentration of ^{13}C-sLex ([L]) = 1.7 mM; Mixing time (τ_m) = 0.15s.

6.3.2 Modeling Study

These data were utilised for the determination of the bound-state conformation of sLex by best-fitting the theoretical TRNOE values derived from a full relaxation matrix simulation to the experimental values by systematically adjusting the conformation of the glycan using a grid-search procedure. The resulting conformation is shown in figure 6.3, and is characterised by the following glycosidic dihedral angles; Neu5Acα2-3Gal: φ, ψ = -43°, -12°; Galβ1-4GlcNAc: φ, ψ = +45°, +19°; Fucα1-3GlcNAc: φ,ψ = +29°, +41°. These values are similar to those determined in the studies of Peters and co-workers (Scheffler, 1997; Scheffler, 1995), which gave rise to glycosidic torsion angles: Neu5Acα2-3Gal: φ, ψ = -76°, +6°; Galβ1-4GlcNAc: φ, ψ = +39°, +12°; Fucα1-3GlcNAc: φ,ψ = +38°, +26°. However they differ significantly from those determined in the recent study of Poppe (1997): Neu5Acα2-3Gal: φ, ψ = -58°, -22°; Galβ1-4GlcNAc: φ, ψ = +24°, +34°; Fucα1-3GlcNAc: φ,ψ = +71°, +14°, particularly with regard to the conformation about the Fucα1-3GlcNAc linkage. The reason for this discrepancy probably derives from the absence of a crucial TRNOE from Fuc CH_3 - Gal H-2 in the previous study (Poppe, 1997), and from the fact that the inter-residue TRNOE between Fuc CH_3 - Gal H-6,6' TRNOE exactly overlaps with the intra-residue TRNOE between Fuc CH_3 -Fuc H-2 due to essentially complete overlap of the proton resonances of Gal H6, H6' and Fuc H-2. It is thus difficult to quantify these TRNOEs independently to any degree of accuracy using homonuclear ^{1}H NMR methods. In contrast, the TRNOEs are well resolved in the three dimensional NOESY-HSQC spectra (Fig 6.2, panel D).

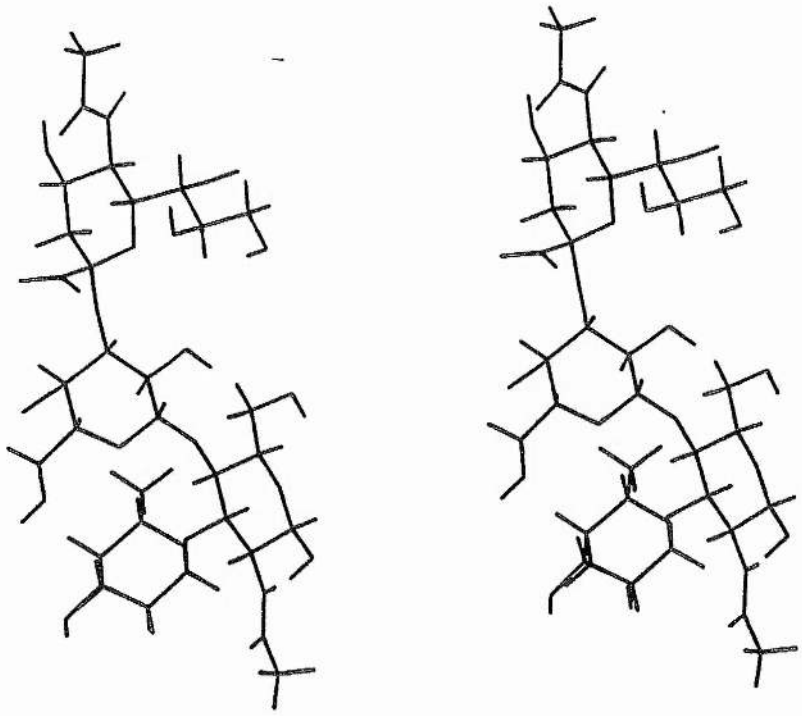

Figure 6.3 – Stereo view of the Bound-state conformation of sLex derived from transferred NOE measurements.

Despite the higher precision with which the intra-ligand TRNOEs can be quantified in NOESY-HSQC spectra, it should be noted that the total number of available TRNOEs limits the accuracy by which the bound-state conformation of the ligand can be determined. Thus, the conformation about the Neu5Acα2-3Gal linkage is defined by a single TRNOE between Gal H-3 -Neu5Ac H-8 in both this study and previous studies (Cooke, 1994; Hensley, 1994; Poppe, 1997, Scheffler, 1997, Scheffler, 1995). While it can be assumed that the glycan adopts a single

conformation in the binding pocket of E-selectin, the discrepancies between the derived values for the glycosidic linkage between studies probably reflects the lack of an adequate number of distance restraints across this glycosidic linkage. Clearly, additional techniques must be developed to obtain additional conformational restraints in systems of this type for example the measurement of dipolar couplings by inducing molecular alignment (chapter 3) or by measuring cross-correlated relaxation effects (chapter 5). An additional factor that in principle limits the accuracy of the bound-state conformation of sLex in all studies to date, is the neglect of the influence of protons within the protein binding site. These by definition cannot be included in full relaxation-matrix simulations since their relative disposition with respect to the glycan is unknown. While in principle the neglect of protein spins from these simulations can lead to erroneous conclusions regarding bound-state conformations (Arepalli,1995; Glaudemans, 1990), the unique associations that are observed in carbohydrate-protein interactions, which involve multiple hydrogen-bond interactions between hydroxyl groups on the glycan and the side-chains of binding-site residues in the protein, result in the effective magnetic isolation of the carbohydrate ligand from the protein. An exception is the situation where a monosaccharide residue in the glycan partakes in a stacking interaction with an aromatic side-chain in the binding site, in which case efficient spin-diffusion is possible involving aromatic side-chain protons due to their proximity to the ligand (Arepalli, 1995; Low, 1997). Fortunately, such stacking interactions can readily be identified as a result of characteristic ring-current shifts of ligand resonances in the presence of the

protein (Low, 1997). Since no such shifts were observed for the sLex/E-selectin complex in this study, even at low ligand:protein ratios (1:1 mole:mole), nor could any ligand-protein TRNOEs be observed at these ratios, these data suggest that the influence of protein spins can be neglected to first order. This conclusion is in accord with saturation-transfer type experiments designed to exclude indirect intra-ligand TRNOE connectivities via protein protons during the course of transferred-NOESY experiments (Poppe, 1997).

The bound-state conformation of sialyl Lewis-x derived from this study may be compared with the solution conformations described in an earlier study (Rutherford, 1994). The conformation about the Neu5Acα2-3Gal linkage (φ, ψ = -43^{o}, -12^{o}) lies closest to minimum 'A' and is in a low-energy region of the potential surface (Breg, 1989; Rutherford, 1994), but not in the global-minimum energy configuration. In contrast, the conformation about the Galβ1-4GlcNAc linkage (φ, ψ = $+45^{o}$, 19^{o}) appears to be in the global minimum energy configuration for the free tetrasaccharide. The conformation about the Fucα1-3GlcNAc linkage (φ, ψ = $+29^{o}$, $+41^{o}$) also lies within the minimum-energy region of the potential surface for the free oligosaccharide. With regard to binding affinity, the oligosaccharide therefore appears to be bound to E-selectin in a conformation very close to the global-minimum energy configuration. The very low affinity of sialyl Lewis-x for E-selectin therefore probably arises from an enthalpy-entropy compensation phenomenon (Dunitz, 1995). A possible candidate in this regard is the substantial configurational entropy of the Neu5Ac

residue, which must be lost on association at the expense of the free energy of binding as the glycan adopts its 'bioactive' conformation (Kolb and Ernst, 1997a; Kolb and Ernst, 1997b).

6.4 Conclusions

This study shows the advantages of using uniformly ^{13}C labeled sugars, which allows the use of the additional dispersion of carbon chemical shifts. The results from this study lead to a bound-state conformation for sialyl Lewis-x that is similar to that proposed by Scheffler *et.al.* (Sheffler, 1997; Sheffler, 1995), but differs substantially from the conformation proposed by Poppe *et al.* (Poppe, 1997) principally in the conformation about the Fucα1-3GlcNAc linkage.

References

Abragam, A. (1961) The principles of Nuclear Magnetism, Clarendon Press, Oxford, p. 309

Acquotti, D., Poppe, L., Dabrowski, J., von der Lieth, C-W., Sonnino, S. and Tettamanti, G. (1990). " Three dimensional structure of the oligosaccharide chain of G_{M1} ganglioside revealed by a distance mapping procedure." *Journal of the American Chemical Society* **112:** 7772 – 7778.

Adams and Lerner, L. (1992) "A simple one-dimensional method for measuring proton exchange rates in water" *Journal of American Chemical Society* **114:** 4827 - 4829

Arepalli, S.R., Glaudemans, C.P.J., Daves, G.D., Kover, P., Bax, A. (1995). "Identification of protein-mediated indirect NOE effects in a disaccharide-Fab complex by transferred ROESY." *Journal of Magnetic Resonance Series B* **106:** 195 - 198

Bastiaan, E.W., Maclean, C., Zijl, P.C.M.v. and Bothner-By, A.A. (1987) " High resolution NMR of liquids and gases: Effects of magnetic field induced molecular alignment." *Ann. Rep. NMR Spectroscopy.* **19:** 35 - 77

Bax, A., Freeman, R., Kemsell, S.P. (1980) "Natural Abundance ^{13}C-^{13}C Coupling Observed via double-quantum coherence" *Journal of the American chemical Society* **102:** 4849-4951

Bax, A., Max, D. and Zax, D. (1992) "Measurement of long-range ^{13}C-^{13}C J couplings in a 20kDa protein-peptide complex." *Journal of the American chemical Society* **114:** 6923 – 6925.

Bax, A. and Tjandra, N. (1997) "High-resolution heteronuclear NMR of human ubiquitin in an aqueous liquid crystalline medium" *Journal of Biomolecular NMR* **10:** 289 - 292

Bevilacqua, M.P., Prober, J.S., Mendrick, D.L., Cotran, R.S. and Gibrone Jnr, M.A. (1987). "Identification of an inducible endothelial-leukocyte adhesion molecule." *Proceedings of the National Academy of Science of the United States of America* **84:** 9238 – 9243

Bevilacqua, M.P., Stengelin, S., Gimbrone Jnr, M.A. and Seed, B. (1989). "Endothelial leukocyte adhesion molecule-1: An inducible receptor for neutrophils related to complement regulatory proteins and lectins." *Science* **243:** 1160 – 1165.

Bevilacqua, V.L., Thomson, D.S. and Prestegard, J.H. (1990) "Conformation of methyl-β-lactoside bound to ricin B-chain" *Biochemistry* **29:** 5529 – 5537.

Bevilacqua, V.L., Kim, Y. and Prestegard, J.H. (1992) "Conformation of β-methylmelibiose bound to ricin B-chain as determined by transferred NOEs." *Biochemistry* **31:** 9339 – 9349.

Bock, K., Lemieux, R.U. (1982). " The conformational properties of sucrose in aqueous solution - intramolecular hydrogen bonding." *Carbohydrate Research* **100:** 63 - 74

Bodenhausen, G., Kogler, H., and Ernst, R.R. (1984) " Selection of coherence-transfer pathways in NMR pulse experiments" *Journal of Magnetic Resonance* **58:** 370 – 388

Boden, N., Corne, S.A., Jolley, K.W., (1987) "Lyotropic Mesomorphism of the cesium pentadecafluorooctanoate/water system" *Journal of Physical Chemistry* **91:** 4092 - 4105

Bothner-By, A.A. et al. (1985a) "Alignment of molecules in a magnetic field." *Magn. Res.* 935 - 938

Bothner-By, A.A. (1985b) "Magnetic field induced alignment of molecules" *Encyclopedia of Magnetic resonance* (eds Grant, D.M) 2932 - 2938 (Wiley, Chichester, 1995)

Brady, J.W. (1986). "Molecular dynamics simulations of α-D-glucose." *Journal of the American Chemical Society* **108:** 8153 - 8160

Brady, J.W. (1987). "Molecular dynamics simulations of β-D-glucose." Carbohydrate Research **165:** 306 - 312

Breg, J., Kroon-Batenburg, L.M.J., Strecker, G., Montreuil, J. and Vliegenthart, J.F.G., (1989) "Conformational analysis of the sialyl(α2-3/6) N-acetyllactosamine structural element occurring in glycoproteins, by two dimensional NOE ^{1}H-NMR spectroscopy in combination with energy calculations by hard-sphere with hydrogen-bonding potential." *European Journal of Biochemistry* **178:** 111 – 120

Brünger, A.T. XPLOR Manual Version 3.1, Yale University, New Haven, CT. 1993.

Brüschweiler, R., Griesinger, C., Ernst, R.R., (1989) "Correlated motion monitored by NMR relaxation in the rotating frame-a source of structural and dynamic information on macromolecules" *Journal of American Chemical Society.* **111:** 8034.

Bundle, D.R., Baumann, H., Brisson, J-R., Gagne, S.M., Zdanov, A. and Cygler, M. (1994) "Solution structure of a trisaccharide-antibody complex" *Biochemistry* **33:** 5183 – 5192.

Campbell, A.P., Skyes, B.D. (1993). " The 2D transferred nOe effect: Theory and Practice." *Annual Review of Biophysics and Biomolecular Structure* **22:** 99 - 122

Casset, F., Imberty, A., Perez, S., Etzler, M.E., Paulsen, H., Peters, T. (1997). "Transferred NOE and rotating frame NOE experiments reflect the size of the bound segments of the Forssman pentasaccharide in the binding site of *Dolichos biflorus* lectin." *European Journal of Biochemistry* **244:** 242 - 250

Cavanagh, J., Fairbrother, W.J., Palmer III, A.G., Skelton, N.J. (1996). "Protein NMR Spectroscopy: Principles and Practice" Academic press.

Chung, J., Tolman, J.R., Howard, K.P., Prestegard, J.H. (1993). "Three-Dimensional ^{13}C-^{13}C correlated experiments on oligosaccharides" *Journal of Magnetic Resonance, Series B* **:102:** 137 – 147

Clausen, H. and Hakomori, S-I. (1989). "ABH and related histo-blood group antigens – Immunochemical differences in carrier isotype and their distribution." *Vox Sanguinis* **56:** 1 - 20

Clore, G.M., Gronenborn, A.M. (1982). " Theory and applications of the transferred nuclear Overhauser effect to the study of the conformations of small ligands bound to proteins." *Journal of Magnetic Resonance* **48:** 402 - 417

Clore, G.M., Gronenborn, A.M (1983a). " Theory of the time-dependant TRNOE: Application to analysis of ligand-protein complexes." *Journal of Magnetic Resonance* **53:** 423 - 442

Clore, G.M., Gronenborn, A.M. (1983b). "Theory of the time-dependant TRNOE: Applications to structural analysis of ligand-protein complexes in solution." *Journal of Magnetic Resonance* **53:** 443 - 442

Clore, G.M., Gronenborn, A.M. (1991). "Applications of 3-dimensional and 4-dimensional heteronuclear NMR spectroscopy to protein structure determination." *Progress in Nuclear Magnetic Resonance Spectroscopy* **23:** 43 - 92

Clore, G.M., Gronenborn, A.M. and Trajndra, N. (1998) "Direct structure refinement against residual dipolar couplings in the presence of rhombicity of unknown magnitude" *Journal of magnetic resonance.* **131:**159-162

Collins, W.P. and Pinol, A. (1983). "Temporal relationships between indices of the fertile period." *Fertil. Steril.* **39,** 647-655

Cooke, R.M., Hale, R.S., Lister, S.G., Shah, G. and Weir, M.P. (1994) "The conformation of the sialyl Lewis^X ligand changes upon binding to E-selectin." *Biochemistry* **33:** 10591 – 10596.

Dabrowski, J. and Poppe, L. (1989) "Hydroxyl and amido groups as long-range sensors in conformational analysis by nuclear Overhauser enhancement: A source of experimental evidence for conformational flexibility of oligosacchardes" *Journal of American Chemical Society* **111:** 1510 - 1511

Dabrowski, U., Dabrowski, J., Grosskurth, H., von der Lieth, C.W., and Ogawa, T. (1993). "Solution conformation of the tetrasaccharide glycoside Xylβ1-2(Manα1-3)Manβ1-4Glcβ1-R from the molla-series glycophingolipids." *Biochemical and Biophysical Research communications* **192:** 1057 – 1065

Dabrowski, J., Kozar, T., Grosskurth, H. and Nifant'ev, N.E. (1995) "Conformaional mobility of oligosaccharides: Experimental evidence for the existance of an "anti" conformer of the Galβ1-3Glcβ1-OMe disaccharide." *Journal of the American Chemical Society* **117:** 5534 – 5539.

Daniels, G.L. et.al. (1993) "ISBT working party on terminology for red cell surface antigens – Sao Paulo report." *Vox Sanguinis* **65**: 77-80.

Davis, A.L., Keeler, J. Laue, E. and Moskau, D. (1992) "Experiments for Recording Pure-Absorption Heteronuclear Correlation Spectra Using Pulsed Field Gradients" *Journal of magnetic resonance* **98:** 207 – 216.

Derome, A.E., (1987). "*Modern NMR techniques for Chemistry Research.*" Pergamon, Oxford

Diehl, P. (1985) Nuclear magnetic resonance of liquid Crystals (Ed. Emsley, J.W.) (Reide, Dodrecht, Netherlands) 147 - 180

Duda, C.A., and Stevens, E.S. (1990) "Lactose conformation in aqueous solution from optical rotation" *Carbohydrate Research* **206(2):** 347 – 351

Dunitz, J.D.(1995) "Win some lose some – Enthalpy-Entropy compensation in weak intermolecular interactions" *Chem. Biol.***2:** 709 – 712

Edge, C. (1994) "The role of glycosylation in disease." Oxford Glycosystems catalogue: 30-31

Edison, A.S., Abildgaard, F., Westler, W.M., Mooberry, E.S., Markley, J.L. (1994) "Practical introduction to the theory and implementaion of multinuclear, multidimensional nuclear magnetic resonance experiments." *Methods in Enzymology* **239:** 3 - 79

Ejchart, A., D., J. and von der Lieth, C.W. (1992). "Solution conformation of monosyllactoses and difucosyllactoses as revealed by rotating-frame NOE-based

distance mapping and molecular dynamics calculations." *Magnetic Resonance in Chemistry* **30:** S105 – S114

Emsley, J.W., and Lindon, J.C., (1975) NMR spectroscopy Using liquid crystal solvents (Pergamon, New York, 1975)

Faber, K.L., Harder, W., Ab, G., Veenhuis, M. (1995) "Review: Methylotrophic yeasts as factories for the production of foreign proteins" *Yeast* **11:** 1331-1344

Farmer II, B.T., Macura, S., Brown, L.R. (1987). "Relay artifacts in ROESY spectra." *Journal of Magnetic Resonance* **72:** 347 - 352

Feng, X., Lee, Y.K., Sandstroem, D., Eden, M., Sebald, A., Levit, M.H., (1996) *Chemical Physics Letters.* **257:** 314

French, A.D. (1988) "Rigid and relaxed-residue conformational analysis of cellobiose using the computer program MM2." *Biopolymers* **27:** 1519 – 1525

French, A.D., Brady, J.W. (1989). *Computer modelling of carbohydrate of carbohydrate molecules.* Washington, American Chemical Society.

Gayathri, C., Bothner-By, A.A., Zijl, P.C.M.v., Maclean, C. "Dipolar Magnetic field effects in NMR spectra of liquids" *Chem. Phys. Lett* **87:** 192 - 196

Genest, D. (1989)." Monte-Carlo simulation study of the influence of internal motions on the molecular conformation deduced from two-dimensional NMR experiments." *Biopolymers* **28:** 1903 - 1911

Glaudemans, C.P.J., Lerner, L., Davies, G.D., Kovac, P., Venable,R., Bax, A. (1990). "Significant conformational changes in an antigenic carbohydrate epitope upon binding to a monoclonal antibody." *Biochemistry* **29:** 10906 - 10911.

Gosser, Y.Q., Howard, K.P., and Prestegard, J.H. (1993). "Three-Dimensional ^{1}H-detected ^{13}C-^{13}C correlation experiments for carbon backbone assignments of enriched natural products" *Journal of Magnetic Resonance, Series B* **101:** 126 – 133

Graves, B.J., Crowther, R.L., Chandran, C., Rumberger, J.M., Li, S., Huang, K.S., Presky, D.H., Familletti, P.C., Wolitzk, B.A. and Burns, D.K. (1994). "Insight into E-selectin/ligand interaction from the crystal structure and mutagenisis of the lec/EGF domains" *Nature* **367:** 532 – 538

Greenwell, P. (1997) "Blood group antigens: molecules seeking a function?" *Glycoconjugate Journal* **14:** 159 – 173.

Griffey, R.H., Redfield, A.G., Loomis, R.E. and Dalhquist, F.W. (1985) "Nuclear magnetic resonance observation and dynamics of specific amide protons in T4 lysozyme" **24:** 817

Gronenborn, A.M. and Clore, G.M. (1995) "Structures of protein complexes by multidimensional heteronuclear magnetic-resonance spectroscopy " *CRC Critical review Biochem. Mol. Biol.* **30:** 351 - 385

Grzesiek, S. and Bax, A. (1993). "The importance of not saturating H_2O in protein NMR. Application to sensitivity enhancement and NOE measurements." *Journal of the American Chemical Society* **115:** 12593 – 12594

Ha, S., Giammona, A., Field, M. (1988). "A revised potential energy surface for molecular mechanics studies of carbohydrates." *Carbohydrate Research* **180:** 207 - 221

Haasnoot, C.A., de Leeuw, F.A.A.M., Altona, C. (1980). " The relationship between proton-proton coupling constants and substituent electronegativities -1." *Tetrahedron* **36:** 2783 - 2792

Harris, R. (1997) *Ph. D. thesis* University of St.Andrews

Harris, R., Kiddle, .G.R., Field, R.A., Ernst, B., Magnani, J.L. and Homans, S.W. (1998). "Stable Isotope assisted NMR studies on ^{13}C-Enriched sialyl Lewis^{x} in solution and bound to E-selectin" *In Print.*

Harris, R., Milton, M., Homans, S.W. (1997) "New NMR techniques for the study of ^{13}C labelled oligosaccharides." *Journal of Biomolecular NMR*, **9:** 47 - 54

Hensley, P., McDevitt, P.J., Brooks, I., Trill, T.J., Field, J.A., McNulty, D.E., Connor, J.R., Griswold, D.E., Kumar, N.V., Kopple, K.D., Carr, S.A., Dalton, B.J. and Johanson, K. (1994). "The Soluble Form of E-selectin is an Asymmetric Monomer" *The Journal of Biological Chemistry* **269:** 23949 – 23958

Hochuli, E., Dobeli, H., And Schacher, A. (1987). "New metal chelate adsorbent selective of proteins and peptide containing neighbouring histidine residues." *Journal of Chromatography* **411:** 177-184

Holak, T.A., Prestegard, J.H., Forman, J.D. (1987). "NME-pseudo-energy approach to the solution structure of acyl carrier protein." *Biochemistry* **26:** 4652 - 4660

Homans, S.W., Pastore, A., Dwek, R.A., Rademacher, T.W. (1987). "Structure and dynamics in oligo-mannose type oligosaccharides." *Biochemistry* **26:** 6649 - 6655

Homans, S.W. (1990). "A molecular mechanical force-field for tge conformational analysis of oligosaccharides - comparison of theoretical and crystal structures of Manα1-3Manβ1-4GlcNAc." *Biochemistry* **29:** 9110 - 9118

Homans, S.W. and Forster, M. (1992) "Application of restrained minimisation, simulated annealing and molecular dynamics simulations for the conformational analysis of oligosaccharides" *Glycobiology* **2:** 143 - 151

Homans, S.W., (1994) In Molecular Glycobiology (Eds. Fukuda, M. and Hindsgaul, O.), IRL Press, New York, NY, U.S.A., pp. 230 - 257

Hwang, T-L. and Shaka, A.J. (1995) "Water suppression that works. Excitation sculpting using arbitrary waveforms and pulse field gradients" *Journal of Magnetic Resonance Series A* **112:** 275 – 279.

Ichikawa, Y. et.al. (1992) "Chemical-enzymatic synthesis and conformational analysis of sialyl Lewis^x and derivatives." *Journal of the American Chemcal Society* **114:** 9283 – 9298.

Imberty, A., Tran, V., Perez, S. (1989). "Relaxed potential energy surfaces of N-linked oligosaccharides - The mannose-α1-3mannose case." *Journal of Computational Chemistry* **11:** 205

Imberty. A. (1997). " Oligosaccharide structures: theory versus experiment." *Current Opinion in Structural Biology* **7:** 617 - 623.

Janknecht, R., de Martynoff, G., Lou, J., Hipskind, R.A., Nordheim, A., and Stunnenberg, H.G. (1991). "Rapid and efficient purification of native histidine-tagged protein expressed by recombinant vaccinia virus" *PNAS* **88:** 8972-8976

Jeffrey, G.A. and Saenger, W. (1991) "Hydrogen bonding in Biological structures." (Springer, Berlin)

Jelesarov, I., Leder, L., Bosshard, H.R. (1996) "Probing the Energetics of Antigen-Antibody recognition by titration microcalorimetry" *A companion to methods in enzymology* **9:** 533-541

Karplus, M. (1959). "Contact electron-spin coupling of nuclear magnetic moments." *Journal of Chemical Physics* **30:** 11 - 18

Karplus, M. (1963). "Vicinal proton coupling in nuclear magnetic resonance." *Journal of the American Chemical Society* **85:** 2870 - 2871

Kay, L.E.; Marion, D.; Bax, A. (1989) *Journal of Magnetic Resonance* **84:** 72 –84

Keeler, J. and Neuhaus, D. (1985). "Comparison and Evaluation of methods for Two-dimensional NMR spectra with Absorption-Mode Lineshapes" *Journal of Magnetic Resonance* **63:** 454 – 472

Keller, P.J. and Vogele, K.E. (1986). "Sensitivity enhancement of INADEQUATE by proton monitoring." *Journal of Magnetic Resonance* **68:** 389 – 392

Knüttel, A., Kimich, R. and Spohn, K.H. (1990) "Indirect ^{13}C tomography and volume-selective spectroscopy via proton NMR" *Journal of magnetic resonance* **86:** 526

Kolb, H.C., Ernst, B. (1997a) "Development of tools for the design of selectin antagonists" *Chem. European Journal* **3:** 1571 – 1578

Kolb, H.C., Ernst, B. (1997b) "Recent progress in the glycodrug area" *Pure and Applied Chemistry* **69:** 1879 – 1884

Kover, K.E., Batta, G., Madi, Z. (1986) "Quantitative 2D heteronuclear spectroscopy – application to a rigid molecule" *Journal of Magnetic Resonance* **69:** 538 - 541

Kover, K.E., Batta, G. (1988) "Sensitivity-Enhanced 2D heteronuclear NOE spectroscopy" *Journal of Magnetic Resonance*, **79:** 206 - 210

Laemmli, U.K. (1970) "Cleavage of structural proteins during the assembly of the head of bacterophage T4" *Nature* **227:** 680-685

Lasky, L.A. (1995) "Selectin-Carbohydrate Interactions and the initiation of the inflammatory response" *Annual Review of Biochemistry* **64:** 113 – 139

Leeflang, B.R., Vliegenthart, J.F.G. (1990) "Relayed NOE experiments for discrimination of exchange effects of overlapping labile protons" *Journal of Magnetic Resonance* **89:** 615

Lemieux, R.U., Bock, K., Delbaere, L.T.J., Koto, S., Rao, V.S. (1980). "The conformations of oligosaccharides related to the ABH human blood group determinants." *Canadian Journal of Chemistry* **58:** 631 - 653

Levine, D.W. and Cooney, G.L., (1973) "Isolation and characterisation of a thermotolerant methanol-utilizing yeast" *Applied Microbiology* **26:** 982-990

Li, Y.C. and Montelione, G.T. (1993). "Solvent saturation-transfer effects in pulse field gradient heteronuclear single quantum coherence (PFG-HSQC) spectra of polypeptides and proteins" *Journal of Magnetic Resonance Series B* **101:** 315 – 319.

Liu, H., Jumar, A., Weisz, K., Schmitz, U., Bishop, K.D. and James, T.L. (1993). "Extracting accurate distance and bounds from 2D NOE exchangeable proton peaks." *Journal of the American Chemical Society* **115:** 1590 – 1591.

Livingston, P.O., Natoli, E.J., Jones-Calves, M., Stockbert, E., Oettgen, H.F. and Old, L.J. (1987). "Vaccines containing purified G_{M2} ganglioside elicit G_{M2} antibodies in melanoma patients." *Proceedings of the National Academy of Sciences of the United States of America* **84:** 2911 – 2915

Lohman, J.A.B. and Maclean, C. (1978) "Allignment effects on high resolution NMR Spectra, induced by the magnetic field." *Chem. Phys* **35:** 269 - 274

London, R.E. (1990) "A Theoretical Evaluation of the significance of scalar relaxation in coupled spin-1/2 systems in macromolecules" *Journal of Magnetic Resonance* **86:** 410 - 415

Low D.G., (1996) *Ph.D. Thesis* University of St.Andrews

Low D.G., Probert, M.A., Embleton G., Seshadri, K., Field, R.A., Homans, S.W., Windust, J. and Davis, P.J.(1997) "Structure of a glycoconjugate in solution and in complex with an antibody Fv fragment" *Glycobiology* **7(3):** 373-381

Lynch, S.R., Pelton, J.G. and Tinoco Jr, I. (1996). "NMR assignment of a 2'-hydroxyl proton from UUCG tetraloop through long-range correlations with ^{13}C." *Magnetic Resonance in Chemistry* **34:** 1179 – 1186.

Maniatis, T., Sambrook, J. and Fritsh, E.F. (1989) "Molecular Cloning: A laboratory manual, secon edition" Cold Spring Harbor Laboratory Press.

McAuliffe, J. and Hindgaul, O. (1997). "Carbohydrate drugs – an ongoing challenge." *Chemistry and Industry* **March (5):** 170 – 174.

McCain, D.C., Markley, J.L (1986) "Internal motions of the 3 hydroxymethyl groups in aqueous sucrose" *Journal of American Chemical Society* **108:** 4259

McCain, D.C., Markley, J.L., (1987) "Stereospecific assignment of the methyl groups H-1 NMR lines of Valine and Leucine in polypeptides by non random C-13 labelling" *Journal of Magnetic Resonance* **73:** 244

Messerle, B.A. Wider, G. Otting, G., Weber, C. and Wüthrich, K. (1989) *Journal of Magnetic Resonance* **85:** 608

Milton, M.J., Homans, S.W. (1995). "Thermodynamics and specificity of oligosaccharide interactions." *Glycoconjugate Journal* **12:** 429

Milton, M.J., Harris, R., Probert, M., Field, R.A. and Homans, S.W. (1998) "New conformational constraints in isotopically ^{13}C enriched oligosaccharides" *Glycobiology* **8:** 147-153

Morrissey, J.H. (1981). " Silver stain or proteins in polyacrylamide gels: A modified procedure with enhanced uniform sensitivity" *Analytical Biochemistry* **117:** 307-310

Neuhaus, D., Williamson, M.P. (1989) The Nuclear Overhauser effect in Structural and Conformatiomnal analysis. VCH.

Neuhaus, D., Van Mierlo, G.P.M. (1992) "Measurement of Heteronuclear NOE Enhancements in Biological Macromolecules – A convenient pulse sequence for use with aqueous solutions" *Journal of Magnetic Resonance* **100:** 221 - 228

Ni, F. (1994). "Recent developments in transferred NOE methods." *Progress in Nuclear Magnetic Resonance Spectroscopy* **26:** 517 - 606

Ni, F., Scheraga, H.A. (1994). " Use of transferred NOE to determine the conformations of ligands bound to proteins." *Accounts of Chemical Research* **27:** 257 - 264

Nilges, M., Clore, G.M.,Gronenborn, A.M. (1988). "Determination of 3-Dimensional structures of proteins from inter-proton distance data by hybrid distance geometry-dynamical simulated annealing calculations." *FEBS Letters* **228:** 317 - 324

—

Nishida, Y., Ohrui, H., and Meguro, H. (1984) "^{1}H studies of (6R) – and (6S) – Deuterated D-Hexoses: Assignment of the preferred rotamers about C5-C6 bond of D-glucose and D-galactose Derivatives in solution" *Tetrahedron Letters* **25 (15):** 1575 - 1578

Noggle, J.H. and Schirmer, R.E. (1971) "The nuclear Overhauser effect, Chemical Applications." Academic Press, London, U.K.

Oettgen, H.F. (1989) *Gangliosides and Cancer.* New York, VCH.

Ohrui, H., Nishida, Y., Watanabe, M., Hori, H., Meguro, H. (1985). "Studies on (6R)-deuterated and (6S)-deuterated (1-6) linked disaccharides - Assignment of the preferred rotamers about the C5-C6 bound of (1-6) disaccharides in solution." *Tetrahedron Letters* **26:** 3251 - 3254

Podkorytov, I.S. (1990). "Seven-pulse sequence DEPT-INADEQUATE." *Journal of Magnetic Resonance* **89:** 313 – 325

Pople, J.A., Schneider, W.G., Bernstein, H.J. (1959) High resolution Nuclear Magnetic Resonance, McGraw-Hill book company. Inc.; New York

Poppe, L. van Halbeek, H.J (1991) "Nuclear Magnetic Resonance of hydroxyl and amido protons of oligosaccharides in aqueous solution: Evidence for strong intermolecular hydrogen bond in sialic acid residues." *Journal Of American Chemical Society* **113:** 363 - 365

Poppe, L., Stuike-Prill, R., Meyer, B. and van Halbeek, H. (1992). " The solution conformation of sialyl(2-6)lactose studied by modern NMR techniques and Monte Carlo simulations." *Journal of Biomolecular NMR* **2:** 109 – 136.

Poppe, L., van Halbeek, H., Acquotti, D. and Sonnino, S. (1994). "Carbohydrate Dynamics at a micellar surface." *Biophysical journal* **66:** 1642 – 1652.

Poppe, L., Brown, G.S., Philo, J.S., Nikrad, P.V. and Shah, B.H. (1997). "Conformation of sLe^x tetrasaccharide, free in solution and bound to E-, P-, and L-selectin." *Journal of the American Chemical Society* **119:** 1727 – 1736

Probert, M.A., Milton, M.J., Harris, R., Schenkman, S., Brown, J.M., Homans, S.W. and Field, R.A. (1997) "Chemoenzymatic synthesis of G_{M3}, $Lewis^x$ and sialyl $Lewis^x$ oligosaccharides in ^{13}C-enriched form" *Tetrahedron Letters.* **38:** 5861-5864.

Reif, B., Köck, M., Kerssebaum, R., Kang, H., Fenical, W., and Griesinger, C., (1996). "ADEQUATE, a New Set of Experiments to Determine the Constitution of

Small Molecules at Natural Abundance" *Journal of Magnetic Resonance Series A*, **118:** 282 – 285

Reif, B., Hennig, M., Griesinger, C. (1997). "Direct Measurement of Angles between bond vectors in high-resolution NMR" *Science* **276:** 1230 – 1233

Rinaldi, R.L. (1983) "Heteronuclear 2D NOE spectroscopy." *Journal of the American Chemical Society* **105:** 5167 - 5168

Rossi, G.L. (1992). "Biological activity in the crystalline state." *Current Opinion in Structural Biology* **2:** 816 – 820

Rutherford, T.J, Partridge, J., Weller, C.T. and Homans, S.W. (1993) "Characterisation of the extent of internal motions in oligosaccharides" *Journal of Biochemistry*, **32:** 12715 - 12724

Rutherford, T.J., Spackman, D.G., Simpson, P.J. and Homans, S.W. (1994). "5 nanosecond molecular dynamics and NMR study of conformational transitions in the sialyl Lewis^x antigen." *Glycobiology* **4:** 59 – 68.

Sanders, J.K.M., Hunter, B.K. (1987). "*Modern NMR Spectroscopy: A guide for chemists.*" Oxford, Oxford University Press

Sanders, C.R., and Schwonek, J.P. (1992) Characterisation of magnetically orientable bilayers in mixtures of dihexanoylphosphatidylcholine and dimyristoylphosphatidylcholine by solid-state NMR" *Biochemistry* **31:** 8898 - 8905

Santoro, J., and King, G.C., "A constant time 2D Overbodenhausen experiment for inverse correlation of isotropically enriched species" *Journal of Magnetic Resonance* (1992) **97:** 202 - 207

Scarsdale, J.N., Ram, P., Orestegard, J.H., Yu, R.K. (1988). "A molecular mechanics NMR pseudo-energy approach to the solution conformation of glycolipids." *Journal of computational Chemistry* **9:** 133

Schauer, R. (1982) *Sialic acids – chemistry, metabolism and function,* Springer-Verlag.

Scheffler, K., Ernst, B., Katopodis, A., Magnani, J.L., Wang, W.T., Weisemann, R. and Peters, T. (1995). "Determination of the bio-active conformation of the carbohydrate ligand in the E-selectin/sialyl Lewis^x complex." *Angewandte Chem. Int. Ed. Engl.* **34(17):** 1841 – 1844

Scheffler, K., Brisson, J.R., Weisemann, R., Magnani, J.L., Wong, W.T., Ernst, B., Peters,T. (1997). Application of homonuclear 3D NMR experiments and 1D analogs

to study the conformation of sialyl Lewis^x bound to E-selectin." *Journal of Biomolecular NMR* **9:** 423 - 436

Schmidt-Rohr, K., (1996). "Torsion Angle Determination in Solid ^{13}C-labeled amino acids and peptides by separated-local-field Double-Quantum NMR" *Journal of American Chemical Society*. **118:** 7601 - 7603

Scorer, C.A., Jeffrey, J.C., McCombie, W.R., Romanos, M.A., and Sreekrishna, K. (1994) "Rapid selection using G418 of High copy number transformants of *Pichia pastoris* for high-level foreign gene expression" *Bio/Technology* **12:** 181-184

Seelig, J., Borle, F. and Cross, T.A. (1985) "Magnetic ordering of phospholipid membranes" *Biochem. Biophys Acta*, **814:** 195-198

Sharon, N. and Lis, H. (1972) "A detailed ^{1}H and ^{13}C NMR study of a repeating disaccharide of hyaluronan: the effects of temperature and counter-ion type." *Carbohydrate Research* **242:** 29 – 51

Shuqun Sheng and van Halbeek, H. (1995) "NMR developments in structural studies of carbohydrates and their complexes" *Biochemical and Biophysical Res Com* 215, No2, 504 - 510

Sklenár and Bax, A. (1987) *Journal of Magnetic resonance* **74:** 469

Sklenár, V. Piotto, M., Leppik, R. and Saudek, V. (1993) "Gradient tailored water suppression for ^{1}H-^{15}N HSQC experiments optimised to retain full sensitivity" *Journal of Magnetic Resonance series A* **102:** 241-243

Sicinska, W., Adams, B. and Lerner, L. (1993). "A detailed ^{1}H and ^{13}C NMR study of a repeating disaccharide of hyaluronan." *Carbohydrate Research* **242:** 29 – 51.

Sørensen, O.W., Freeman, R., Frenkiel, T., Mareci, T.H., and Schuck, R. (1982). "Observation of ^{13}C-^{13}C couplings with enhanced sensitivity" *Journal of Magnetic Resonance* **46:** 180 – 184

Sparks, S.W. and Ellis, P.D. (1985). "DEPT Polarization Transfer for the INADEQUATE Experiment" *Journal of Magnetic Resonance* **62:** 1 – 11

States, D.J., Haberkorn, R.A. and Ruben, D.J. (1982). "A 2-dimensional nuclear Overhauser experiment with pure absorption phase in 4 quadrants." *Journal of Magnetic Resonance* **48:** 286 – 292.

Stein, P.E., Boodhoo, A., Tyrrel, J.G., Brunton, J.L. and Read, R.J. (1992) "Crystal structure of the cell binding B oligomer verotoxin-1 from *E.coli.*" *Nature* **355:** 748 – 749.

Stoddart, J.F. (1971) "*Stereochemistry of Carbohydrates*" New York, Wiley

Stonehouse, J. (1994). *Ph.D. Thesis*, University of Cambridge.

Stott, K., and Keeler, J. (1996) Gradient-Enhanced One-dimensional Heteronuclear NOE Experiments with ^{1}H detection" *Magnetic resonance in Chemistry* **34:** 554 - 558

Thogerson, H., Lemieux, R.U., Bock, K., Meyer, B. (1982). "Further justification for exo-anomeric effect. Conformatioinal analysis based on nuclear magnetic resonance spectroscopy of oligosaccharides." *Canadian Journal of Chemistry* **60:** 44-57.

Tjandra, N., Grzesiek, S. and Bax, A.J. (1996) "Magnetic field dependence of Nitrogen-proton J splittings in ^{15}N enriched human ubiquitin resulting from relaxation interference and residual dipolar coupling" *Journal of American Chemistry* **118:** 6264 - 6270

Tjandra, N., Bax, A. (1997a) "Direct measurement of distances and angles in biomolecules by NMR in a dilute liquid crystalline medium" *Science* **278:** 1111 - 1114

Tjandra, N. Bax, A. (1997b) "Measurement of dipolar contributions to $^{1}J_{CH}$ splittings from magnetic-field dependence of J modulation in two-dimensional NMR spectra". *Journal of Magnetic resonance* **124:** 512 - 515

Tjandra, N. Omichinski, J.G., Gronenborn, A.M., Clore, G.M. and Bax, A. (1997) "Use of dipolar ^{1}H-^{15}N and ^{1}H-^{13}C couplings in the structure determination of magnetically oriented macromolecules in solution" *Nature Structural Biology* **4:** 732 - 738

Tolman, J.R., Flanagan, J.M., Kennedy, M.A. and Prestergard, J.H. (1995) "Nuclear magnetic dipole interactions in field-oriented proteins: Information for structure determination in solution" *Proc. Natl. Acad. Sci* **92:** 9279 - 9283

Torda, A.E., Scheek, R.M. and van Gunsteren, W.F. (1989). "Time-dependent distance restraints in molecular dynamics simulations." *Chemical Physical Letters* **157(4):** 289 – 294.

Torda, A.E., Scheek, R.M. and van Gunsteren, W.F. (1990). "Time-averaged nuclear Overhauser effect distance restraints applied to tendamistat." *Journal of Molecular Biology* **214:** 223 – 235.

Trinh, C.H., Hemmington, S.D., Verhoeyen, M.E. and Phillips, S.E.V. (1997). "Antibody fragment Fv4155 bound to two closely related steroid hormones: the structural basis of fine specificity" *Structure* **5(7):** 937-948

Tropp, J. (1980) "Dipolar relaxation and nuclear Overhauser effects in non-rigid molecules: The effect of fluctuating internuclear distances." *Journal Chemical Physics* **72:** 6035 – 6044.

Tvaroska, I., Bleha, T. (1989). "REVIEW: Anomeric and Exo-anomeric effects in carbohydrate chemistry." *Advances in Carbohydrate Chemistry and Biochemistry* **47:** 45-123

Van Halbeek, H. (1994a) "NMR spectroscopy of hydroxyl protons in supercooled carbohydrates" *Nature Structural Biology*, **1:** 215 - 216

Van Halbeek, H. (1994b) "NMR developments in structural studies of carbohydrates and their complexes" *Current Opinion in Structural Biology* **4:** 697 - 709

Varki, A. (1993) "Biological roles of oligosaccharides: all of the theories are correct." *Glycobiology* **3**: 98 - 130

Vliegenthart, J.F.G., Dorland, L. and van Halbeek, H. (1983). "High resolution, ^{1}H-nuclear magnetic resonance spectroscopy as a tool in the structural analysis of

carbohydrates related to glycoproteins." *Advances in Carbohydrate Chemistry Biochemistry*, **41:** 209 - 374

Vold, R.R., and Prosser, P.S. (1996) "Magnetically oriented phospholipid bilayered micelles for structural studies of polypeptides. Does the ideal Bicelle exist?" *Journal of Magnetic Resonance* **B113:** 267 - 271

von Itzstein, M., Wu, W-Y. and KoK, G.B. (1993). "Rational drug design of potent sialidase-based inhibitors of influenza virus repetition." *Nature* **363:** 418 – 423.

Vuister, G.W., Delaglio, F. and Bax, A. (1993) "The use of coupling constants as a probe for protein backbone conformation" *Journal of Biomolecular NMR* **3:** 67 -80

Wang, C. and Pardi, A. (1987) *Journal of Magnetic Resonance* **71:** 154

Wang, A.C. and Bax, A.J. (1996) "Determination of the Backbone dihedral angles in human ubiquitin from reparametrized Karplus Equations" *Journal of American Chemical* **118:**2483 - 2494

Watkins, W.M. and Morgan, W.J.T. (1959) *Vox Sanguinis* **4:** 97 – 119.

Weiner, S.J., Kollman, P.A., Case, D.A., Chandra Singh, U., Ghio, C., Alagona, G., Profeta, S.P., Weiner, P. (1984). "A new force-field for molecular mechanical

simulations of nucleic acids and proteins." *Journal of the American Chemical Society* **106:** 765 - 784

Weiner, S.J., Kollman, P.A., Nguyen, D.T., Case, D.A. (1986). "An all atom force-field for simulations of protein and nucleic acids." *Journal of Computaional Chemistry* **7:** 230 - 252

Werbelow, L.G. and Grant, D.M, (1974) *Advances in Magnetic Resonance* **9:** 189

Wiseman, T., Williston, S., Brandts, J.F., and Lin, L.N. (1989). "Rapid measurement of binding constants and heats of binding using a new titration calorimeter" *Analytical Biochemistry* **179:** 131-137

Wu, G.D., Serianni, A.s., Barker, R. (1983). "Stereo-selective deuterium-exchange of methylene protons in methyl tetrafurnosides - hydroxymethyl group conformations in methyl pentafuranosides." *Journal of Organic Chemisty* **48:** 1750 – 1757.

Wright, C.S. (1992) "Crystal structure of a wheat germ agglutinin/glycophorin-sialoglycopeptide receptor complex. *Journal of Molecular Biology* **267:** 14345 – 14352

Wright, C.S. and Kellog, G.E. (1996) "Differences in the hydropathic properties of ligand binding at four independent sites in wheat germ agglutinin-oligosaccharide crystal complexes." *Protein Science* **5**: 1466 – 1476.

Wüthrich, K. NMR of Proteins and Nucleic Acids (Wiley, New York; 1986)

Yan, Z.Y., Bush, C.A. (1990). "Molecular dynamics simulations and conformational mobility of blood group oligosaccharides." *Biopolymers* **29:** 799

Yu, C. and Levy, G.C. (1984). "Two-dimensional heteronuclear NOE (HOESY) experiments – investigation of dipolar interactions between heteronuclei and nearby protons." *Journal of the American Chemical Society* **106**: 6533 - 6537